

10-24-2018

## Study of Rheology and Flow Behavior of Magneto-Rheological Fluids Under the Influence of a Magnetic Field and Its Potential Applications for Drilling and Completion Operations

John Edwin Estrada Giraldo

*Louisiana State University and Agricultural and Mechanical College*

Follow this and additional works at: [https://digitalcommons.lsu.edu/gradschool\\_theses](https://digitalcommons.lsu.edu/gradschool_theses)



Part of the [Other Engineering Commons](#)

---

### Recommended Citation

Estrada Giraldo, John Edwin, "Study of Rheology and Flow Behavior of Magneto-Rheological Fluids Under the Influence of a Magnetic Field and Its Potential Applications for Drilling and Completion Operations" (2018). *LSU Master's Theses*. 4826.

[https://digitalcommons.lsu.edu/gradschool\\_theses/4826](https://digitalcommons.lsu.edu/gradschool_theses/4826)

This Thesis is brought to you for free and open access by the Graduate School at LSU Digital Commons. It has been accepted for inclusion in LSU Master's Theses by an authorized graduate school editor of LSU Digital Commons. For more information, please contact [gradetd@lsu.edu](mailto:gradetd@lsu.edu).

**STUDY OF RHEOLOGY AND FLOW BEHAVIOR OF MAGNETO-RHEOLOGICAL FLUIDS  
UNDER THE INFLUENCE OF A MAGNETIC FIELD AND ITS POTENTIAL APPLICATIONS  
FOR DRILLING AND COMPLETION OPERATIONS**

A Thesis

Submitted to the Graduate Faculty of the  
Louisiana State University and  
Agricultural and Mechanical College  
in partial fulfillment of the  
requirements for the degree of  
Master of Science

in

The Craft and Hawkins Department of  
Petroleum Engineering

by

John Edwin Estrada Giraldo  
B.S., National University of Colombia, Medellín, 2008  
December 2018

## **ACKNOWLEDGMENTS**

I want to thank my advisor Dr. Babak Akbari who, throughout my time at Louisiana State University guided me through the development of this research. All his support is truly appreciated since it was a novel topic of great interest to me. Not only he was a source of technical skills and critical thinking, but also taught me essential skills like organization and problem solving.

I would also like to thank Garrett Nielsen, my research fellow, who worked with me to build the experimental setup and with whom I developed a good friendship.

I must express my very profound gratitude to my family for providing their unconditional support throughout this process. All this idea started in South Carolina when I told them my plans of coming to LSU. I received their immediate support to this personal goal.

I would like to thank my committee members, Dr. Mauricio Almeida and Dr. Mayank Tyagi for their time and advice to strengthen the quality of this research. Their opinions were highly valuable to conduct this research from different points of view.

I would like to thank PERTT lab staff, specially to Mr. Douglas Hoy and Jeannette Wooden because all their guidance and logistics made the development of this project feasible. Similarly, I want to thank Chevron Innovative Research Support (CIRS) and LSU Leveraging Innovation for Technology Transfer (LIFT) for providing the funding and training necessary to build the experimental setup to perform a prove of concepts.

Finally, I am grateful to my LSU classmates and friends who supported all the aspects of my academic life. Thank you, LSU, for providing the space to gather that many talented and friendly people.

## TABLE OF CONTENTS

ACKNOWLEDGMENTS .....	ii
ABSTRACT.....	v
INTRODUCTION .....	1
BACKGROUND .....	4
2.1.    Magnetorheological Fluids (MRF) .....	4
2.2.    Magnetizable Particles in an MRF .....	6
2.3.    Base Fluid in an MRF.....	6
2.4.    Additives in an MRF .....	7
2.5.    Challenges in MRF design .....	7
2.6.    Temperature Effect in an MRF.....	8
2.7.    Rheological Models.....	8
2.8.    Proposed Applications for Drilling and Completion Operations.....	9
MATERIALS AND EXPERIMENTAL METHODS .....	18
3.1.    Design of the Magnetorheological Fluid.....	18
3.2.    Experimental Setup .....	23
RESULTS AND DISCUSSION .....	34
4.1.    MRF mixing, rheology and settling ratio .....	34
4.2.    Sample S0 .....	35
4.3.    Sample S5 .....	37
4.4.    Particle Settling .....	41
4.5.    MRF behavior in Flow Loop .....	43
4.6.    Pressure Drop Estimation vs Results .....	54
UPSCALING TO MODEL FROM PROTOTYPE .....	64
5.1.    Dimensionless Analysis.....	64
5.2.    Mason Number and Bingham Number:.....	71
CONCLUSIONS AND FUTURE WORK .....	74
REFERENCES .....	79
APPENDIX A: MAGNETIC FIELD MEASUREMENTS AT VISCOMETER BOB. ....	83

APPENDIX B: CERTIFICATE OF ANALYSIS CARBONYL IRON POWDER (AMERICAN ELEMENTS) .....	85
APPENDIX C: MAGNETIC FIELD READINGS AT THE PERMANENT MAGNETS .....	86
APPENDIX D: PUMP MOTOR SPECIFICATIONS .....	87
APPENDIX E: PRESSURE RELIEF VALVE DISCHARGE ORIFICE AREA DETERMINATION ....	88
APPENDIX F: STUDY OF RHEOLOGY AND SETTLING RATIO OF SAMPLES S1, S2, S3, S4, S6, S7A, S7B, S8A, S8B, S9 AND S9A.....	90
APPENDIX G EXAMPLE OF CALCULATION FOR PRESSURE DROP.....	104
VITA .....	108

## **ABSTRACT**

The use of magnetorheological fluids (MRF) is presented as an alternative to overcome some of the problems encountered in the drilling and completion of a well. The magnetorheological fluids can modify their rheological properties instantaneously under the influence of a magnetic field. In this thesis, MRF consist of a base fluid, magnetizable particles and a polymer that supports the particles. The magnetizable particles align in the direction of the magnetic field, thus modifying the rheology of the mixture. Because of this characteristic, the use of this fluid can have advantages in controlling fluid losses while drilling in narrow operating windows, to provide a tunable sealing mechanism that could work as a packer, to provide a set-on-demand slurry, and as a novel mechanism for releasing stuck pipe. Using existing correlations for estimating the pressure drop in pipes and annuli and a model to estimate the yield stress of the fluid based on concentration of the magnetizable particles and the magnetic field strength, it is possible to determine the pressure drop caused by the fluid behavior when in presence of a magnetic field. The rheological properties of the MRF are measured in a rotational rheometer with two electromagnets attached to the measuring cup. The magnetic field is varied, and the shear stress and viscosity are measured at different shear rates and magnetic field strengths. The settling ratio is evaluated comparing different carrier fluids, magnetizable particle concentration and use of surfactants. On an experimental setup, different MRF samples are circulated on a flow loop resembling circulation geometry where the pressure drop of the fluid is measured in linear sections and compared to the models. The experimental setup also serves as a small-scale well where different applications for this type of fluid could be tested. The objective of the project is to determine if the pressure drop generated by these samples when magnetized can be high enough to control a fluid loss, to create a strong sealing mechanism as an open-hole packer or other potential mechanisms.

## INTRODUCTION

Although little is known by the public in general about the smart-fluids, its discovery is attributed to Jacob Rabinow in 1949 (Kolekar, 2014) but just in the recent decade this type of fluid has been used at an industrial scale. Nowadays, they are providing a turning point in how the fluid mechanics works. These smart-fluids, also known as magnetorheological fluids (MRF), consist on a suspension of magnetic particles in a liquid. Under the influence of a magnetic field, the suspended magnetic particles interact to form a new structure that resists shear deformation or flow. The interaction of these particles and the magnetic field creates a form of columnar structure that restricts the motion of the fluid, therefore, increasing its rheological properties (Kolekar, 2014). This feature has attracted scientists and technology companies to use these fluids to overcome old engineering limitations. Several applications that use MRF are found in dampers, bridges, body armors and shock absorbers systems (Modular & Series, 2017). Thus, as the MRF have revolutionized different industries and how the fluid mechanic works, the Oil and Gas Industry can benefit from using this type of fluids providing innovative solutions for drilling and completions operations. Although the conventional drilling fluids in the Oil and Gas Industry have been used extensively for several decades, these fluids remain limited to crucial application where the Magnetorheological fluids can be proven more beneficial. These applications where the MRF can be more beneficial will be explained later in this document. The drilling fluids in the Industry are a mixture of a carrier phase, either water or oil, and chemical additives designed to set the required properties of this fluid. Two of these properties are viscosity and yield stress, known in fluid mechanics as rheological properties. Setting the rheological properties of a drilling fluid is important because they determine its flow behavior downhole, the debris removal capacity while drilling, and the expected operational pressures to maintain the wellbore stability, among other implications. An MRF can be a drilling mud, a cementing slurry, a completions fluid, or any other type of fluid used while drilling and completing a well. Conventionally, drilling fluids rheological properties can only be varied at surface by adding chemical additives and cannot be tuned once these fluids are pumped downhole (Nair et al., 2015) other than variations caused by temperature, or pseudoplastic behavior at

different flow rates. This imposes a natural limitation for these fluids, making any rheological change time consuming, non-immediately reactive and frequently expensive because of the high amount of volume to be treated with chemicals to convey a solution.

Conversely, the rheology in Magnetorheological Drilling Fluids, which is the addition of magnetic particles to the conventional drilling fluid is not chemically dependent. In fact, the change of the rheological properties of an MRF is tuned according the intensity and direction of a magnetic field applied to the fluid (Vryzas et al., 2017). This feature allows that any rheological change can be achieved even downhole or at surface when a magnetic field of a certain intensity is applied to the MRF with fixed magnets or electromagnets (Brian Mitchell et al., 2008). Thus, the MRF are capable to develop a rapid and localized rheology modification that can be translated into a restriction to flow under the influence of a magnetic field.

As there is a variety of drilling fluid systems available for specific applications in the industry, likewise different MRF combinations can exhibit numerous behaviors. Therefore, this document presents a detailed study of different Magnetorheological Fluids, ranging from different base fluids such as water and hydrocarbon, different magnetic particle concentration and different mixture stabilizers. Theory suggests that under the appropriate conditions, the MRF can transition from a liquid to a semi-solid form (Hajalilou et al., 2016). In consequence, it can be claimed that if this fluid solidifies intentionally in the annulus, a controlled restriction of the annulus could be achieved, like a packer would do when activated. Assuming this is possible, several applications can be envisioned to solve operational problems during the drilling a completion of a well. These proposed applications are explained later.

Chapter 2 provides a theoretical background of the Magnetorheological Fluids. This includes the preparation of an MRF, the effects of modifying the magnetic particle concentration, the base fluid, the particle size and the temperature. Additionally, the proposed applications of this type of fluid for solving operational problems such as: releasing stuck pipe, fluid loss control for narrow operating windows, or cement slurry segregation during Plug & Abandonment in multiple annuli. The elements and features shown in the drawings are not necessarily drawn to scale, emphasis instead being placed upon clearly illustrating



the principles of the examples. Additionally, certain dimensions may be exaggerated to help visually convey certain principles.

Chapter 3 includes the materials used in this study to analyze the MRF. A rotational viscometer with a magnetic kit is used to measure the rheology of the different MRF fluid samples at different magnetic field strengths. Additionally, the flow-loop built to test the MRF behavior in a concentric annulus is described in detail.

Chapter 4 presents the results and analysis from this study. Particularly, shows the effect of the base fluid and the stabilizers on the settling of the magnetic particles. Since the magnetic particles have a high specific gravity, the particle settling is an issue that need special attention during the preparation of the MRF. The settling ratio after prolonged periods of time (days) are presented in this report. Similarly, the response of the magnetic field depended yield stress of the various samples is presented and analyzed. The results also include the pressure drop analysis of different samples of MRF circulated in the flow-loop. Correlations to history match the pressure drop based on the rheology properties of the MRF are presented and evaluated. Chapter 5 describes the dimensionless analysis through the Buckingham Pi Theorem to estimate the pressure behavior upscaled to more realistic wellbore conditions of geometry and flow rates from the conditions measured in the prototype.

Chapter 6 summarizes the results and the conclusions of this study. Based on the results obtained, the recommendations for future works are presented.

## BACKGROUND

### 2.1. Magnetorheological Fluids (MRF)

The magnetorheological fluids (MRF) are a mixture of a carrier, the magnetizable particles and a stabilizer to avoid the sedimentation of the particles. Under the influence of a magnetic field the magnetizable particles align in the direction of the magnetic field, forming a structure that is capable to vary the rheology of the MRF.

The rheological properties of the MRF are variable depending on 3 factors:

1. the magnetizable particles volume fraction (dispersed phase),
2. the carrier fluid (continuous phase) and
3. the strength of the magnetic field.

The fluid structure, once a magnetic field is applied, is accountable for the formation and reversibility from a free-flowing liquid to a semi-solid. The reversibility is of extraordinary importance and requires to be tuned for each application presented in this paper, some applications require fast reversibility while others need delayed reversibility. The reversibility depends on the grade of the magnetizable particles available on the market, namely Carbonyl Iron Powder (CIP) the one used for this research. The CIP is an iron powder manufactured through thermal decomposition and is one of the most common magnetic particles used for MR applications. Because of its high magnetic susceptibility, these particles align easily in the direction of the magnetic field. The commercialized CIP can be hard grade or soft grade. On the one hand, soft grade magnetic materials can be easily magnetized and demagnetized, which provides a better control over the MRF. On the other hand, hard grade magnetic materials can maintain the magnetized fluid structure without the presence of the magnetic field (Hajalilou et al., 2016). This characteristic is of vital importance because depending on the intended application, an appropriate magnetic material needs to be considered to create an immediate or delayed stiffening.

Another crucial factor for the design and stability of the MRF is the magnetizable particle size, being the range of 0.1-10  $\mu\text{m}$  the optimum size to prevent particle sedimentation due to their unusually high density

(7.5 g/cm<sup>3</sup>). Carbonyl Iron Powder (CIP) is the preferable magnetizable particle to prepare MRF because of the high saturation magnetization and low coercivity (Ashtiani, Hashemabadi, & Ghaffari, 2015; Hajalilou et al., 2016). Additionally, the particle size determines the chain-like formation on the SEM micrographs as observed in Fig. 1. The chains are less stable in the micron size particles but well defined and structured in the Nano-size domain. The more regular the chain formation, the better the rheological response of the MRF.

Although the conventional drilling fluids in the oil industry have been used extensively for several decades, their rheological properties can only be set at the surface by adding chemical additives and cannot be tuned once these fluids are pumped downhole. This imposes a limitation for these fluids, making any rheological change time consuming, non-immediately reactive and frequently expensive because of the high amount of volume to be treated with chemicals. Particularly, the rheology in Magnetorheological Drilling Fluids, which is the addition of magnetic particles to the conventional drilling fluid, are not chemically dependent. Furthermore, the change of the rheological properties of a MRF is tuned according to the intensity and direction of a magnetic field applied to the fluid (Vryzas et al. 2017). This feature allows that any rheological change can be achieved even downhole or at surface when a magnetic field of a certain intensity is applied to the MRF with fixed magnets or electromagnets (Zitha & Wessel, 2002). In addition, the possibility of a fluid creating a fluid barrier when a magnetic field is applied provides an advantage where potential application in the industry can be evaluated.

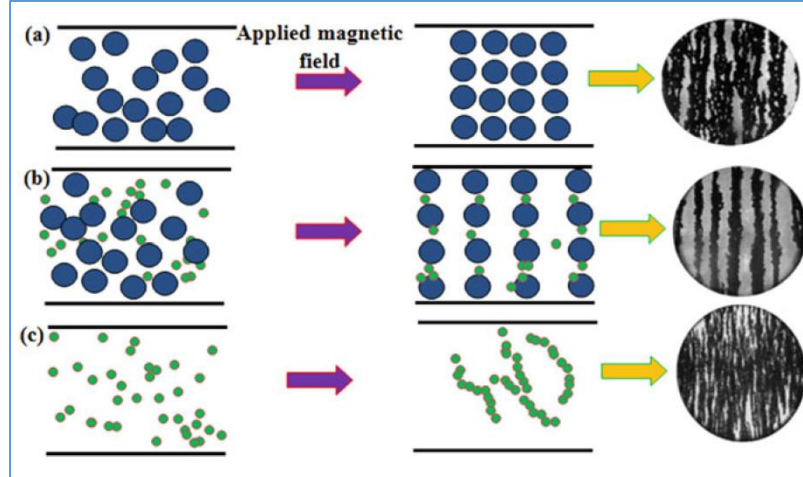


Fig. 1. Effect of magnetic field on (a) micron size particles (b) mixed nano and micron size particles, and (c) nano size particles in the MRF (Hajalilou et al., 2016).

## 2.2. Magnetizable Particles in an MRF

The magnetizable particles are divided into two different classes, metallic alloys (Fe-based) and ceramic materials (Ferrites). The later are principally metal oxides or iron oxides. Researches have been attracted to use iron oxides due to the low magnetism is retained by these particles by removing the applied field, this is also called soft magnetic effect. The most common magnetic materials used for MRF preparation include: Iron Powders, Carbonyl Iron and its composites, Magnetite and iron oxides, among others. These particles have a higher specific gravity and are prone to particle settling (Hajalilou et al., 2016). In this study, soft Carbonyl Iron Particles from American Elements were used in entire experimental phase. Specific characteristics of these particles are depicted in Appendix B.

## 2.3. Base Fluid in an MRF

The base fluid is the continuous phase where the magnetizable particles are dispersed and suspended. A wide variety of base fluids include petroleum-based oils, mineral oils, water, paraffin oils, silicon oil, polyether, glycols, cement slurries among others (Ashtiani et al., 2015). Important features that the base fluid must provide comprise temperature stability, non-corrosive, non-reactive with the magnetic particles, environmentally friendly and cost-effective. Perhaps one of the features that is well studied in this report

includes the ability of the base fluid in combination with additives to maintain the magnetizable particles suspended in motion and static. It is important to note that the base fluid rheology affects directly the rheology of the MRF in both states, active and inactive.

#### **2.4. Additives in an MRF**

Generally, the additives in the MRF are added to prevent the particle settling, to modify the initial viscosity and to produce a stable suspension. To prevent the particle settling, stabilizers such as polymers, thixotropic materials or gelling agents are added to form weak structures that hold the magnetizable particles. Certain surfactants like stearates form a network of swollen strands that traps the particles and collects them (Ashtiani et al., 2015). This feature creates a stabilizing effect to overcome the settling of the magnetizable particles. Thixotropic additives may include synthetic colloidal clay Laponite RD from BYK USA (Rich, Doyle, & McKinley, 2012). The rheological behavior and settling ratio of MRF with Laponite RD is presented in this report. Other studies suggest the use of grease as stabilizers in ion-based particles in silicon oil (Elizabeth Premalatha et al., 2012). Different studies have been performed in silicon oil carrier fluids with a combination of fatty acids such as stearic acid demonstrated good results in terms of magnetorheological effect and low settling ratio (Ashtiani & Hashemabadi, 2015). The rheological behavior and settling ratio of MRF with stearic acid in silicon oil is presented in this report. Other authors have studied the effect of polar and non-polar Polyalphaolefins (PAO) and Dioctyl Sebacate (DOS) in combination with organoclays (Hills & Yurgelevic, 2003) to overcome the particle sedimentation. The use of other additives such as Bentonite and Carbonyl Methyl Cellulose (CMC) is included in this report.

#### **2.5. Challenges in MRF design**

To make an MRF competitive in the market this type of fluids need to have certain characteristics that include chemical stability, high magnetic saturation, operation in a wide range of temperatures, a high yield stress in the presence of a magnetic field and low apparent viscosity in the absence of magnetic field, and good stability against sedimentation (Ashtiani et al., 2015). Yet, the challenges in developing competitive

MRF are focused to prevent the sedimentation. In that sense, different stabilization techniques are being studied. The main techniques are described as follows:

- Coating magnetizable particles: Coating the magnetizable particles with organic polymers reduces the particle settling by reducing the difference between the density of the magnetizable particles and the carrier fluid. Some of these techniques have some negative effects such as reducing the magnetic field dependent yield stress (Cho et al, 2004).
- Spherical Nanoparticles: These particles include iron and its compounds, graphite fibers, carbon nanotubes, fumed silica, etc. Since the nanoparticles have a lower mass and higher surface area in comparison to the magnetizable particles, they can effectively prevent the settling ratio (Y. D. Liu, Choi, & Choi, 2012).
- Modification of the carrier fluid with stabilization additives: Most of these modifications are described in section 2.4 of this report.

## **2.6. Temperature Effect in an MRF**

The temperature has a direct impact in the behavior of the MRF. Principally, the temperature affects the magnetization behavior of the magnetizable particles, the base fluid shear viscosity, and the carrier fluid thermal expansion (Ashtiani et al., 2015). The particle magnetization decreases as the temperature increases, this can be explained because the temperature accelerates the atomic motion causing a reduction in the magnetic moment per unit mass of the CIP. However, the CIP is unaffected at temperatures below 300°C [572°F]. At temperatures larger than 500° [932°F] the weight percentage increases due to the oxidation layer becoming thicker produces an increased sedimentation (Wang et al., 2014). In that sense, the CIP is a good candidate for applications under the most common downhole environments in drilling and completions.

## **2.7. Rheological Models**

The importance of the MRF is the relevance between the Shear Stress and the Shear Rate. As explained before, the magnetizable particles are dispersed randomly in the carrier fluid in the absence of a magnetic

field. In this scenario, the rheological properties are associated strictly to the rheology of the carrier fluid. On the other hand, when a magnetic field is applied to the fluid, the magnetizable particles interact and make chains-like structures through the dipole-dipole interaction between the particles in the direction of the magnetic field (Kang Hyun Song et al., 2009). In consequence, the chain-like formation of the particles produces a restriction of the fluid to flow and the MRF exhibits a viscoelastic behavior as a function of the magnetic field dependent yield stress (Goncalves, Güth, & Maas, 2015). If a high enough magnetic field dependent yield stress is generated, the fluid can alter to a semi-solid form.

The fluids depending on the type of response of the shear stress under different shear rates can be categorized into Newtonian or Non-Newtonians. The MRF and most common drilling fluid exhibit a non-Newtonian response since the shear stress at different shear rates is not linear. Moreover, an initial shear (or yield) stress must be exceeded to initiate the flow. The best model that represents this type of behavior was introduced by Herschel and Bulkley (Tang & Kalyon, 2004) and three different factors determine the relationship between the Shear Stress and the Shear Rate: yield shear stress ( $\tau_0$ ), the flow index ( $n$ ), and the fluid consistency ( $k$ ).

$$\tau = \tau_0 + k\dot{\gamma}^n \quad (\text{Eq. 1})$$

The fluid consistency is a constant of proportionality, the flow index measures the degree to which the fluid is shear thinning  $n < 1$  or shear thickening  $n > 1$ .

## **2.8. Proposed Applications for Drilling and Completion Operations**

### **2.8.1. Use of MRF for releasing stuck pipe.**

During differential sticking, the well can be circulated. That is, the mud or any treatment can be pumped downhole and recovered at the surface. This provides an advantage compared to mechanical sticking when well circulation can be impaired. In general, the release mechanism during a differential sticking includes:

- a. Reduce the mud weight (mud density) to decrease the fluid hydrostatic pressure in the wellbore and hence the pressure differential with the formation. This mechanism can be limited when the formation integrity is at risk.
- b. Use spotting fluids intended to degrade the mud cake, reducing the contact areas of the formation and the stuck tool.
- c. A combination of the previous two mechanisms.

Problems encountered while applying these mechanisms:

Reducing the mud weight can make the wellbore susceptible to wellbore instability, leading to wall collapse or formation fluid migration to the wellbore due to an underbalance condition. Additionally, to significantly reduce the hydrostatic over the problematic zone, a long column of light fluid needs to be in the wellbore, changing the pressure profile of the well. Experience has shown that the spotting fluids need a soaking time to effectively degrade the mud cake. This waiting time is non-productive time, and it delays the drilling operations and increases the operational costs.

MRF advantages:

The MRF can provide a competitive solution to overcome this problem. When MRF is activated in the annulus, it could form an open-hole packer that withstands the hydrostatic pressure above it. The pressure below the packer can be varied (e.g., reduced) locally to decrease the differential pressure over the stuck pipe to a point that the formation fluids pressure can help to release the pipe.

In view of the stuck pipe problem and limitations on the conventional techniques used to address it, one example described herein uses a tool with permanent magnets with a coil tubing set or wireline to set a packer to release a differential sticking.

The Fig. 2. depicts the proposal to release a stuck pipe with coiled tubing. (a) differential sticking can occur when the wellbore pressure is larger than the formation pressure. Also, drilling in depleted or subnormal pressurized formation can cause differential sticking. (b) A coiled tubing is run along permanent magnets to a location above the stuck pipe (c) MRF is pumped through the coiled tubing and up to the annulus to solidify in front of the magnets creating a seal mechanism (d) Nitrogen is pumped through the coiled tubing



enters to the annulus coiled tubing-drill-string (e) The nitrogen expands in the annulus while travelling up to surface decreasing the hydrostatic column (f) Once the formation pressure is higher than the wellbore pressure the first one pushes back pipe to the wellbore and thus releasing it.

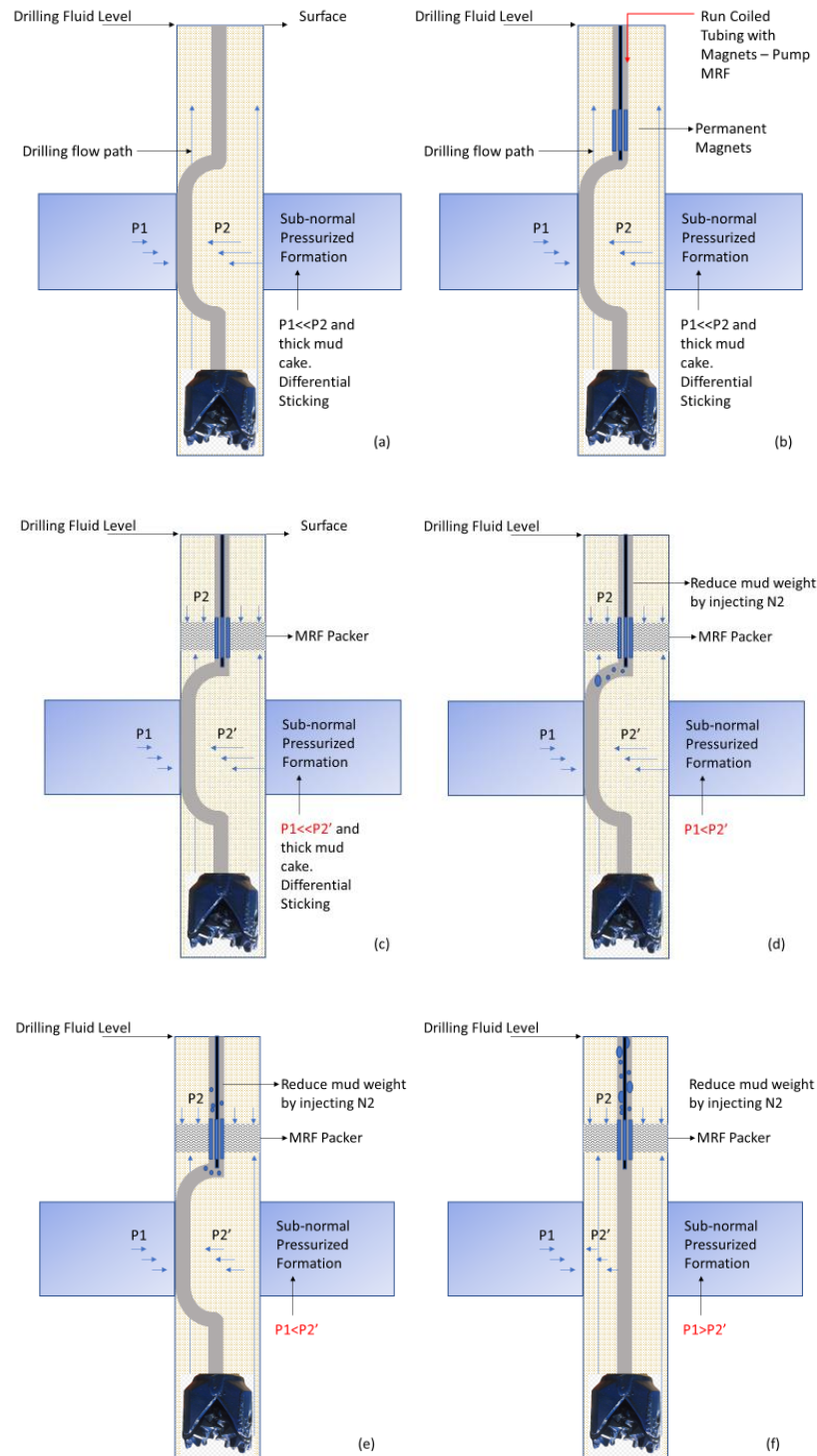


Fig. 2. Releasing stuck pipe with Coiled Tubing

### 2.8.2. Use of MRF as a fluid loss controller while drilling.

How fluid losses are currently cured in the industry:

By using conventional drilling fluids, one mitigation alternative is adding high size solids, also known as bridging agents or lost-circulation materials (LCM) (Ghalambor et al., 2014). Although LCMs have been extensively used, using large size solids can damage the producing formation and reduce the oil or gas productivity in the long run (Alexeyenko & Aramco, 2014). Additionally, the concentration and particle size can be limited to avoid damaging the expensive BHA, particularly the motor and other components. In severe cases, the LCM is not enough to control the fluid losses (Javier U. et al., 2016). The operators can either continue drilling with the problem, which can lead to other potential problems, or to pull out of hole the BHA and run a string to balance a cement plug. In either case, the operator needs to make economic decisions when fluid loss occurs (Whitfill, Wang, & Systems, 2005). In severe cases, the cement slurry itself is not capable to cure fluid losses because of its fluid nature. The cement slurry, in that sense, will continue flowing through the thief zone until the setting time is reached, generally 2-3 hours, leaving the near wellbore zone exposed to additional thief zones and more fluid losses. Some later techniques include the cuttings produced in casing drilling to reduce the mud losses in thief zones (Karimi et al., 2011). However, this application produces a plastering effect around the casing that encourages further analysis related to stuck pipe risks. In addition, the author mentions the application on Casing Drilling, not on Conventional Drilling which is the mainstream in the industry.

MRF Advantages:

If an MR cement slurry is used, the gelling or semisolid effect is created immediately and near the wellbore as other low-solids shear-dependent cement systems have been used in the past (Javier U. et al., 2016). A balanced plug technique for placing the MR cement slurry is required with the particularity that a longer stinger with a magnet arrangement is used to activate the fluid. After the fluid is balanced and the stinger pulled out, the magnets are left in contact with the fluid and activate it near the wellbore. It is necessary to place a fiber glass pipe to break the connection and trip out the pipe after the cement is set. A PDC bit must drill-out the cement and the tool that has the magnets.

The process is illustrated in Fig. 3. (a) the cement slurry is balanced (spotted) in front of the problematic zone (b) The fluid tends to migrate to the thief zone. Below there is an arrangement of magnets that need to be placed in contact with the MRF. Thus, the pipe is pulled out of hole to complete the activation. (c) With soft grade CIP, the magnets need to be in contact constantly with the MRF to create the semi-solid effect. Wait on cement until is set and brake the glass fiber pipe to recover the drill pipe. (d) The cement and magnets are drilled-out and drilling resumed.

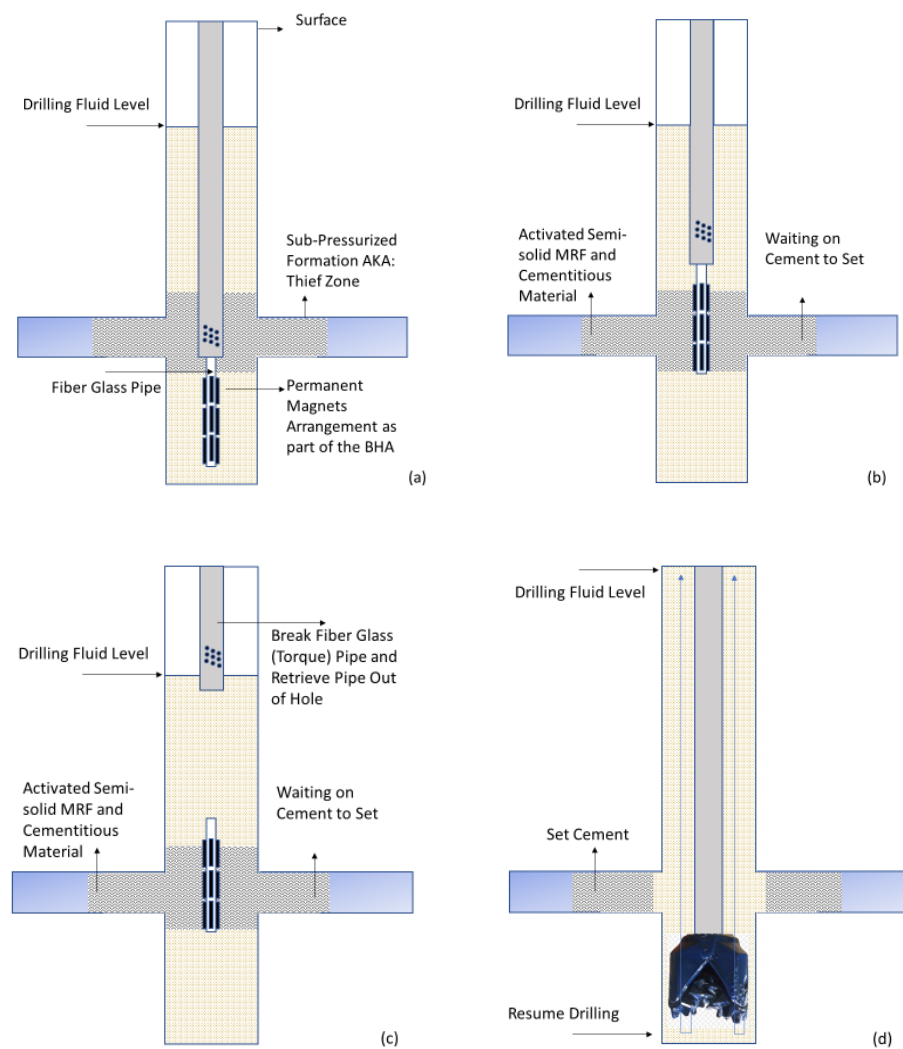


Fig. 3. Releasing stuck pipe with Coiled Tubing

### 2.8.3. Use of MRF as an open-hole packer

#### Limitation of current packers:

Current technology available for open hole packers relies on mechanic, swellable setting mechanisms and lately inflatable packers (Loginov & International, 2015). Those with mechanic activation can do so when hydraulic force is applied to the packer (Almond et al., 2002) also as a form of straddle packers by reciprocating the drillpipe can be problematic (Brown, Thomas, & Milne, 1990; Daneshy, 2011). Some packers can be activated applying weight over the packer or in combination with hydraulic force, this combination of mechanical and hydraulic force has posed challenges in completing long horizontal wells selectively where a fluid migration behind the packer has been recorded (Abbasy & Ritchie, 2010; Bårdsen et al., 2014; Malik et al., 2016). On the other hand, swellable packers are made from a reactive rubber that swells in contact with a fluid such as oil, water, brine. Although these types of packers are commonly used, they can present a sort of disadvantages that, in our perceptive, can be solved using MRF packers. Open hole completions have proved to enhance production in comparison to cemented completions (Rivenbark & Appleton, 2013). An evaluation of the most convenient type of completions is designed according the wellbore stability, type of formation, geomechanics, etc. In that sense, the application of open hole packers with the use of MRF suppose an alternative to promote the open hole completions when applicable.

#### Advantages of MRF packers:

Fig. 4 illustrate a prototype for an MR open-hole packer.

- Adaptability to well geometry: Open holes have diversified sizes and shapes. Wellbore can be cylindrical or elliptical, can be in-gauge or washed-out. The widespread practice is to run caliper logs to determine these characteristics. However, washout or elliptical holes challenge the effectiveness of the open hole packers that are designed primarily for circular in-gauge holes (Hecker et al., 2011). The MRF packers take advantage at the early fluid stage to fully adapt the open hole size and shape. The later activation of the fluid provides a more reliable sealing mechanism.

- Time response: Swellable packer activation can take hours to fully expand. When hydraulic packers in horizontal and extended reach wells require to drop a ball to provide seal and be capable to increase pressure, the time the ball needs to be displaced to the ball seat can take several minutes. The MRF packers provide an immediate (milliseconds) activation once the fluid is in contact with the magnetic field.
- Avoid premature setting: Mechanically-activated packers are susceptible to be set in tortuous wells. MR packers can be activated only when the magnets are placed in the position and the fluid is pumped.
- Damage Resistance: Running into the hole a packer with the rubber (elements) exposed to the harsh surface of the wellbore can risk the integrity of the material. The MRF packers remains fluid while running in hole, which makes it unsusceptible to shear damage when in contact with the wellbore.
- This prototype is theoretical and based on the hypothesis established in this report. The packers used in the industry must have a qualification according API 11D1/ISO14310 V0, that requires a full functioning under downhole conditions under stresses and high temperatures (Stair & Makowiecki, 2016). This study presents a very early stage of development of potential applications that the author of this report envisions possible after further research on the matter.

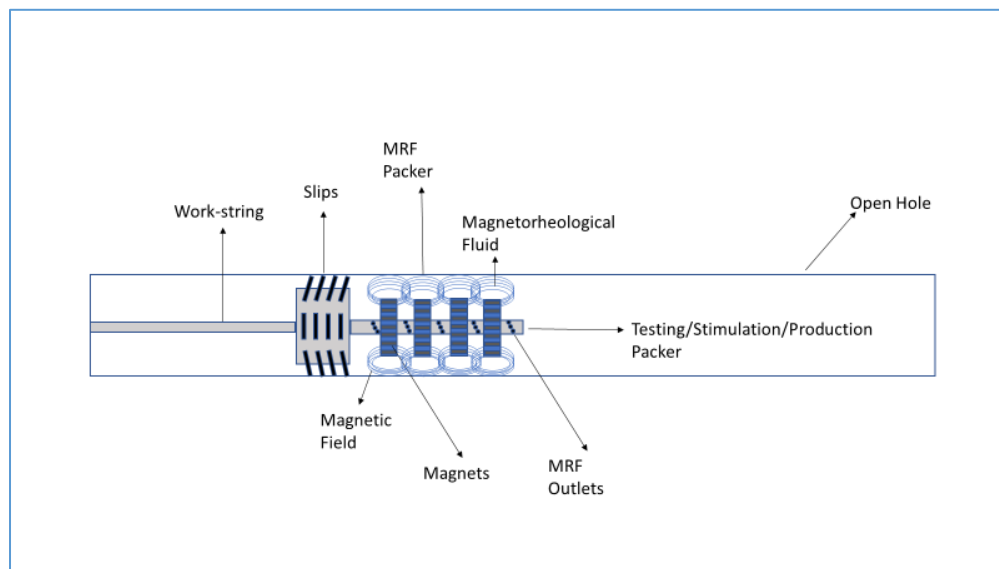


Fig. 4. Prototype open-hole packer

#### 2.8.4. Use of MRF packer for plug and abandonment (P&A)

When a well is not currently profitable, the operators can decide to abandon the well temporarily or permanently. Nowadays, the Oil industry is facing its busiest times on plug and abandonment of their wells. Under the US Law, the 30 CFR Part 250 establishes the guidelines for decommissioning activities. The state of the art relies on cement slurries placed in the well in order to:

- Provide downhole isolation of hydrocarbons and sulfur zones.
- Protect freshwater aquifers; and
- Prevent migration of formation fluids within the wellbore or to the seafloor.

**What is one of the challenges with P&A?** 30 CFR 250.1715 describes how a well must be permanently abandoned. However, technology opportunities appear in multiple annuli to properly abandon. The fact that every section may have been drilled with different mud weight makes the fluid segregation a severe problem to properly set a cement plug. The unstable flow behavior of unset cement slurry plug resting on top of lighter mud is not desired and can lead to improper isolation (Beirute, 1978). MRF is proposed as an alternative to accurately place the cement at the right depth.

**Why are MRF advantageous?** The multiple annuli are perforated to communicate among them. A cement slurry is pumped generally through one of the annuli for what is called “reverse circulation”. Once the fluid reaches the perforations it fills the different annuli that are interconnected through the perforations, as shown in Fig. 5. However, the fluid segregation due to the density difference between the mud and the cement slurry the placement accuracy can be diminished and potentially not comply with the regulation. In that sense, a mechanism could place a set of magnets to activate the MRF slurry in the annuli creating enough solidification to set at the desired depth. Extensive evaluation of cement slurries with magnetizable particles has been performed (Sriramya Duddukuri Nair & Ferron, 2014).

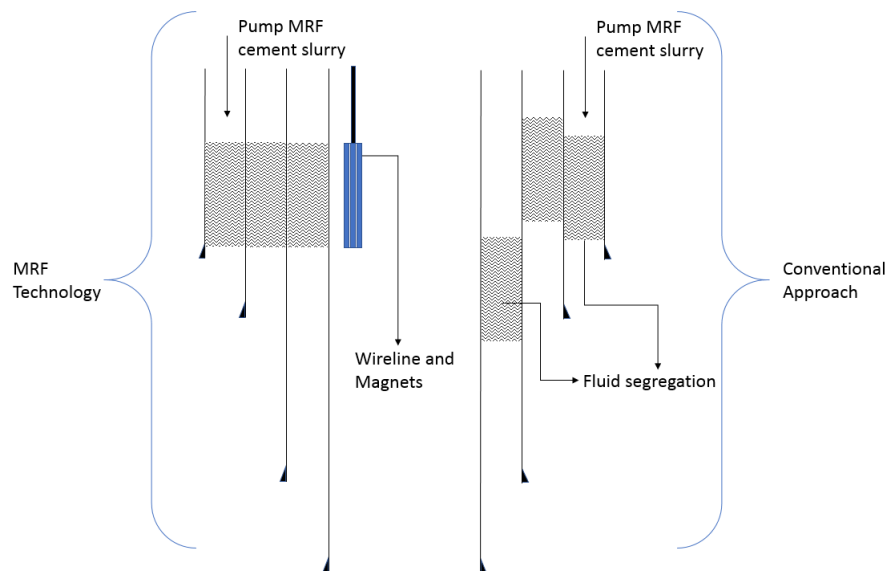


Fig. 5. Plug and Abandonment Application

## MATERIALS AND EXPERIMENTAL METHODS

### 3.1. Design of the Magnetorheological Fluid

The magnetorheological fluids are combination of a base fluid, a magnetizable particle, and in some cases stabilizers or surfactants to overcome sedimentation. The yield stress, settling rate, and viscosity of these fluids are a function of the concentration of the magnetizable particles ( $C$ ), the magnetic field strength ( $H$ ), and type of carrier fluid and surfactants. The selection of the magnetizable particles is a key aspect in developing a strong and stable magnetic effect. The selection criteria are based on the magnetic behavior, the particle size, volume fraction, morphology, and material type. The Carbonyl Iron Powder (CIP) shown in Fig. 6 is the preferred material to prepare MRF due to its highest magnitude of saturation magnetization and lowest coercivity (Hajalilou, Amri Mazlan, Lavvafi, & Shameli, 2016). The saturation magnetization is important because if an external applied field is stronger, the better the alignment of the particles. On the other hand, the coercivity is the intrinsic property of particles to be magnetized or demagnetized. Soft grade particles have low coercivity whereas on hard grade materials is high (Park et al., 2001). Therefore, for MRF preparation a soft grade is preferred to obtain better control over the rheology by tuning the external field.



Fig. 6. Carbonyl Iron Powder in dry state

Another important factor to determine and evaluate is the magnetizable particles volume fraction. Since different models have suggested the chain-like structure formation in the direction of the magnetic field and consequently the increase of the MRF yield stress (Bossis et al., 1997), the concentration of the CIP needs



to be evaluated. The theory suggests that higher volume fractions produce thicker chains and many transversal connections between the magnetizable particles (Hajalilou et al., 2016). In that sense, it is expected to see an increase in the field dependent shear stress as the concentration of CIP increases. Considering the fact that the CIP has a very high specific gravity, it is expected that very high concentration of the particles will contribute to particle settling. The type of carrier fluid also can have a direct implication of the maximum volume fraction. For example, (Liu et al., 2013) reported that when CIP is mixed in a silicone oil the critical concentration is 20% volume fraction before the particle settling becomes evident. Other authors have reported a higher critical concentration in water base carrier fluids (Rich et al., 2012). Different types of base fluids have been tested in the past such as petroleum-based oils, paraffin oils, water, polyether, glycols and silicon oil (Hajalilou et al., 2016). Perhaps the most important aspect to consider in selecting the type of carrier is the temperature stability, non-reactive or non-corrosive reactions with the magnetizable particles, availability, price or environmental considerations. For this research, only two carrier fluids are tested, silicon oil and water.

Finally, additives known as stabilizers are used primarily to reduce the magnetizable particles settling, to produce a stable suspension, improve lubrication and change the initial rheology of the MRF (Ashtiani et al., 2015). These additives include thixotropic agents, viscosity and anti-friction compounds. Some of the most common agents used include guar gum, silica, bentonite and organoclays. A summary of the different samples tested can be found in the following table.

Table 1. Design of the different MRF tested at different concentration of CIP by wt%

Sample Name	Carrier Fluid	Stabilizer	Other Additives	Concentration of CIP %wt tested							
				0%	1%	2%	5%	10%	12%	N/A	N/A
S0	Water	Bentonite	None	0%	1%	2%	5%	10%	12%	N/A	N/A
S1	Silicone Oil	Stearic Acid 3%	None	0%	1%	2%	5%	10%	15%	20%	N/A
S2	Water	Laponite RD 3%	Caustic Soda and Sodium Bicarbonate	0%	N/A	N/A	5%	10%	N/A	N/A	N/A
S3	Water	Laponite RD 1%	Caustic Soda and Sodium Bicarbonate	0%	N/A	N/A	5%	10%	N/A	N/A	N/A
S4	Water	Laponite RD 2%	Caustic Soda and Sodium Bicarbonate	0%	N/A	N/A	5%	10%	15%	N/A	N/A
S5	Water	Laponite RD 1.5%	Caustic Soda and Sodium Bicarbonate	0%	N/A	N/A	5%	10%	15%	20%	25%
S6	Silicone Oil	Stearic Acid 1%	None	N/A	N/A	N/A	N/A	N/A	N/A	20%	N/A
S7a	Water	Bentonite 10%	None	0%	N/A	N/A	5%	N/A	N/A	20%	N/A
S7b	Water	Bentonite 10%	CMC 2.6 [g]	0%	N/A	N/A	N/A	N/A	N/A	N/A	N/A
S8a	Water	Bentonite 10 g	CMC 3.5 [g]	0%	N/A	N/A	N/A	10%	15%	20%	N/A
S8b	Water	Bentonite 20 g	CMC 3.5 [g]	0%	N/A	N/A	N/A	N/A	N/A	N/A	N/A
S9	Water	Kelzan XC 1 g/cm3	None	0%	N/A	N/A	N/A	N/A	N/A	N/A	N/A
S9a	Water	Kelzan XC 2 g/cm3	None	0%	N/A	N/A	N/A	N/A	15%	N/A	N/A

The design of the MRF mixture consists of testing different MRF properties:

#### 3.1.1. Mixability

This process consists on mixing all the constituents of the MRF together in a Hamilton Beach Scovill Mixer Model 936 in a metallic universal cup (#110E). An efficient and simple Magnetorheological Fluid (MR) is obtained from a homogeneous dispersion of the magnetizable particles with the carrier fluid. The best results are obtained when the stabilizer is added to the carrier fluid and mixed at 17,000 rpm for ten minutes. The mixture should produce a fluid with flat and low thixotropy and a clear vortex while mixing. Then, the magnetizable particles are added and mixed at 10,000 rpm for ten more minutes. A visual observation that the particles do not aggregate is a good indicative that the MRF is mixable and potentially pumpable at the field.

#### 3.1.2. Rheology Measurement (ON/OFF State)

A MRF capable to find applications in drilling and completion operations must show a high yield stress in the presence of a magnetic field and low apparent viscosity in the absence of a magnetic field (Ashtiani et al., 2015). Different types of apparatuses are found in the literature to measure the rheology of a MRF (Laun et al., 1996) such as concentric-cylinder rotation viscometer, plate-plate rotational rheometers and capillary viscometers (Sairam, Pangu, & Gajji, 2015). For this research, a Couette type double concentric cylinder viscometer is used (M3600 Viscometer- Grace Instruments) in combination with two fixed electromagnets to impose a magnetic field perpendicular to the plane of shear. A rotating cylinder that creates a defined shear rate and the shear stress is measured indirectly by the torque generated on the bob. The two electromagnetic poles are separated 3" distance. Each pole can produce at its surface 3000 Gauss. For a complete magnetic field strength information refer to Appendix A. The rheological properties response can be measured at several magnetic fields. Photos of the experimental device are shown in Fig. 7 and 8.

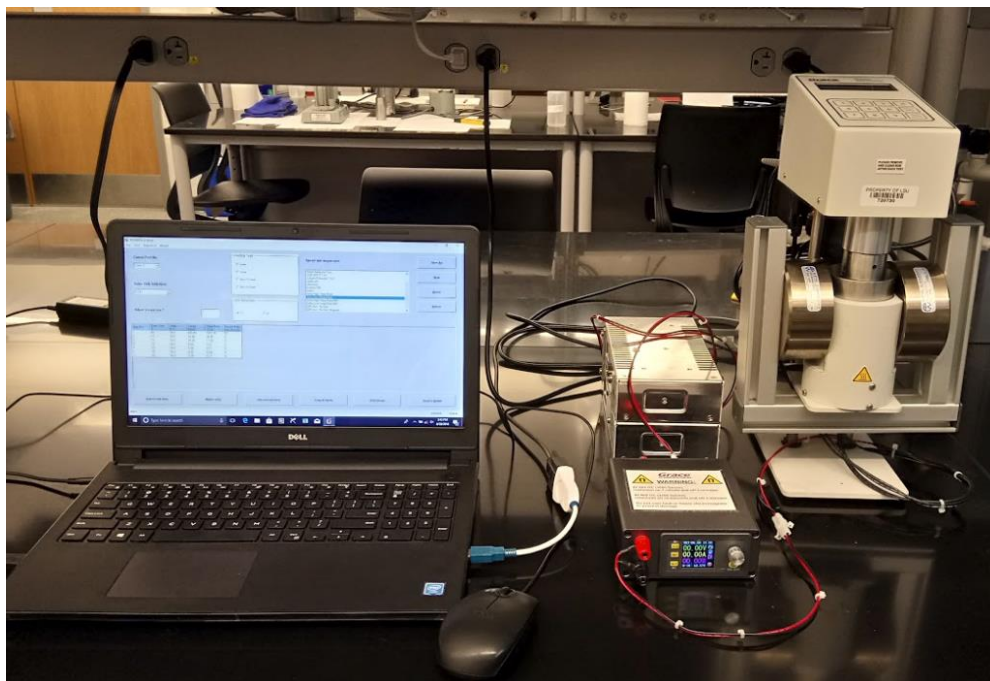


Fig. 7. M3600 Viscometer, voltage graduator and electromagnets

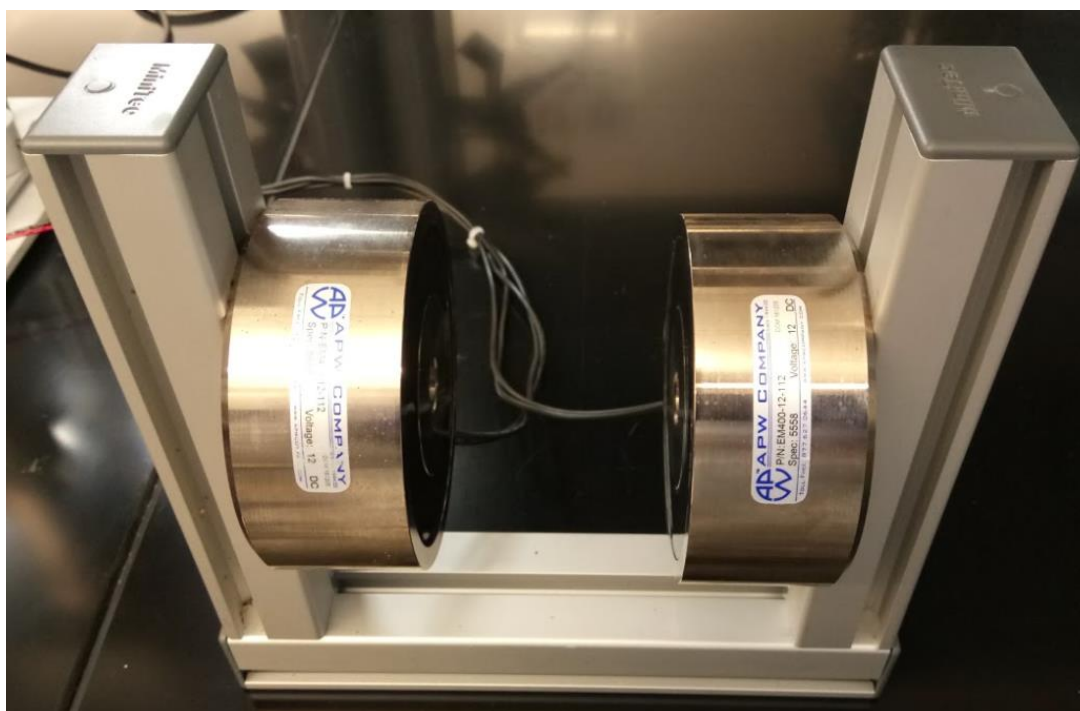


Fig. 8. Flat-faced round holding solenoid electromagnet

### 3.1.3. Settling Ratio

Because the magnetizable particles have a specific gravity of 7.86 g/mL, which is at least five times larger than the liquid phase, without the proper stabilizing agents, a separation of the solid and liquid phase will

occur. Such separation can have a detrimental effect on the ability of the MRF to exhibit repeatable performance (Hills & Yurgelevic, 2003). Therefore, the use of polymeric thickeners or finely divided solids such colloidal clays can reduce the settling ratio of the particles. In that sense, the mixture suspends the magnetizable particles due to the thixotropic properties of the polymers or clays. The type and amount of stabilizer needs to be properly determined because an unnecessarily high concentration will produce an unacceptable high viscosity and shear stress of the MRF. Similarly, a too low concentration will not suspend the magnetizable particles. The process of measuring the settling ratio consists of collecting a fixed amount of volume of MRF and visually inspecting the segregation on a translucent container at room conditions. More specific sedimentation behavior can be studied using Turbiscan MA200 (Joseph et al., 2011). This equipment is not available for this research.

### **3.2. Experimental Setup**

The experimental setup used to evaluate the MRF behavior in a flow loop is depicted as follows. The objective of the setup is to flow the MRF through two concentric pipes that simulate a workstring and an annulus of a well and determine how the pressure drop in the annulus is affected as a function of the magnetic field generated. The arrangement of the Neodymium magnets creates a magnitude and orientation of the magnetic field and consequently, an alteration of the rheology of the MRF.

The inner pipe (workstring) has an outside diameter (OD) of 1.66-in and inside diameter (ID) of 1.5-in. This pipe is made of carbon steel and the magnets are placed intentionally in the outer wall to evaluate if the magnetic field generates a rheology change only in the annulus while allowing the MRF to flow unaffected inside the workstring. The outer pipe representing the openhole is a stainless-steel pipe schedule 304 with an OD of 4.5-in and ID of 4.0-in. Four thredolets are welded on the outer pipe to install modular pressure transducers Honeywell FP2000 to read the pressure along the annulus. One additional pressure transducer is installed downstream of the pump to read the drillpipe pressure. The permanent magnets are arranged equidistant in between transducers P3 and P4 as shown in Fig. 9 and Fig. 10.

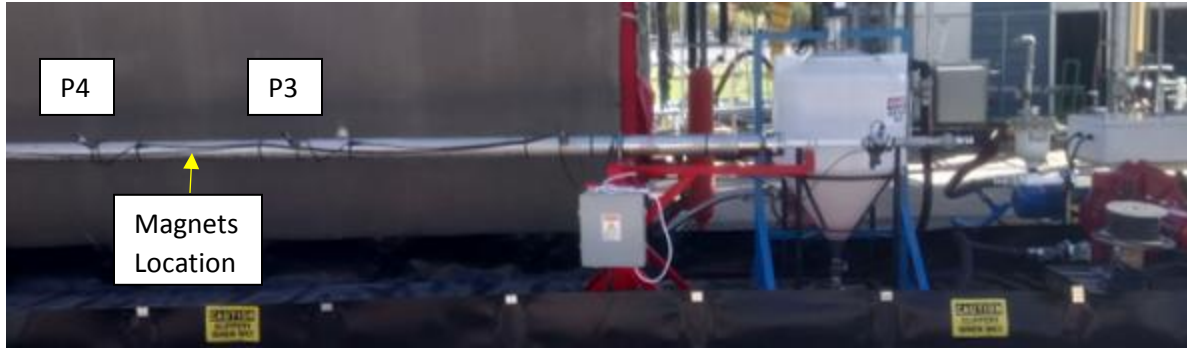


Fig. 9. Experimental Setup

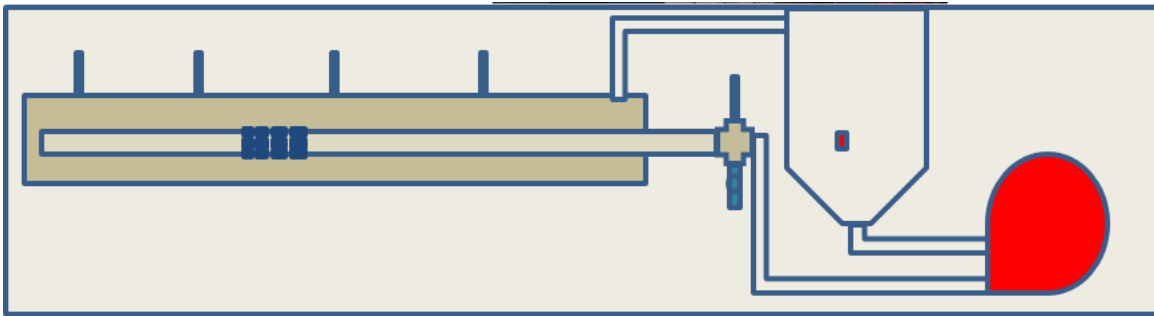


Fig. 10. Experimental Setup Schematic

### 3.2.1. Circulating System

The circulating system consists of a pipe/annulus arrangement, a mud tank, a pump and hoses to connect these various subcomponents. The pipe/annulus arrangement is horizontal.

The pump selected to run the experiments is peristaltic Watson Marlow Bredel 40. In this type of pump, the fluid is pushed from the inlet to the outlet through a hose squeezed by some rollers. This positive displacement pump prevents the MRF to be in contact with moving parts to avoid any contamination. Also, this pump allows a constant flow rate whilst the back pressure is altered. The later feature is important for establishing the relationship between the rheology and pressure drop developed by the MRF when flowing next to the magnets. The MRF is mixed in an 85 gal mud tank with 45 grades pitched blade turbine impellers connected to mixer motor. The electric motor for the mixer is located far enough from the MRF to avoid any premature activation. The experimental setup fluid sequence is shown as follows in Fig. 11. The MRF is pumped by the peristaltic pump (1) and a pulsation dampener Blacoh C905ND (2) is used to reduce the pressure pulsation. The MRF enters the drillpipe (3) and is pumped through the annulus where the pressure

transducers (4) read the pressure drop. The MRF fluid reaches the outlet (flowline) and dumped to the mud tank (5) to be circulated again to the system (6).

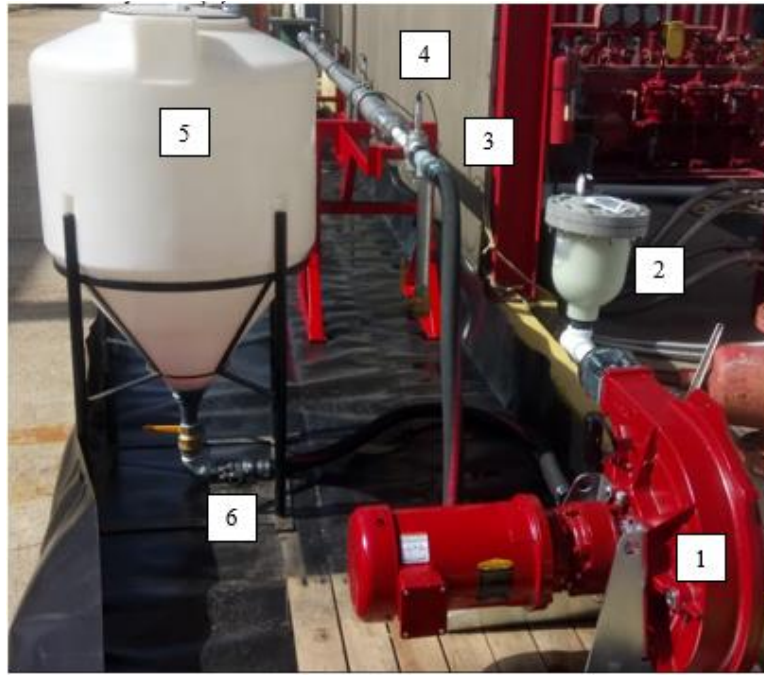


Fig. 11. Circulating System

The mud tank has a return pipe that connects to the return hose. This return pipe allows for the fluid to be returned closer to the bottom of the tank to reduce any potential cavitation due to suction from the pump. The outlet from the conical bottom goes to the inlet for the pump. This outlet has a ball-valve to allow for service of the hose and/or pump if necessary. The hose that connects the mud tank to the pump inlet is connected through cam-and-groove type connections for easy removal and servicing.

### 3.2.2. Power System

This system provides the energy to the main components of the experimental setup. These components are the pump motor (Baldor VEM3611T) and Mud Tank Agitator (Grovhac 500 series), both part of the circulation system. Additionally, the power system supplies the energy to the data acquisition system. For this experimental setup two sources of power are used, a 480 Volts alternating current (AC) and 120 Volts AC.

480 Volts:

- Pump Motor, connection shown in Fig. 12.

120 Volts:

- Mud Tank Agitator (Grovhac 500 series)
- Data Acquisition System: Laptop, pressure transducers (Honeywell FP2000), DAQ Board (NI cDAQ 9174) and Module (NI 9203).

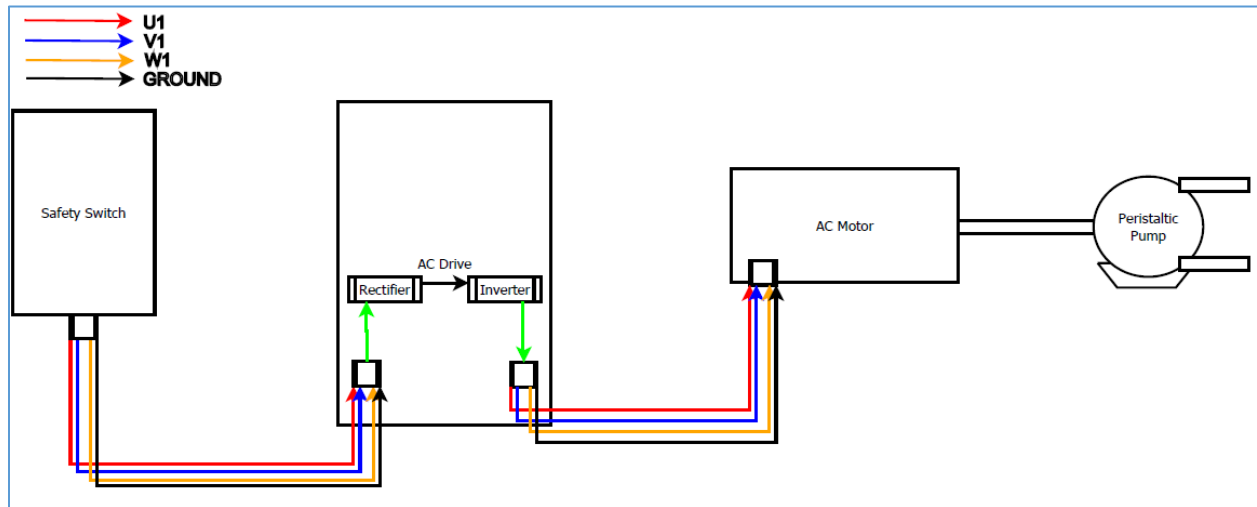


Fig. 12. High Voltage Connection

High Voltage Diagram of Connections

The Fig. 13 describes the main components of the high voltage connection:



Fig. 13. Simplified High Voltage Power System



1. Safety Switch: Is used as a disconnecting means for a service entrance and as a fault protection for the pump motor. The Westinghouse Heavy Duty Safety Switch RHFN361 is a 3 Poles 480/600 VAC, 30 Amps, fused and with NEMA 3R enclosure.
2. Watertight IEC 309 Pin and Sleeve Receptacle: The Hubbell 430R7W receptacle is the point of connection for the power cable. Made from toughened Nylon is a 3 Pole/ 4 wired rated for 3 HP, 480V AC and 30 Amps.
3. Watertight IEC 309 Pin and Sleeve Plug: The Hubbell 430P7W plug is mounted (terminated) on a power cord and interface with the receptacle.
4. Power Cord: The Ultrex VN Unshielded tray cable 10 AWG THHN/THWN-2 with four copper conductors rated for 600V and 32/40 Amps ROHS compliant.
5. AC Drive: The ABB ACS355 is a wall mountable drive for controlling asynchronous AC induction motors and permanent magnet synchronous motors. According to the AC Drive user's manual, a rectifier converts three-phase AC voltage to DC voltage. The capacitor bank of the intermediate circuit stabilizes the DC voltage. The inverter converts the DC voltage back to AC voltage for the AC motor. The brake chopper connects the external brake resistor to the intermediate DC circuit when the voltage in the circuit exceeds its maximum limit (27).
6. AC Motor: The Baldor motor VEM3611T provides the mechanical energy to rotate the positive displacement pump (Bredel 40). This motor is a standard general purpose type motor with a synchronous speed of 1800 rpm @60Hz, 460 V, three phase, 3 HP with totally enclosed, fan cooled (TEFC) enclosure. The hose pump has a planetary gearbox that enables a wide range of reductions, torques and connections from the electric motor to the pump, refer to Appendix D to specifications of the AC Motor.

### 3.2.3. Data Acquisition System

#### Hardware

The data acquisition system contains five pressure transducers, hardware and software to read and chart the pressures in the flow-loop. The sequence of data transmission and components are shown in Fig. 14 and depicted as follows:

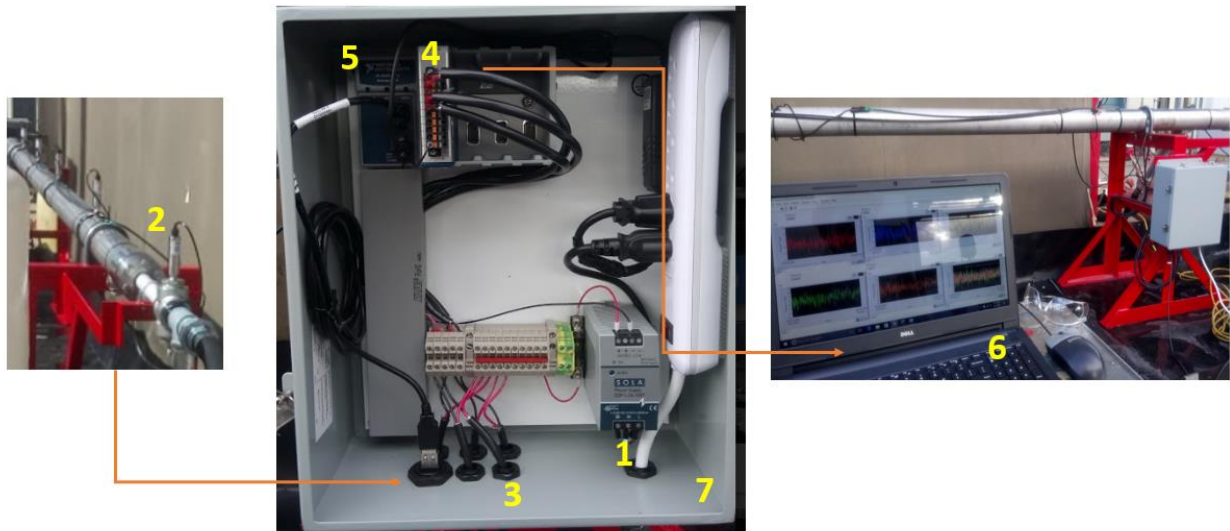


Fig. 14. Data transmission Components

1. SolaHD Power Supply: Provides the power required by the pressure transducers to operate.
2. Pressure Transducer Honeywell FP2000: A modular pressure transducer with 0.25% accuracy, 750 psi maximum pressure. It has a current amplifier (4 to 20 mA 2 wire) and a frequency response of 300 Hz.  $\frac{1}{4}$  -18 NPT male pressure port and polyurethane cable. These pressure transducers were used for the pressure drop measurements with sample S0, however the low accuracy high fluctuation of the values represented a challenge to record and interpret them. Therefore, OMEGA PX309-100AI pressure transducers were later obtained with 100 psi maximum pressure, and 0.25% BSL FS static accuracy
3. Data Cable: Shielded cable AWG 15.
4. NI 9203 Module: It is an 8-Channel,  $\pm$  20 mA analog input module. Receives the input signals from the pressure transducers.

5. NI cDAQ 9174 Chassis: This chassis provides the data transfer between the I/O Modules and the external host (Laptop).
6. LabView: Software used for capturing the pressure measurements in the system.
7. Junction Box Hoffman A1412NF: It is a 14-gauge steel NEMA type 4 junction box to protect the data acquisition hardware from rain and dust. The hardware diagram is explained in Fig. 15.

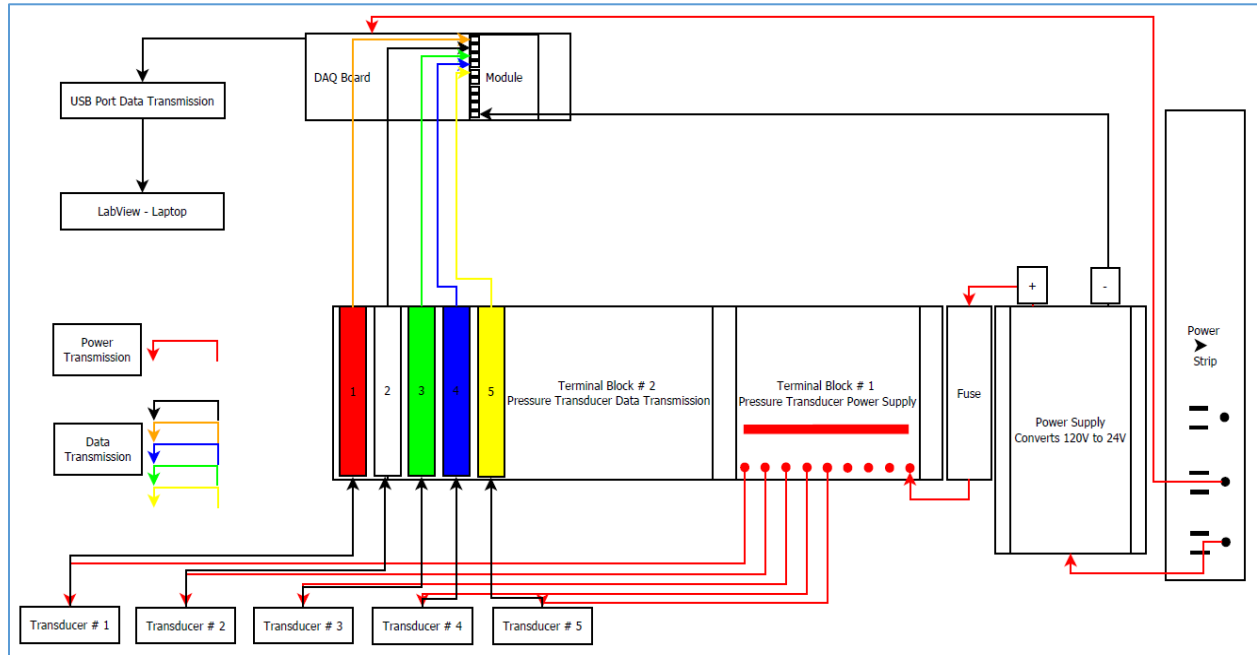


Fig. 15. Junction Box Data Acquisition Schematics.

## Software

The software used to transform the data from the pressure transducer to a computer interface is LabView by National Instruments. The DAQ board is connected directly to the computer through a USB cable and the software transforms the mA produced by the pressure transducers into pressure data. The calibration was performed using Instruments and Standards that are traceable to the United States National Institute of Standards and Technology. The AUTO Mensor 1200 (range 0-100 psia) is a pneumatic and integrated electrical pressure generator used to calibrate the pressure transducers. A data acquisition control unit HP 34970A DMM is used to record the current signal [mA] to the corresponding pressure [psi]. A hydraulic deadweight test was used to confirm the calibration values. Fig. 16 represents the schematic of the virtual

interface to collect the pressure independently from each transducer. The data collected is both raw and filtered. A manual input of the VFD frequency is available to correlate the flow rate and the pressure.

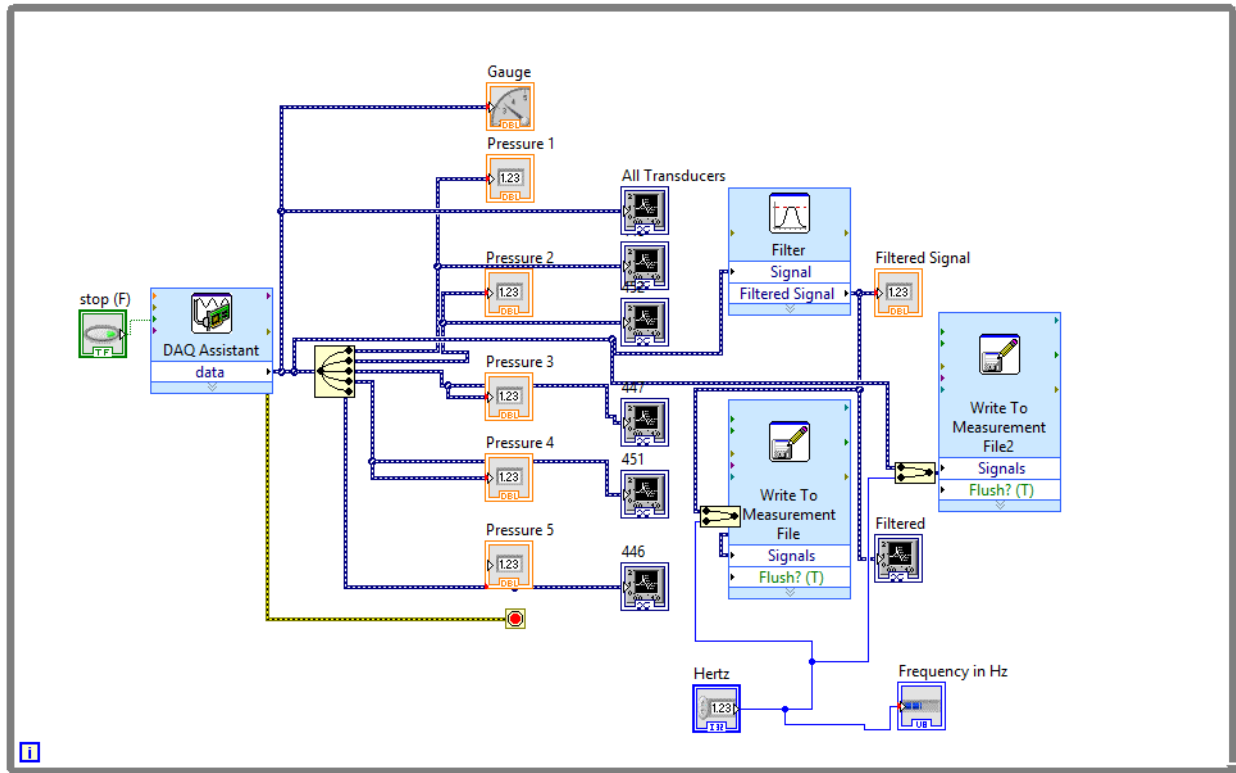


Fig. 16. Virtual Interface from LabView to data recording

### 3.2.4. Permanent Magnets

Permanent magnets are used to generate the magnetic field to activate the MRF. Two different sets of magnets were used as described as follows in Table 2:

Table 2. Permanent Magnet Characteristics

	Set 1	Set 2
<b>Material</b>	Neodymium (NdFEB)	Neodymium (NdFEB)
<b>Grade</b>	N45H	N45H
<b>Max Temp [F]</b>	248	248
<b>Coating</b>	Nickel (Ni)	Nickel (Ni)
<b>Magnetization</b>	Inside Curve to Outside Curve	Inside Curve to Outside Curve
<b>Dimensions</b>		
<b>[mm]</b>	54X46X20	43X39X5

Four different rings of magnets are aligned in the inner pipe (magnet arrangement) and secured with epoxy resin as shown in Fig. 17.

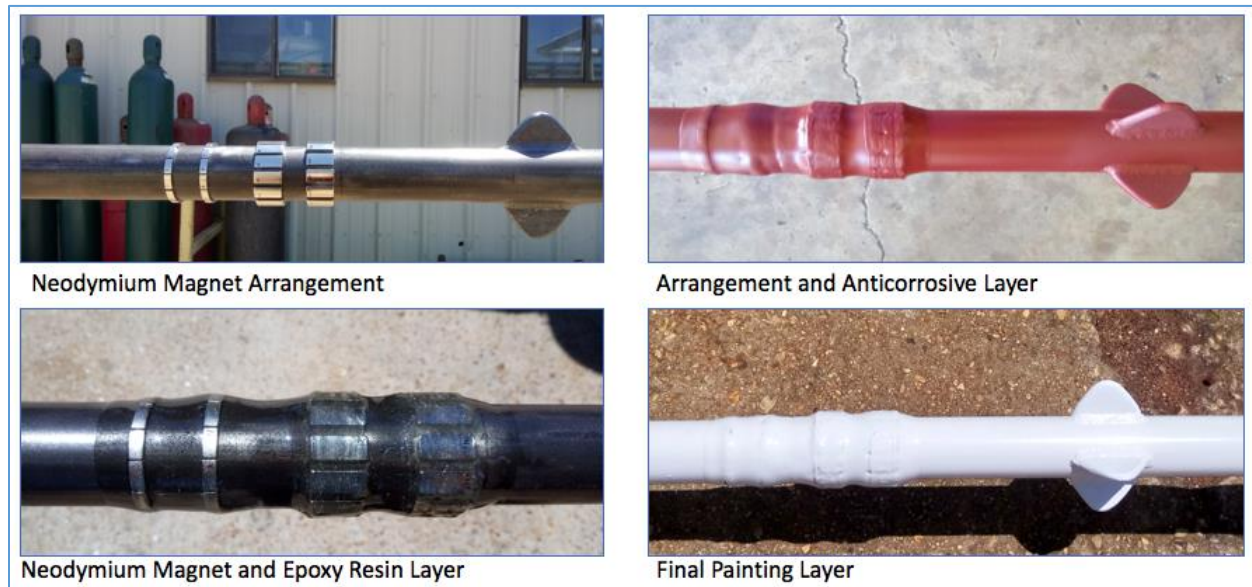


Fig. 17. Neodymium permanent magnets arrangement

### 3.2.5. Magnetic Probe

The Extech MF100 AC/DC magnetic field meter Fig. 18 is used to measure the magnetic strength at different distances from the permanent magnets and the also at the measurement zone in the M3600 viscometer.



Fig. 18. Extech MF 100 Magnetic Probe

### 3.2.6. Safety Considerations

#### Pressure Relief Valve (PRV):

To protect the personnel and the equipment, a PRV was designed to discharge the contained fluid under pressures higher than 100 psi in a controlled manner. For spring operated valves, the sizing is a function of the volumetric discharge flow rate, the set pressure and the overpressure. The minimum area of the discharge orifice is determined by the Eq. 2 (*Back to Basics*, 2013):

$$A = \frac{Q}{38 K_d K_w K_v} \sqrt{\frac{G}{P_1 - P_2}} \quad (\text{Eq. 2})$$

Where A is the discharge orifice area [in<sup>2</sup>], Q is the volumetric flow of liquid [gpm],  $K_d$  is the effective discharge coefficient [unitless] that can be obtained from ASME and Pressure Vessel Inspectors for code-certified devices.  $K_w$  is the adjustment factor for backpressure [unitless] that can be obtained from Fig. E1 in Appendix E.  $K_v$  is the adjustment factor for viscosity [unitless] that can be obtained from Fig. E2 in Appendix E. G is the specific gravity of the flowing fluid referenced to water [unitless].  $P_1$  is the allowable overpressure [psi] and  $P_2$  is the backpressure [psi].

Given the conditions expected on the flow-loop and using Eq. 2, the minimum orifice area is 0.229-in<sup>2</sup> equivalent to a minimum discharge orifice diameter of 0.54-in. Therefore, a galvanized PRV discharge orifice of diameter 1-in was installed to the system after the pulsation dampener.

#### Spill Containment:

At PERTT facility, any spill must be contained to avoid the CIP particles reaching nearby natural drainage or entering the facility's skimmers. Therefore, the spill containment is a geomembrane created from low density polyethylene (LPDE). It has a thickness of 40mil and is 30' by 5' by 1'. This is U.V and chemical resistant and can contain a spill volume of 26.7 bbl (1122 gal) equivalent to 7 times the maximum volume of magnetorheological fluid to be prepared and circulated as in Fig. 19. This in compliance with regulation from EPA for spill containment (40CFR 264.193).



Fig. 19. Geomembrane for spill containment

## RESULTS AND DISCUSSION

### 4.1. MRF mixing, rheology and settling ratio

Different additives and different carrier fluids produce a rheological behavior. The objective of this study is to determine a proper combination of carrier fluid, stabilizer and concentration of CIP that produce a competitive MRF. In that sense, an MRF that is easily mixable, that produces a high yield stress, good repeatability of the results, and low or negligible magnetizable particle sedimentation. The following table summarizes the different samples tested at the laboratory.

Table 3. Summary of samples tested

S M	Carrier Fluid	Stabilizer	Other Additives	Concentration of CIP %wt tested						Primary Reason for Rejection
S0	Water	Bentonite	None	1%	2%	5%	10%	12%		None
S1	Silicone Oil	Stearic Acid 3%	None	1%	2%	5%	10%	15%	20%	High Settling Ratio
S2	Water	Laponite RD 3%	Caustic Soda and Sodium Bicarbonate			5%	10%			Extreme Gelation
S3	Water	Laponite RD 1%	Caustic Soda and Sodium Bicarbonate			5%	10%			High Settling Ratio
S4	Water	Laponite RD 2%	Caustic Soda and Sodium Bicarbonate			5%	10%	15%		High Gelation
S5	Water	Laponite RD 1.5%	Caustic Soda and Sodium Bicarbonate			5%	10%	15%	20%	None
S6	Silicone Oil	Stearic Acid 1%	None						20%	Extreme Gelation and extremely high rheologies without magnetic field

Table 3 continued next page



S M	Carrier Fluid	Stabilizer	Other Additives	Concentration of CIP %wt tested						Primary Reason for Rejection
S7 a	Water	Bentonite 10%	None			5%			20%	Do not produces Vortex. Probably unpumpable
S7 b	Water	Bentonite 10%	CMC 2.6 [g]						0%	Do not produces Vortex. Probably non- pumpable
S8 a	Water	Bentonite 10 g	CMC 3.5 [g]				10%	15%	20%	Produces corrosion of CIP
S8 b	Water	Bentonite 20 g	CMC 3.5 [g]							Do not produces Vortex. Probably non- pumpable
S9	Water	Kelzan XC 1 g/cm <sup>3</sup>	None							Produces a low quantity of foam
S9 a	Water	Kelzan XC 2 g/cm <sup>3</sup>	None					15%		Produces a high quantity of foam

The mixing, rheological properties and settling ratios of samples S1,S2, S3, S4, S6, S7, S8 and S8 are included on the Appendix F. On the other hand, the experimental results of samples S0 and S5, those that exhibited the best features among the samples tested, are shown as follows:

#### 4.2. Sample S0

The MRF is prepared with Carbonyl Iron Powder – Soft Grade. These particles have a purity of 99.5% (metal basis) and a specific gravity of 7.86 g/mL at 77°F, find specifications at appendix B. The CIP is also the weighing material for the sample fluid. Additionally, bentonite with a specific gravity of 2.5 g/mL is added as the viscosity agent commonly used for drilling fluid preparations. The carrier fluid is fresh water. General information of the sample fluid is presented in Table 4:

Table 4. Fluid Characteristics

Property	Value
Bentonite [wt%]	5.89
CIP [wt%]	0.44-10.5
Density Range [ppg]	9.0-9.3

The sample was tested at different concentrations of CIP measuring the rheology at different magnetic fields. The rheology behavior is presented in Fig. 20:

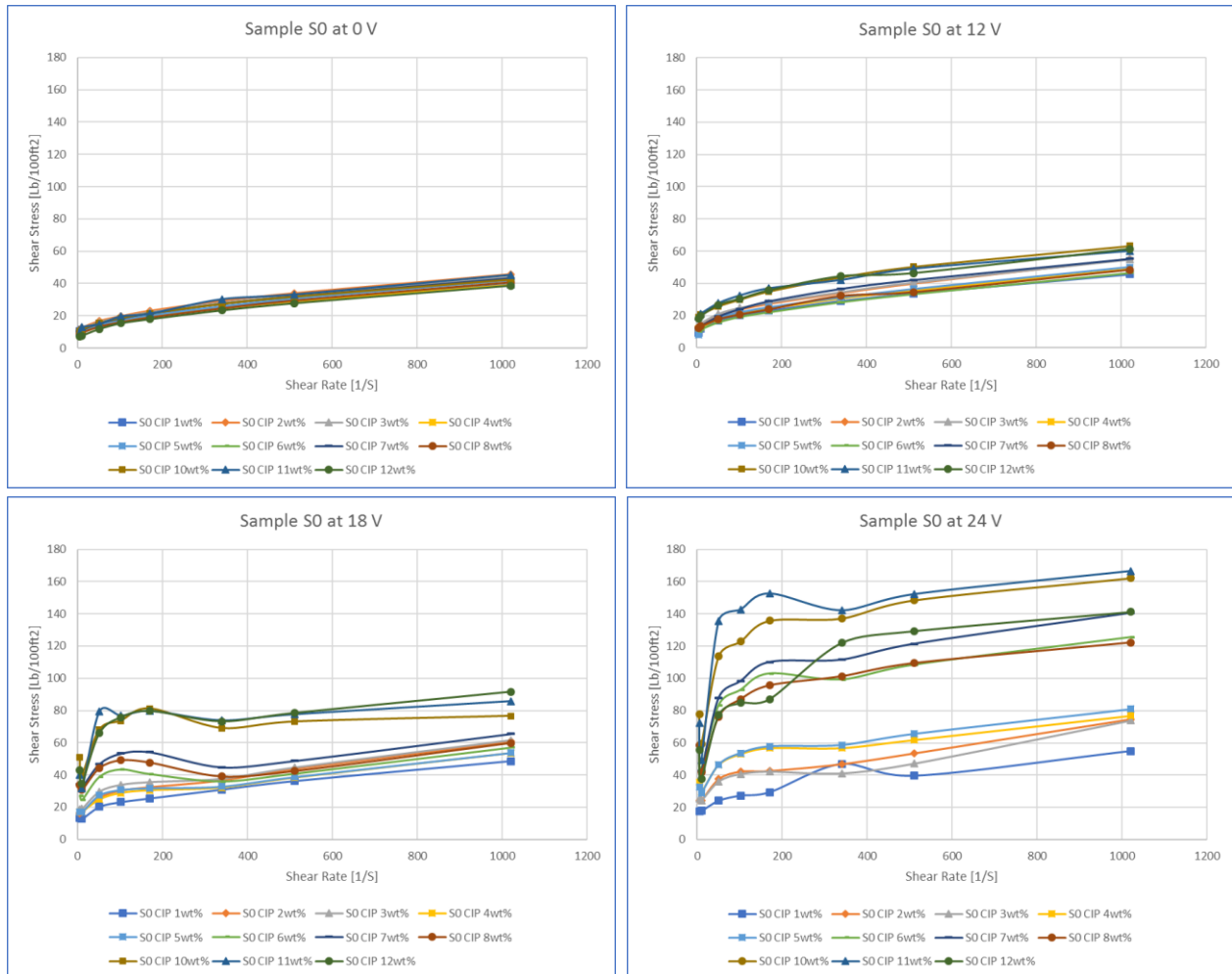


Fig. 20. Rheology behavior of Sample S0 at different magnetic fields.

Without the presence of a magnetic field at 0 Volts, all the samples exhibit a similar shear stress when increasing the concentration of the CIP. On the opposite case, at 24 Volts, the shear stress behavior spreads out as the concentration of the CIP is varied. This is an indication that the shear stress change at different shear rates is a function of the concentration of the CIP. Additionally, the rheogram at 24 V indicates that

in general the shear stress increases as the concentration of the CIP increases. Perhaps, this is not the case for the concentration of CIP 12% wt at 24 Volts that exhibited a lower shear stress in comparison to samples with lower concentration of CIP. Additionally, an evident particle sedimentation was observed at the bottom of the measuring cup for this specific CIP concentration. In that sense, it can be inferred that the decrease in the shear stress response is a consequence of the sedimentation. It is reasonable to think that either, the stabilizer concentration or type is not enough for the concentration of CIP or that after the cycles of magnetization and demagnetization of the particles, they form aggregates that are more prone to settling. The particle settling was studied at different periods of time showing negligible sedimentations. The fluid is circulated in the experimental setup at the minimum concentration of CIP (0.44 wt%), the pressure drop is measured and recorded. The CIP concentration is increased sequentially until reaching the maximum concentration (10.5 % wt)

#### **4.3. Sample S5**

The sample S5 is a mixture of Laponite RD in water. The Laponite RD is a highly shear thinning silicate used to stabilize emulsions. The Laponite RD is insoluble in water but hydrates and swells in water to form a colorless dispersion. According to the manufacture (BYK, USA) at concentrations higher than 2% in water, highly thixotropic gels can be produced. The appearance of the Laponite RD in dry state is of a free-flowing white powder. To avoid the degradation of the Laponite RD pallets, the pH was increased to 10 by adding 1.8 mM NaOH and 4.1 mM NaHCO<sub>3</sub>. Once the Laponite RD is added to the system the polymer reacts, and a more viscous fluid forms, having the consistency of a thin cross-linked gel. Also, in static conditions the fluid gelled rapidly. The gels were broken easily by applying shear to the system. The experimentation confirmed that concentration of Laponite RD higher than 2% form strong gels that make the rheology measurement difficult. On the other hand, concentration of Laponite RD lower than 1.5% produce a very thin fluid that does not hold the CIP particles in suspension. Therefore, different concentration of Laponite RD were tested to optimize the design i.e. good mixability and suspension and an almost flat gel development. Consequently, a Laponite RD concentration of 1.5wt% (Sample 5) yielded

the best results in terms of rheology behavior and low settling ratio. Furthermore, the rheology measurements showed good repeatability i.e. same or similar results after a repetition of successive experiments. Also, the shear stress increases in a coherent pattern as the CIP concentration and the magnetic field increased as shown in Fig. 21. Another interesting trend is observed at shear rates larger than  $400 \text{ s}^{-1}$  where the shear stress decreased as the shear rate increase. The theory associates this type of behavior to thixotropic fluids or fluids that form strong gels at low shear rates. In this sense, it is logical to accept an MRF with gelling properties that withhold the high density magnetizable particles static or at low shear rates and that behaves more as a conventional pseudoplastic fluid at higher shear rates.

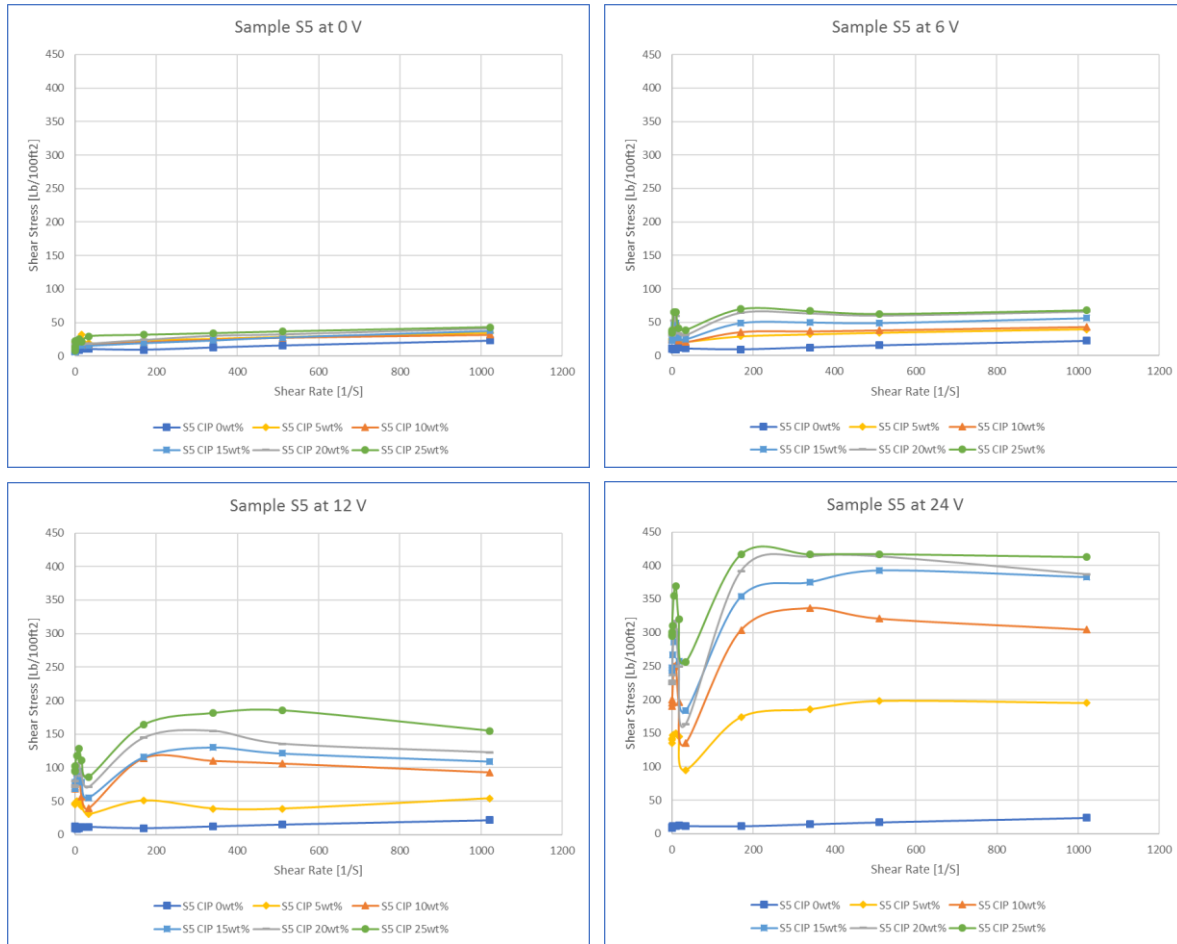


Fig. 21. Rheology Measurements of Sample S5

The gelling effect is still evident at very low shear rates but reduced in comparison to sample 4, see Appendix F. Similarly, comparing with sample 4 at the same CIP concentration, sample 5 shows more stable values close to 400 Lb/100 ft<sup>2</sup>.

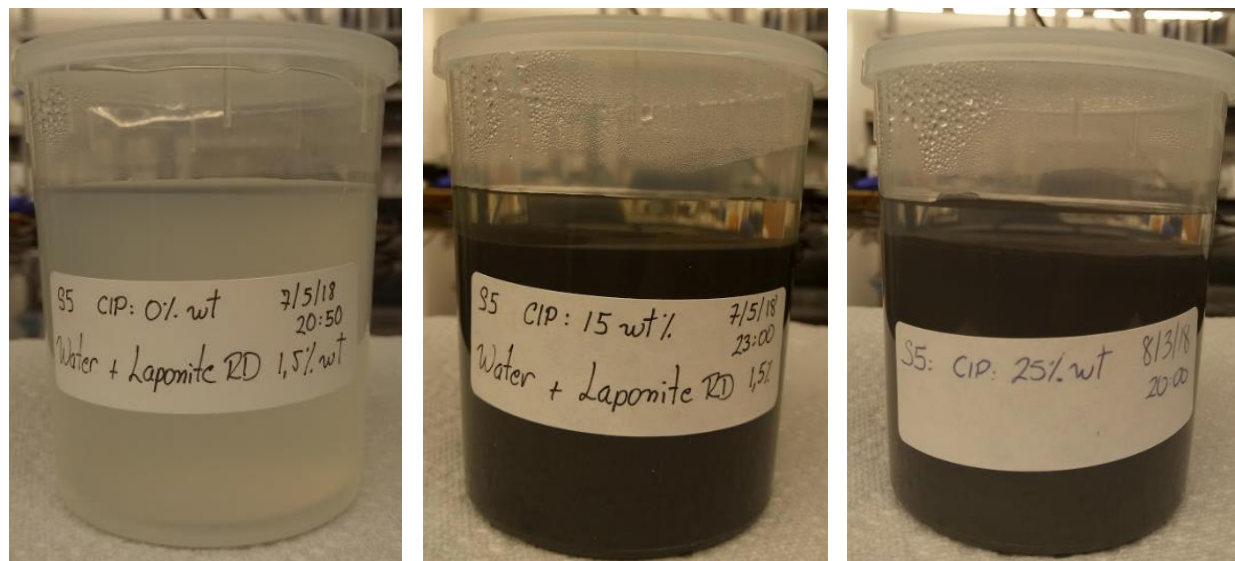


Fig. 22. Settling Ratio of Sample S5 after 77 days of mixed

Sample 5 showed the best behavior among the candidate as MRF based on the criteria of MRF stability, mixability, results repeatability, good shear stress development and low particle sedimentation.

Further supporting this claim, comparison charts for the different samples S0, S1, S5 and S8a with a CIP concentration of 10wt% at 0 and 24 Volts is presented in Fig. 23. Only these samples are presented to avoid a busy chart and because these represent the main variation in terms of carrier fluid and stabilizer. The dashed line represents the sample at 0V and the continuous line at 24V, this to establish a point of comparison of ON/OFF states i.e. with or without magnetic field, respectively. The sample S5 showed a significant increase of the shear stress of an order of 20 times under the influence of the magnetic field. Also, its shear stress under the influence of the magnetic field is one of the highest among the samples tested. Consequently, it is thought that higher flow-restriction can be achieved.

The sample S0 has a good development of shear stress under the influence of the magnetic field but is almost half of the one developed by Sample S5. The sample S1 showed the highest values of shear stress but the high viscosity and shear stress in absence of magnetic field is a setback for that sample.

The sample S8a exhibits a good development of shear stress but as shown in Appendix F, this mixture produces an aggravated corrosion issue of the CIP particles with time. This phenomenon was broadly observed during the experimental phase included sample S0, future studies are required to determine the main causes. One hypothesis is that the montmorillonite, the main component of the Bentonite, a mineral from the group of phyllosilicates that is structurally formed by aluminum and magnesium arranged octahedrally in form of oxides and hydroxides, is provoking the accelerated oxidation of the ferrous components of the CIP. Therefore, the ferric oxide  $\text{Fe}_2\text{O}_3$  responsible for the brown color in the sample is forming from either the dissolved  $\text{O}_2$  in the water or from the oxygen free radicals from the Silicon Dioxide  $\text{SiO}_2$  that constitutes about 61.4% of the Montmorillonite. The other samples that did not contain bentonite as the stabilizer and water as carrier fluid did not exhibit any corrosion even after two months of preparation whereas the samples containing bentonite all corroded. This suggests that the  $\text{O}_2$  dissolved in water is not the main constituent of this phenomenon. Refer to Fig. F14 on Appendix F to see the oxidation of the sample.

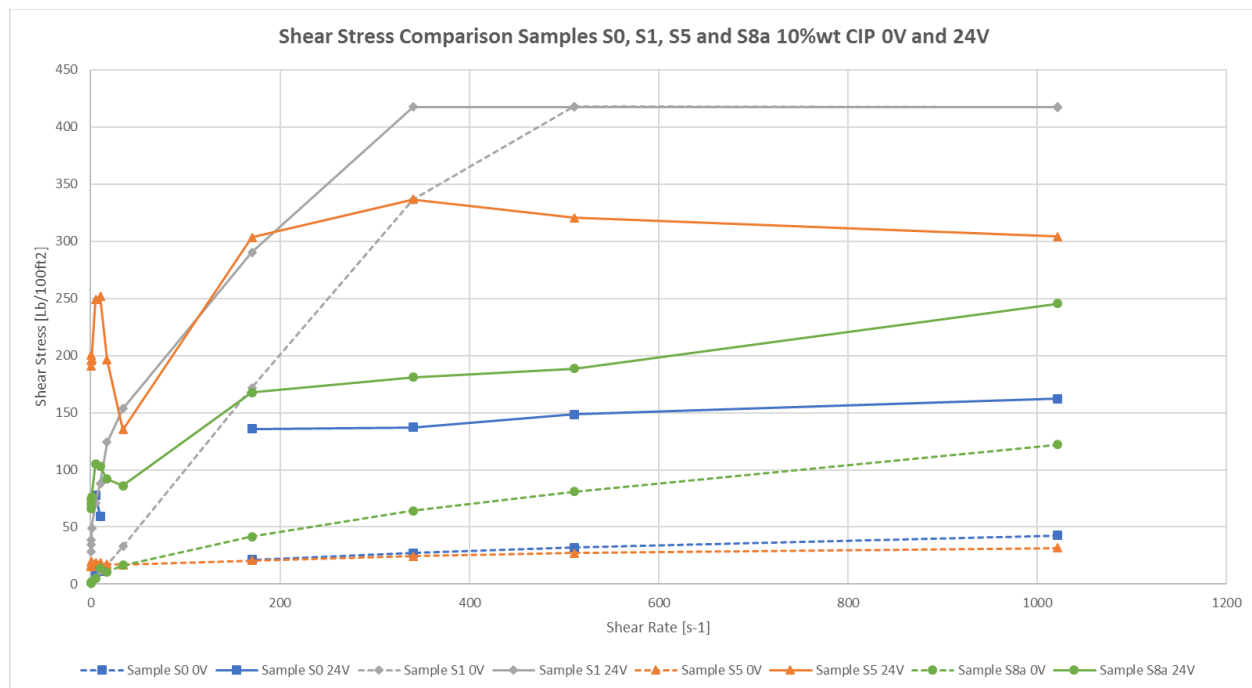


Fig. 23. Rheology Comparison of Different Samples with CIP 10% wt

#### 4.4. Particle Settling

Another important aspect for the selection of the MRF is the settling ratio. The settling ratio or sedimentation ratio is defined as the volume of the supernatant liquid over the volume of the total suspension. Table 5. Summarizes the settling ratio expressed as the percentage of free fluid that does not contain CIP. When the CIP concentration is 0%, the settling ratio measured represents the free fluid from the mixture.

Table 5. Settling Ratio Evaluation at 24, 48 hours, 30 days and 60 days

Sample	Hours after mixed				
	24	48	168	720	1440
<b>S1 CIP0%</b>	1%	1%	20.00%	20.00%	20.00%
<b>S1 CIP5%</b>	2%	2%	20.50%	20.50%	20.50%
<b>S1 CIP20%</b>	3%	3%	45.30%	45.30%	45.30%
<b>S2 CIP0%</b>	0%	0%	0%	0%	0%
<b>S2 CIP5%</b>	0%	0%	0%	0%	0%
<b>S2 CIP10%</b>	0%	0%	0%	0%	0%
<b>S3 CIP0%</b>	0%	0%	13%	14%	14%
<b>S3 CIP5%</b>	0%	0%	28.40%	28.80%	28.80%
<b>S3 CIP10%</b>	0%	0%	31.20%	31.50%	31.50%
<b>S4 CIP0%</b>	0%	0%	0%	0%	0%
<b>S4 CIP5%</b>	0%	0%	4.70%	5.70%	5.70%
<b>S4 CIP10%</b>	0%	0%	5.30%	6.20%	6.20%
<b>S4 CIP15%</b>	0%	0%	6.80%	7.10%	7.10%
<b>S5 CIP0%</b>	0%	0%	0%	0%	0%
<b>S5 CIP10%</b>	0%	0%	7.50%	8.60%	8.60%
<b>S5 CIP15%</b>	0%	0%	7.60%	8.70%	8.70%
<b>S5 CIP20%</b>	0%	0%	7.40%	8.80%	8.80%
<b>S5 CIP25%</b>	0%	2%	12.40%	12.86%	12.86%
<b>S6 CIP20%</b>	0%	12.40%	40.50%	42.50%	42.50%
<b>S7a CIP20%</b>	0%	0%	0%	0%	0%
<b>S8a CIP20%</b>	0%	0%	5.60%	18.90%	18.91%
<b>S9a CIP15%</b>	0%	0%	7.60%	8.40%	8.40%

The Fig 24. Represents the settling ratio per sample at different concentrations of CIP:

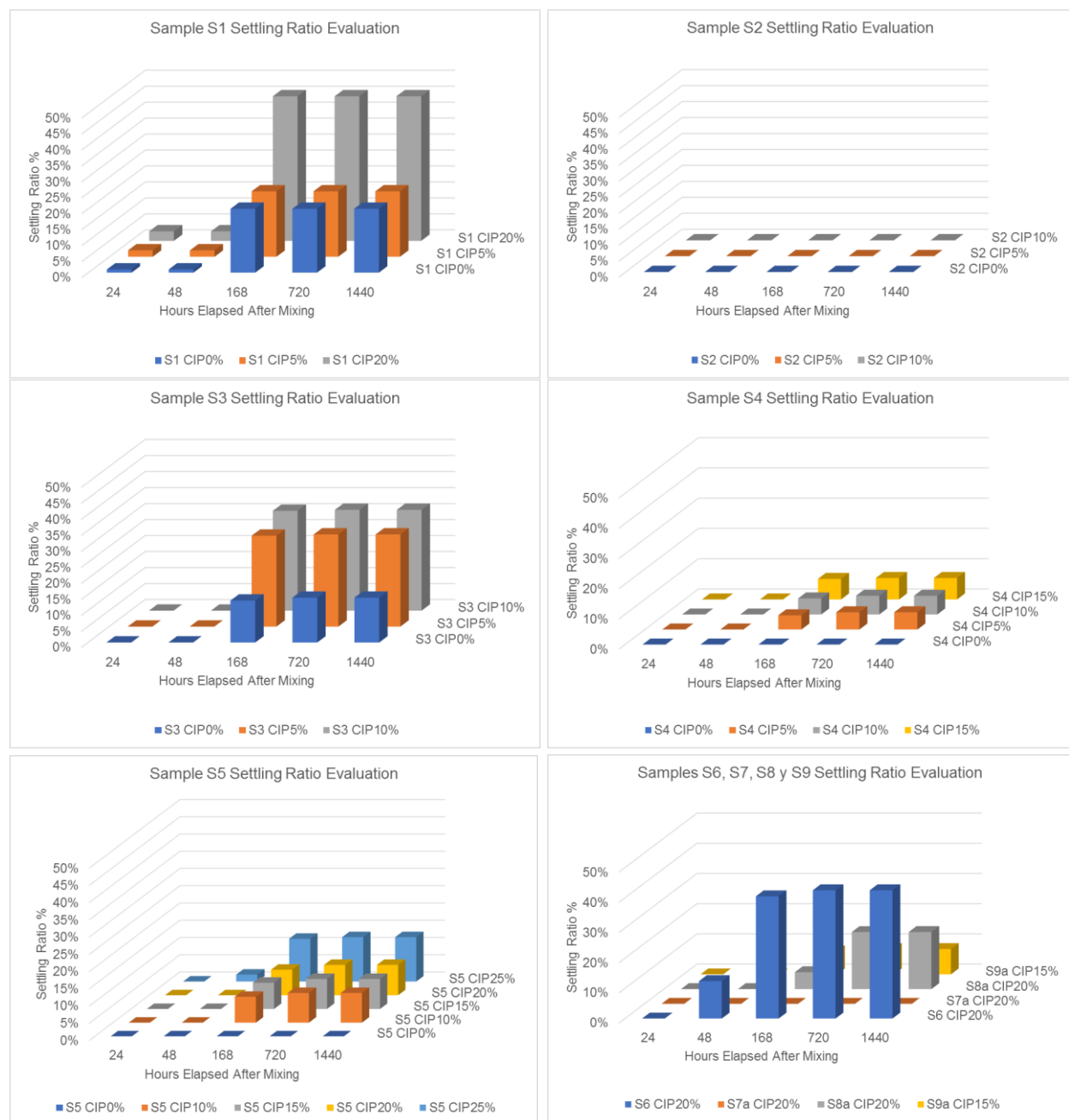


Fig. 24. Settling ratio evaluation at 24, 48, 168, 720 and 1440 hours.

The samples that contained silicone oil as the carrier fluid and stearic acid as the stabilizer (Sample S1 and S6) are the ones that exhibited the highest and fastest sedimentation among the samples. Although the theory presented this mixture as a good option to avoid particle settling, a high viscosity silicone oil alone seems not to yield the expected results. For future works, mixing an emulsion and defining the proper



emulsifier to increase the interfacial tension could provide better results in terms of lowering the settling ratio. On the other hand, the samples with carrier fluid water and Laponite RD exhibited a higher sedimentation control as the concentration of Laponite RD increased. However, extremely high concentration of Laponite RD (larger than 2%) produce aggravated gelation that behaves more as a cross-linked fluid. As presented before, the MRF require to remain fluid in OFF states and only present higher rheology under the influence of the magnetic field. The optimum concentration of Laponite RD is 1.5% because it has low rheology and good control against particle settling. Finally, among all the samples, the particle settling is developed at an early stage between the first week after mixed (168 hours) and later than that the settling ration remains steady.

#### **4.5. MRF behavior in Flow Loop**

Once the best MRF candidates (Sample S0 and S5) were selected in terms of good mixability, considerable increase in shear stress under the influence of the magnetic field, and low settling ratio, these samples were mixed and circulated at a large-scale flow-loop, see Fig. 25. The flow-loop consists of two concentric pipes resembling circulation geometry where the pressure drop of the fluid is measured in linear sections and compared to the models. The objectives of this experimental phase include: (a) Evaluate the pressure drop or restriction to flow, if any, of the circulated MRF in the sections containing a magnetic field and sections without it, (b) Evaluate the build-up or agglomeration of magnetizable particles, if any, in front of the permanent magnets by comparing the inlet-outlet density and by the visual observation of the magnets after the circulation of the MRF, (c) Evaluate the pressure change or restriction to flow, if any, of the system when an external magnetic field is applied in the outlet hose of the system, (d) Evaluate the durability of the MRF against corrosion in environments that contain steel and other contaminants.

#### **Overview of the results:**

The first sample to be tested was Sample S0, composed of water as the carrier fluid, Bentonite 5.89%wt as the stabilizer and the addition of CIP up to 10.5%wt as the magnetizable particles. The sample was circulated at different flow rates at different concentrations of CIP. The pressure drop across the system

was monitored. The results exhibit a minor increase in the pressure drop in front of the magnets. Unfortunately, after 12 days of mixing the sample and after remaining static for a period of 60 hours inside the experimental setup the mixture developed an exacerbated gelation accompanied with traces of corrosion of the fluid. Fig. 27 and 28 display the pressure behavior of the circulation of the gelled Sample S0. The pressure transducers used for this experiment had a low sensibility at the low-pressure ranges observed during the experiments. Because of this, a high fluctuation of the pressure readings made interpretation of the results difficult. A new set of pressure transducers with higher sensibility to lower pressures was acquired to run the experiments with sample S5. Because of this issue, this document does not include a comparison in pressure drop behavior comparing sample S0 and sample S5. On the contrary, this document presents an independent analysis per sample.

On the other hand, the sample S5 was mixed and circulated in the experimental setup. The results showed a very similar pressure drop compared to the one obtained with sample S1 being in the order of 0.52 psi for the same concentration of CIP of 10%wt. The main difference between the two samples is that the sample S5 after being static and circulated in the experimental setup for a period of more than 30 days did not show traces of oxidation.

## Flow Loop

The pressure transducer number P1, P2, P3, P4 and P5 are arranged as the following diagram:

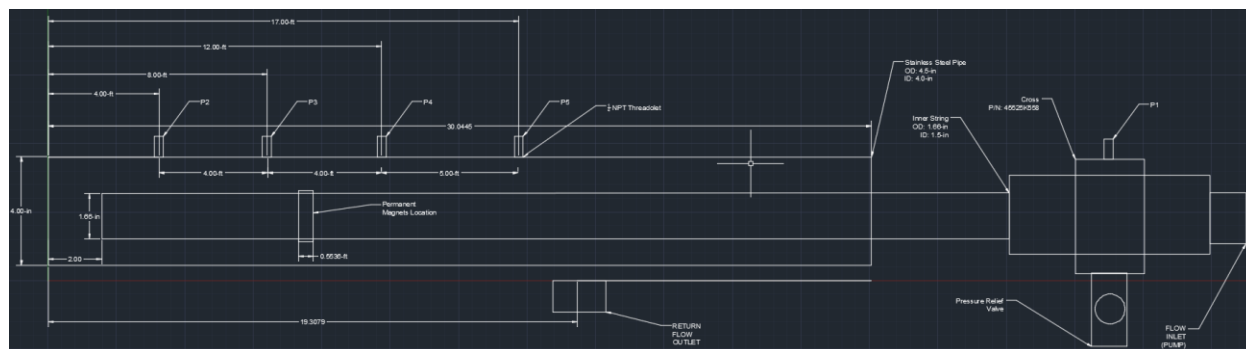


Fig. 25. Flow-loop schematic with location of the pressure transducers and direction of the flow (update with my own schematic).

### Circulation of Sample S0:

The base fluid (water and bentonite) is mixed in the drum to prepare 60 gal of fluid. The drum is connected to the peristaltic pump, a positive displacement pump, that circulates the mixture to the experimental setup. The pump is connected to the inner pipe (1.66-in OD) and the fluid is circulated to inside the pipe and later to the annulus formed by the inner pipe and the outer pipe (4.00-in ID). Inside the annulus, the fluid flows in front of the section with magnets and sections without magnets. The pressure transducers located in the outer pipe measure the pressure at the annulus. According to the theory of pressure drop in pipe and annuli, the friction pressure loss is a function of the flow rate. Similarly, the shear stress is a function of the shear rate exerted on the fluid. Therefore, the fluid is circulated at different flow rates to evaluate the pressure drop behavior. The base fluid (water and bentonite) provides a pressure behavior without magnetizable particles. To evaluate the effect of the magnetizable particles on the pressure drop, CIP is added incrementally and circulated at different flow rates to evaluate the fluid behavior in the experimental setup. The fluid was circulated in the experimental setup at the minimum concentration of CIP (0.447 wt%), the pressure drop was measured and recorded. The following results were published at the OTC conference (Estrada, Akbari, & Nielsen, 2018). The CIP was added incrementally until reaching the maximum concentration (10.5 %wt). The annulus pressure drops between transducers P4-P3, where the magnet arrangement is located, was recorded and the results are presented in table 6.

Table 6. CIP concentration vs Pressure Drop for Sample S0

<b>Carbonyl Iron Particles Concentration [wt%]</b>	<b>Pressure Drop Trasducers P4 - P3 [psi] at 21.1 gpm</b>
0.447	0.5103
0.894	0.664
1.341	1.031
1.788	1.222
3.576	1.345
4.917	1.3536
5.588	1.3647
6.258	1.4363

Continued Table 6 on next page

<b>Carbonyl Iron Particles Concentration [wt%]</b>	<b>Pressure Drop Transducers P4 - P3 [psi] at 21.1 gpm</b>
6.929	1.5698
7.599	1.6352
8.270	1.3118
8.941	1.1033
9.611	1.4151
10.505	1.333

The results showed an additional pressure drop across the magnets as a function of the concentration of the CIP. Additionally, the pressure drop measurements show a steady increase until a CIP concentration of 7.599 %wt. This is interpreted as a maximum saturation where the magnetizable particles are affected by the magnetic field strength. The saturation behavior and its implications are intended to be analyzed with further experimentation later in this report in section 4.6 Pressure Drop Estimation vs Results. The values of the pressure drop in the section without magnets is not presented since they showed intensified fluctuation that yielded positive and negative values, making difficult to establish a credible point of comparison. In summary, the pressure drop increases as the concentration of the CIP is increased as shown in Fig. 26. The comparison between the sections with and without magnetic field is properly performed at studying the circulation of sample S5 in the next section.

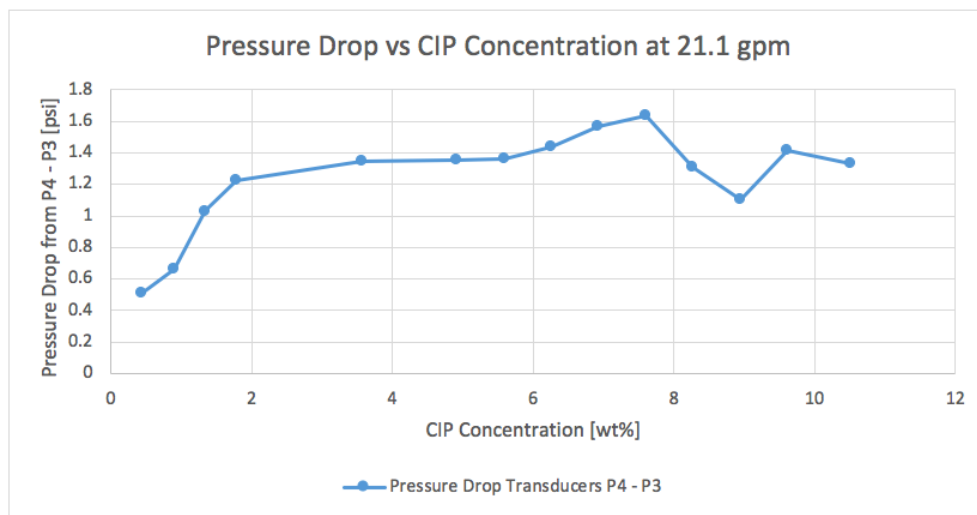


Fig. 26. Pressure Drop vs CIP concentration

The MRF with a CIP concentration of wt%10.5 was held static for a period of 60 hours inside the experimental setup to evaluate its behavior. When the fluid was circulated after this period, the pressure drop across the magnets showed an increased in comparison to the measurements previously presented i.e. at 21.1 gpm the pressure drop across the magnets was 1.33 psi whereas the new measurement rounded 3.11 psi, see Fig. 27. An evaluation of the causes of this behavior is currently being carried out because the main factors to contaminate a drilling mud where not present. These factors generally are Calcium-Ions contamination, Biocarbonate and carbonate contamination, presence of hydrogen sulfide and ions  $\text{Na}^+\text{Cl}^-$ . However, none of these factors were present during the experimentation. The main hypothesis is associated with the oxidation produced by the silicon oxides present in the montmorillonite, the main mineral component of the Bentonite, the details were presented at the end of the section 4.3 of this document. However, the author does not encounter a relationship between the oxidation and the pressure drop.

Based on the results presented in Fig. 28, the rheology of the MRF can be modified according to the magnetic field strength and magnetizable concentration. At evaluating the pressure behavior for the gelled MRF, the fluid rheology did not play the dominant role in the packing and/or pressure drop. Instead, the built-up iron particles in front of the magnets created a mechanical restriction as shown in Figure 29. This can be inferred because the pressure drop measured experimentally is extremely higher than the estimated based on the rheological parameters. On the other hand, considering the flow restriction due to the reduction of the annular flow area in front of the packer Fig. 30 the calculations of the pressure drop estimation gets closer to the measure pressure drop.

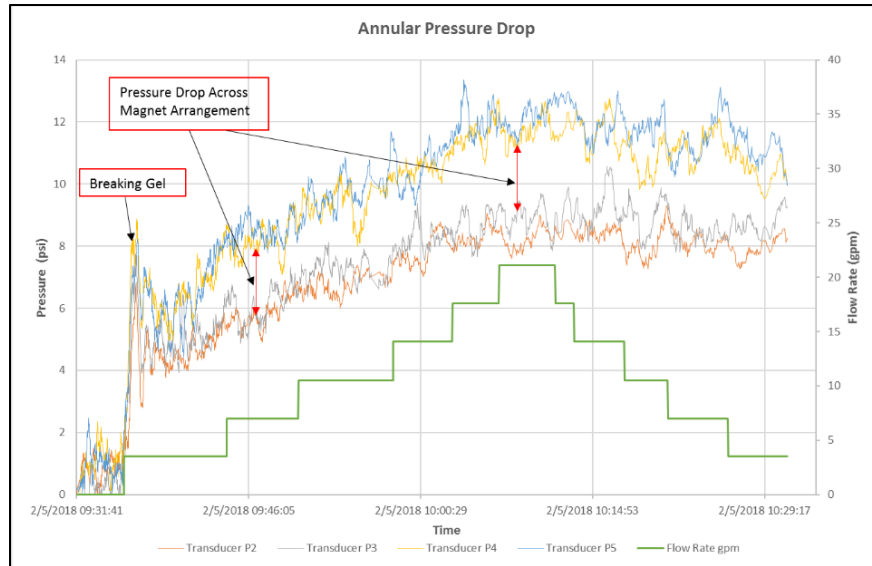


Fig. 27. Pressure Drop Measurement at different flow rates MRF CIP wt% 10.5 after 60 hours static

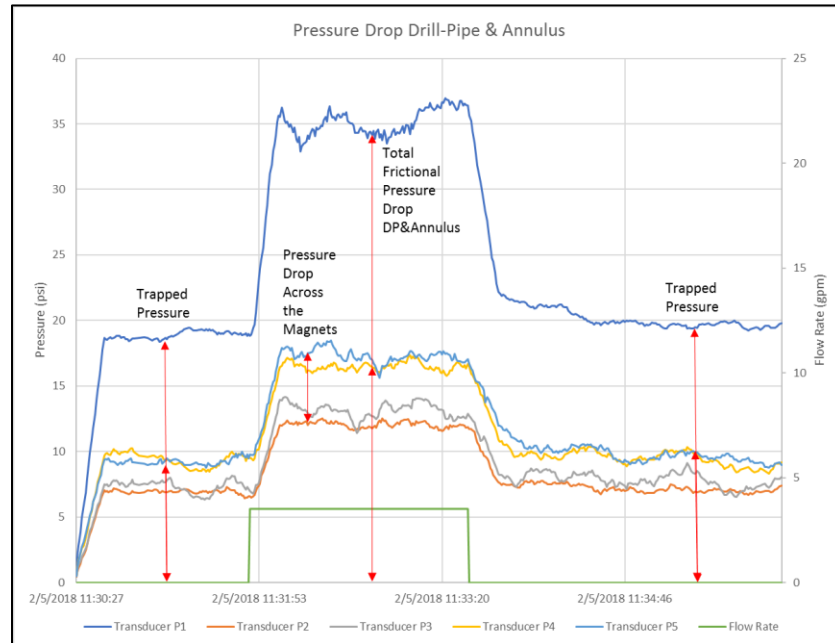


Fig. 28. Pressure Drop Measurement Drill-Pipe & Annulus with MRF CIP wt% 10.5 after 60 hours static

Finally, the MRF was drained and the inner pipe with the magnets is extracted to visually evaluate the packing effect. As shown in Fig. 29 a clear packing effect is observed and the CIP are aligned in the direction of the magnetic field. The MRF pseudo-packer has a good consistency and requires a moderate to high lateral stress to remove the particles. Once particles are removed away from the magnets, the pseudo-packer restores to its liquid form.



Fig. 29. CIP particle build-up in front of the permanent magnets

### Circulation of Sample S5:

Tests following the same parameters as followed with sample S0 were performed as follows: Water, Laponite RD 1.5% wt, and CIP: 0%, 2.5%, 5%, 7.5%, 10%, 12.5%, 15%, 17.5%, and 20% by weight. Higher sensitivity pressure transducers for low pressure were installed to improve the accuracy on the readings. As follows the two extreme scenarios are presented CIP 20% wt and CIP 0% wt

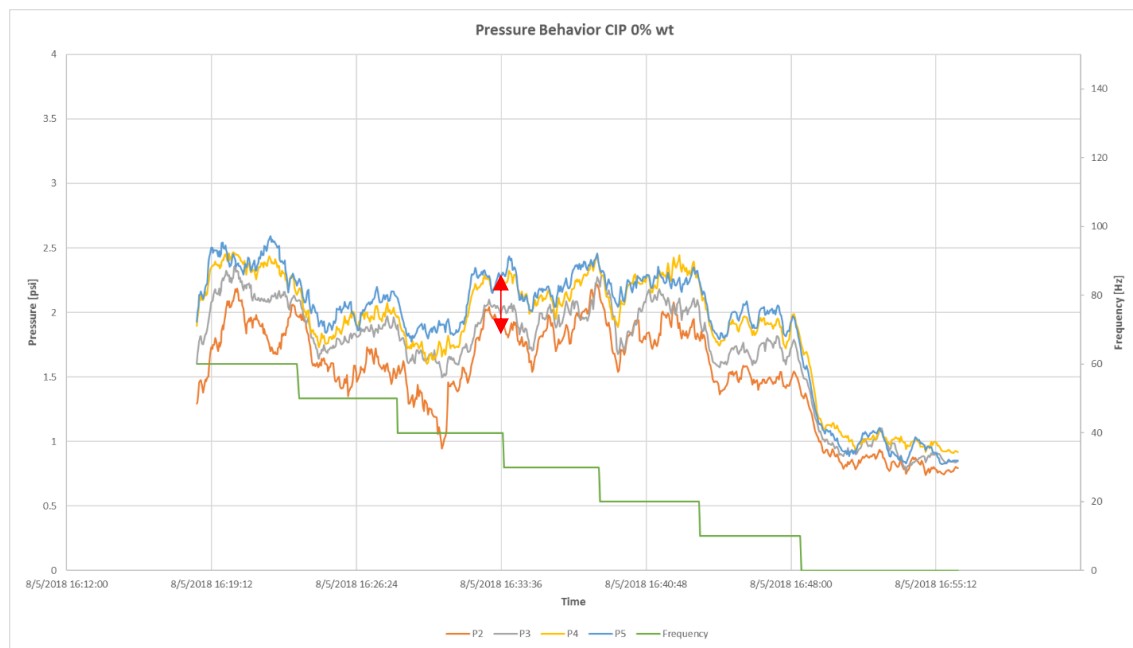


Fig. 30. Circulation of sample S5 at different flowrates without CIP

Fig. 30. Displays the pressure behavior of the sample S5 without any content of CIP. In other words, the pressure drop is only generated by the intrinsic rheological properties of the admixture. In general terms, the four curves have a similar trend and the spread out among them is minimum, consistent with a pressure drop behavior of a fluid of low to moderate rheology.

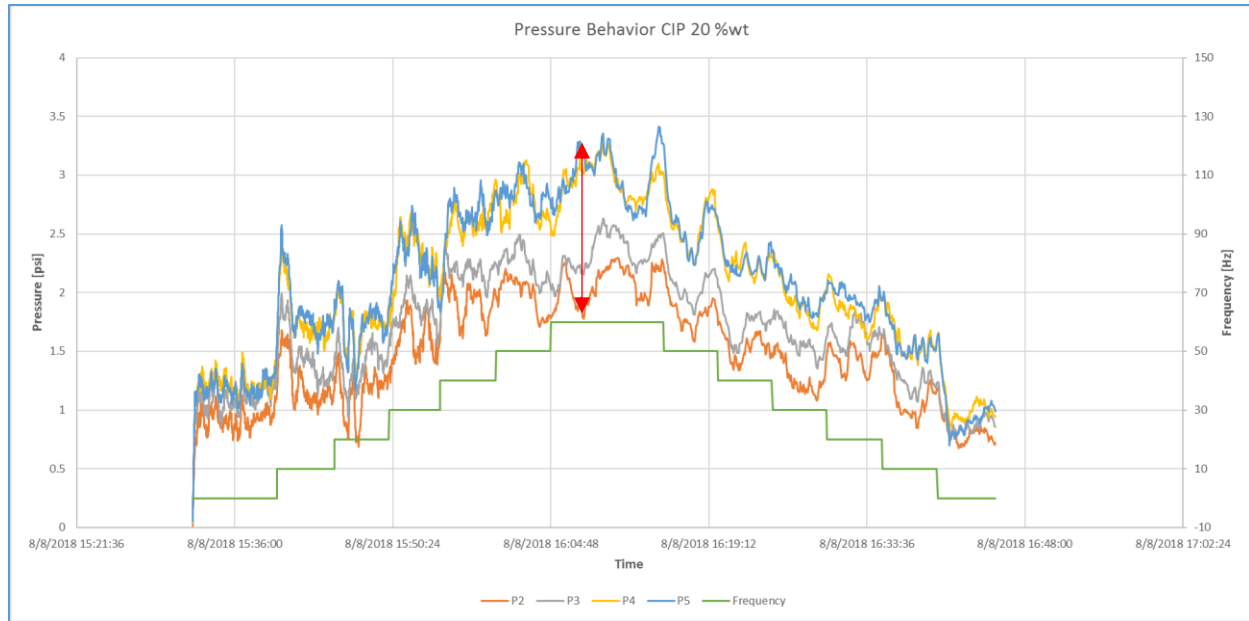


Fig. 31. Circulation of sample S5 with a concentration of CIP of 20%wt

On the other hand, Fig. 31 displays a clear spread out of the curves, particularly at higher rates between the pressure readings upstream the magnets (P4 and P5) and downstream the magnets (P3 and P2). Also, the pressure drop in the section that contains the magnets (P4 and P3) is considerably larger than the pressure drop of the section of the same length that does not contain the magnets (P4 and P5). In that sense, a flow restriction is being developed in front of the magnets that is creating an additional pressure drop. The additional pressure drop generated by the magnets is low (0.6 psi). However, it must be considered that the magnet arrangement length is short. An upscaled model of the generated pressure drop is presented in section 4.7. The hypothesis is that if a longer magnet arrangement, or of a higher magnetic field strength is used, the pressure drop can be increased.

Another observation from Fig. 31 is that the pressure drop across the magnets increases as the flow rate increases (reference green curve). This can be explained from the friction loss equations presented in section 4.6. The friction loss is as a function of the annular cross-sectional area and the flow rate. As the flow rate increases, the friction loss increases proportionally. As the annular cross-sectional area decreases, the friction loss increases. Another consideration is that the pressure drop is also a function of the yield stress of the fluid for non-newtonian fluids. Therefore, the pressure drop is also a function of the CIP concentration



of the MRF and the intensity of the magnetic field. As observed in Fig. 29, when the MRF is in contact with the permanent magnets, the particles build-up in front of the magnets. It can be interpreted that as the particles build-up, the cross-sectional area decreases, and hence, increasing the frictional losses. Similarly, as the shear stress increases in front of the magnets, the pressure drop increases.

Considering the option of evaluating the effect of a magnetic field in the system, a set of electromagnets was strategically placed surrounding the outlet hose (the return line from the flow loop towards the mud tank), see Fig. 32. A magnetic field was induced to the returning MRF as emulating a choke for Managed Pressure Drilling Operations.

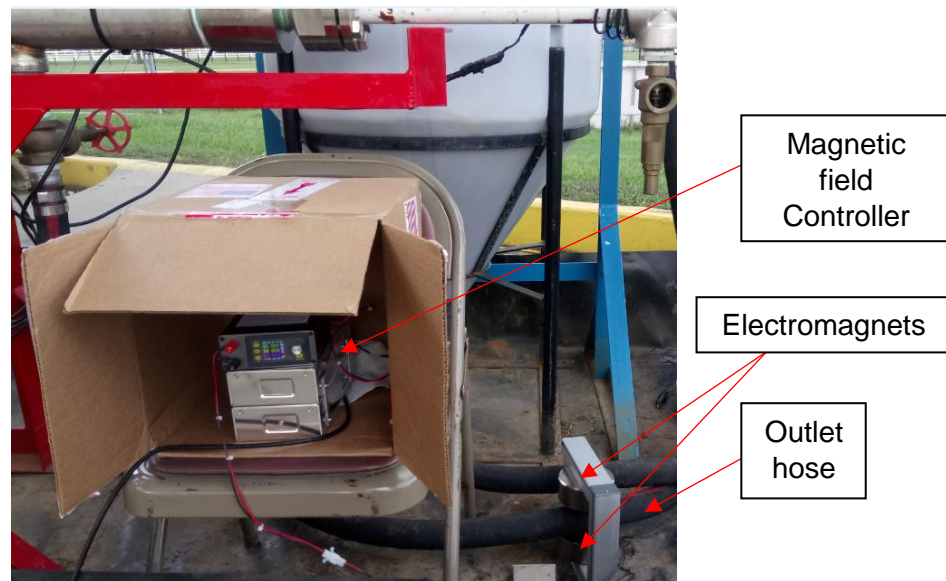


Fig. 32. Electromagnet choke with circulating MRF

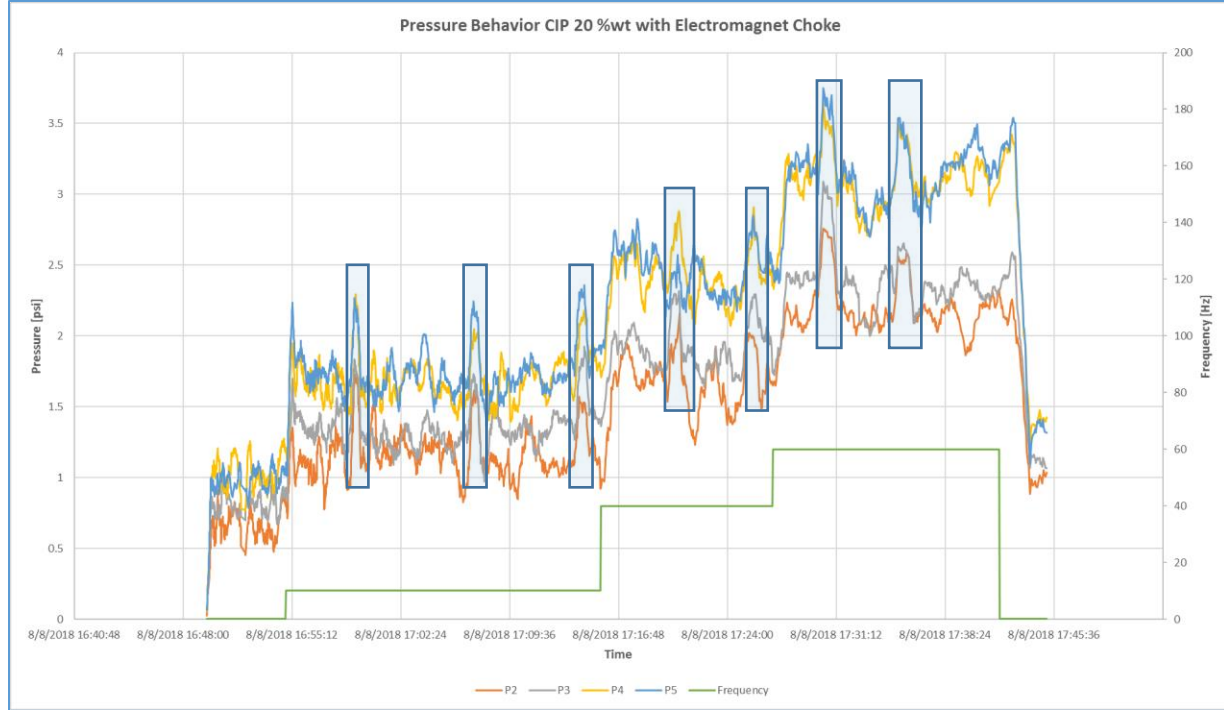


Fig. 33. Pressure behavior of flowing MRF with electromagnet choke

In Fig. 33 the pressure behavior of the MRF flowing in the experimental setup was evaluated. The blue squares indicate the moment at which a magnetic field is induced. As observed, the pressure in all the transducers increased simultaneously at a same proportion of 0.5 to 0.8 psi per activation. This is the main principle of Managed Pressure Drilling (MPD) where a surface choke aperture regulates the amount of back pressure to apply to the system to regulate the bottom hole pressure. To the best of the author's knowledge, a dedicated person regulates the aperture of the choke according to drilling condition because the choke is manually operated. The novelty of a suitably configured magnetic choke is that it can act rapidly responding to a computer-based sensing to produce a back pressure in controlled and automated mode for MPD applications when an MRF flows in the system.

#### **In-and-Out Density:**

The circulating samples S5 at different CIP concentration were taken before the cycle (during mixing) and after the cycle (taken from the return while circulating) in the flow-loop. The density was measured, and the results are summarized in the Table 7.

Table 7. Density of the circulating sample S5 at different concentrations of CIP

<b>CIP wt%</b>	<b>Density Taken Before Circulation [g/cm3]</b>	<b>Density Taken after circulation [g/cm3]</b>	<b>Density Taken Before Circulation [Lb/gal]</b>	<b>Density Taken after circulation [Lb/gal]</b>
<b>5</b>	1.0852	1.0277	9.039716	8.560741
<b>7.5</b>	1.0938	1.0847	9.111354	9.035551
<b>12.5</b>	1.1529	1.1514	9.603657	9.591162
<b>15</b>	1.2023	1.1541	10.015159	9.613653

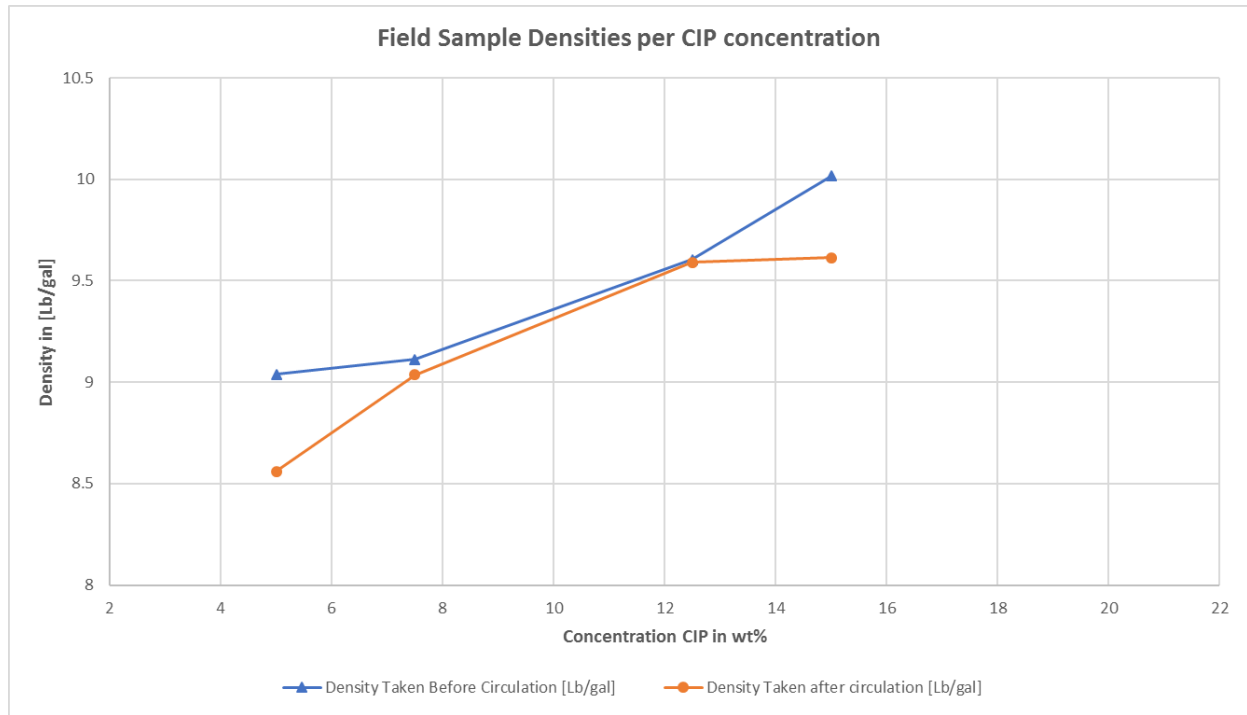


Fig. 34. Density of the circulating sample S5 at different concentrations of CIP

As expected, the density increased as the CIP were added because of the high specific gravity of the CIP. In general, the density taken before the cycle was slightly higher in comparison to the one taken after the circulation. This can be explained because the CIP was added to the drum and later circulated and homogenized with the fluid inside the flow loop which triggered a further dispersion of the particles. Another reason could be the accumulation or build-up of CIP particles across the magnets, consequently reducing the concentration of the outgoing fluid.

#### 4.6. Pressure Drop Estimation vs Results

Different models have been developed to study the behavior of the fluid in pipe and annuli. Some specific models have been developed for MRF in concentric and eccentric annuli using the Bingham-plastic model to simulate cement with ferrous particles in front of drilling mud (Ermila, Eustes, & Mokhtari, 2012). On the other hand, other models estimate the pressure losses of fluids modeled as Herschel-Bulkley in laminar, transitional and turbulent flow in both concentric and eccentric annuli (Kelessidis, Dalamarinis, & Maglione, 2011). Most of the drilling fluid including cement slurries, drilling mud as well as Magnetorheological fluids are best modeled as Herschel-Bulkley rather than Bingham-plastic. The Herschel-Bulkley model also called Yield Power Law describes the flow of pseudoplastic fluids that require a yield stress to initiate flow and whose apparent viscosity is a function of the shear rate. The Herschel-Bulkley uses three different factors to determine the relationship between the Shear Stress and the Shear Rate: yield shear stress ( $\tau_0$ ), the flow index ( $n$ ), and the fluid consistency ( $k$ ).

$$\tau = \tau_0 + k\dot{\gamma}^n \quad (\text{Eq. 1})$$

The fluid consistency is a constant of proportionality, the flow index measures the degree to which the fluid is shear thinning  $n < 1$  or shear thickening  $n > 1$ .

There are approximations to estimate these three parameters that involve a curve fit from the shear stresses measured at the viscometer at different shear rates. The flow regime, the rheological properties, the flow rate and the flowing geometry are key factors at determining the pressure loss in a system. The approach of the following method considers the pressure drop by fixed lengths in the geometrical sections, pipe or annulus (American Petroleum Institute, 2009).

The average velocity of the fluid in pipe or annulus is inversely proportional to the cross-sectional area of the conduit:

$$V_p = \frac{24.51 Q}{d_p^2} \quad (\text{Eq. 2})$$

$$V_a = \frac{24.51 Q}{d_h^2 - d_p^2} \quad (\text{Eq. 3})$$

Where  $V_p$  and  $V_a$  correspond to the average velocity [ft/min] in pipe and annulus, respectively.  $Q$  is the flow rate [gpm].  $d_h$  and  $d_p$  are the diameter [in] of the outside geometry and pipe, respectively.

The nominal shear rate  $\gamma$  first must to be converted to shear rate at the wall  $\gamma_w$  to calculate the pressure drop. The well geometry correction factor  $B_a$  is a function of the rheological parameter flow index  $n$  and the type of conduit.

$$B_a = \left[ \frac{(3-\alpha)n+1}{(4-\alpha)} \right] \left[ 1 + \frac{\alpha}{2} \right] \quad (\text{Eq. 4})$$

Where  $\alpha$  is 0 for geometry factor for pipe and 1 for annulus.

The field viscometer correction factor  $B_x$  is also a function of the flow index  $n$  and the type of bob/sleeve combination.

$$B_x = \left[ \frac{X^{\frac{2}{n}}}{nX^2} \right] \left[ \frac{X^2-1}{X^{\frac{2}{n}-1}} \right] \quad (\text{Eq. 5})$$

Where  $X$  is the 1.0678 in the standard bob/sleeve combinations R1B1.

The combined geometry shear-rate factor is defined as  $G$

$$G = \frac{B_a}{B_x} \quad (\text{Eq. 6})$$

The shear rate at the wall  $\gamma_w$  required to determine the shear stress at the wall is calculated as follows:

$$\gamma_w = \frac{1.6GV_p}{d_p} \quad \text{or} \quad \gamma_w = \frac{1.6GV_a}{d_h-d_p} \quad (\text{Eq. 7})$$

The frictional pressure losses are directly proportional to the shear stress at the wall  $\tau_w$ , where  $\tau_f$  is the shear stress at the wall in viscometer units.

$$(\text{Eq. 8})$$

$\tau_w$  in engineering units.

$$\tau_w = 1.066\tau_f \quad (\text{Eq. 9})$$

The frictional losses are also a function of the flow patterns characterized by laminar, transitional and turbulent flow regimes.

The Reynolds number (generalized) determines the flow regime and applies for both pipe and annulus.

$$N_{ReG} = \frac{\rho V^2}{19.36 \tau_w} \quad (\text{Eq. 10})$$

Where  $\rho$  is the density in [Lb/gal] of the fluid and  $V$  is the average velocity for pipe or annulus in [ft/min].

The critical Reynolds number  $N_{CRe}$  is the value of  $N_{ReG}$  where the flow regime changes from laminar flow to transitional flow.

$$N_{CRe} = 3470 - 1370n \quad (\text{Eq. 11})$$

The pressure losses in pipes and annuli are a function of the Fanning friction factor  $f$  which is a function of the rheological properties, the flow regime and generalized Reynolds number. A generalized expression of Fanning friction factor  $f$  for any Reynolds number and flow regime includes intermediate terms for laminar  $f_{lam}$ , transitional  $f_{trans}$  and turbulent  $f_{turb}$  flow regimes.

$$f_{lam} = \frac{16}{N_{ReG}} \quad (\text{Eq. 12})$$

$$f_{trans} = \frac{16 N_{ReG}}{N_{CRe}^2} \quad (\text{Eq. 13})$$

$$f_{turb} = \frac{a}{N_{ReG}^b} \quad (\text{Eq. 14})$$

Where

$$a = \frac{\log_{10}(n) + 3.93}{50} \quad (\text{Eq. 15})$$

$$b = \frac{1.75 - \log_{10}(n)}{7} \quad (\text{Eq. 16})$$

The pipe roughness effect on friction increases in fully developed turbulent flow. Since this is not case of the current experiment, the pipe roughness effect is considered negligible.

$$f_{intermediate} = (f_{transitional}^{-8} + f_{turbulent}^{-8})^{-1/8} \quad (\text{Eq. 17})$$

$$f = (f_{intermediate}^{12} + f_{laminar}^{12})^{1/12} \quad (\text{Eq. 18})$$

Where  $f$  is the Fanning friction factor, dimensionless.

Finally, the pressure drop expression for a fixed length  $L$  is expressed as follows:

$$\Delta P_{pipe} = \frac{1.076 \rho V_p^2 f L}{10^5 d_p} \quad (\text{Eq. 19})$$

$$\Delta P_{annulus} = \frac{1.076 \rho V_a^2 f L}{10^5 (d_h - d_p)} \quad (\text{Eq. 20})$$

By using Eq. 1 to Eq. 20 it is possible to compare the pressure drop calculated from the rheology measurements and the measured pressure drop at the flow-loop. The importance of a good fitting is that an upscaling can be performed to establish the required rheologies, CIP concentration, or magnetic field intensity to induce a determined flow restriction.

Estimation of the field dependent yield stress:

The predicted yield stress as a function of the applied magnetic field from several MRF available from Lord Corporation, a company specialized in this type of fluids, can be modeled as proposed by Carlson (Goncalves et al., 2015):

$$\tau_y = C * 271700 * \phi^{1.5239} * \tanh(6.33 * H) \quad (\text{Eq. 21})$$

Where  $\phi$  is the particle volume fraction,  $\tau_y$  is the field dependent yield stress [Pa]  $H$  is the field strength [A/m]. The constant  $C$  depends on the type of carrier fluid as follows:

$C = 0.95$  , for silicone oil

$C = 1$  , for hydrocarbon oil

$C = 1.16$  , for water

The evaluation of the pressure drop as a function of the rheological properties can be estimated. As the rheology of the MRF is also a function of the magnetic field intensity, the magnetic field is measured at eight different locations at the bob of the viscometer radially as shown in Appendix A. Similarly, the magnetic field intensity is measured at different locations in the arrangement of permanent magnets used in the flow-loop. The average magnetic field measured at the middle of the clearance between the workstring (inner-pipe) and outer pipe i.e. at 0.5-in from the top of the magnets is considered as a representative magnetic field at which the flowing MRF is exposed. The magnetic field strength right in

front of the magnet is very high ( $\sim 280$  mT) and may produce an over estimation of the pressure drop. Similarly, the magnetic field intensity close to the outer pipe is extremely low ( $< 17$  mT) and may produce a negligible pressure drop effect. Therefore, a value of approximately 70 mT is used for following calculations. A more representative magnetic field as function of the distance from the magnetic field could be more representative and accurate. However, not all these representative magnetic field can be produced at the bob. In that sense, the average magnetic field intensity measured at the bob of the viscometer that better represents a magnetic field of  $\sim 70$  mT is when the electromagnets are exposed to 24 Volts. The magnetic field is measured with the magnetic probe at different locations of the bob, details in Appendix A. Therefore, the pressure drop estimation based on the rheology measurements are based on the shear stress obtained at different shear rates when the electromagnets produce a similar magnetic field as the permanent magnets to the flowing MRF in the experimental setup.

Additionally, only a small section of the work-string contains the permanent magnets. Therefore, the pressure drop estimation accounts for a zero or non-magnetic field in the sections without permanent magnets and  $\sim 70$  mT in the sections with permanent magnets. The shear stress values to estimate the pressure drop in the sections without magnetic field are those recorded at the viscometer when the electromagnets are completely off.

The following table summarizes the results obtained. The sample S5 with 1.5% wt Laponite RD at different concentrations of CIP (0, 5, 10, 15 and 20% wt) was circulated in the flow-loop at different flow rates and the pressure drop measured: Pressure transducers P5 and P4 located at 4 feet to each other, this section does not contain any permanent magnet and the MRF has not been exposed to any magnetic field. Pressure transducers P4 and P3 located at 4 feet to each other, this section contains the arrangement of the permanent magnets and a section without magnets. Finally, pressure transducers P3 and P2 located at 5 feet to each other, this section does not contain any permanent magnet but the MRF has been exposed to the magnetic field on the section before. The purpose of the later section is to evaluate the MRF behavior after being exposed to the permanent magnets later in time. Table 8 is summarized in Fig. 35, 36 and 38.



Table 8. Pressure Drop Measured vs Calculated

			Pressure Drop Measured					Pressure Drop Calculated from Rheology				
			CIP%wt					CIP%wt				
	Flow Rate [gpm]	Flow Rate [Hz]	0	5	10	15	20	0	5	10	15	20
P5/P4 [Pressure Drop in psi]	3.52	10	0.120 174	0.076 86	0.086 38	0.088 98	0.088 887	0.081 081	0.145 339	0.145 167	0.098 116	0.120 276
	7.03	20	0.065 281	0.094 31	0.077 76	0.084 98	0.090 72	0.081 442	0.152 336	0.146 658	0.109 088	0.128 988
	10.55	30	0.120 396	0.069 739	0.103 34	0.098 98	0.115 254	0.081 827	0.156 584	0.147 975	0.116 066	0.135 163
	14.07	40	0.071 334	0.118 198	0.110 49	0.109 18	0.148 249	0.082 227	0.159 67	0.149 191	0.121 286	0.140 11
	17.58	50	0.075 967	0.129 392	0.115 01	0.117 51	0.167 533	0.082 64	0.162 105	0.150 336	0.125 496	0.144 308
	21.10	60	0.054 98	0.055 683	0.047 669	0.067 319	0.079 354	0.083 063	0.164 123	0.151 428	0.129 044	0.147 992
P4/P3 [Pressure Drop in psi]	3.52	10	0.089 325	0.157 051	0.277 604	0.312 858	0.390 88	0.084 378	0.250 85	0.303 203	0.311 608	0.350 814
	7.03	20	0.109 266	0.174 773	0.276 786	0.382 466	0.408 595	0.084 784	0.285 4	0.346 067	0.371 007	0.413 391
	10.55	30	0.108 606	0.254 741	0.375 591	0.409 054	0.445 914	0.085 208	0.318 104	0.389 272	0.428 03	0.474 601
	14.07	40	0.102 727	0.275 38	0.340 783	0.440 784	0.525 463	0.085 644	0.350 153	0.432 904	0.484 344	0.535 598
	17.58	50	0.096 877	0.315 793	0.418 255	0.479 929	0.517 179	0.086 088	0.381 93	0.476 982	0.540 489	0.596 773
	21.10	60	0.110 448	0.482 179	0.525 685	0.631 239	0.657 694	0.086 54	0.413 605	0.521 507	0.596 705	0.658 303
P3/P2 [Pressure Drop in psi]	3.52	10	0.019 85	0.019 165	0.029 079	0.058 6	0.018 323	0.081 081	0.145 339	0.145 167	0.098 116	0.120 276
	7.03	20	0.017 517	0.097 005	0.001 783	0.094 55	0.027 253	0.081 442	0.152 336	0.146 658	0.109 088	0.128 988
	10.55	30	0.010 458	0.015 159	0.044 36	0.030 61	0.061 232	0.081 827	0.156 584	0.147 975	0.116 066	0.135 163
	14.07	40	0.025 327	0.019 34	0.003 049	0.091 88	0.084 462	0.082 227	0.159 67	0.149 191	0.121 286	0.140 11
	17.58	50	0.023 148	0.021 697	0.001 72	0.037 27	0.080 168	0.082 64	0.162 105	0.150 336	0.125 496	0.144 308
	21.10	60	0.027 514	0.011 223	0.018 116	0.202 12	0.077 717	0.083 063	0.164 123	0.151 428	0.129 044	0.147 992

Table 9. Pump Variable Frequency Drive (VFD) frequency [Hz] equivalence to flow rate [gpm]

Flow Rate [gpm]	Flow Rate [Hz]
3.52	10
7.03	20
10.55	30
14.07	40
17.58	50
21.10	60

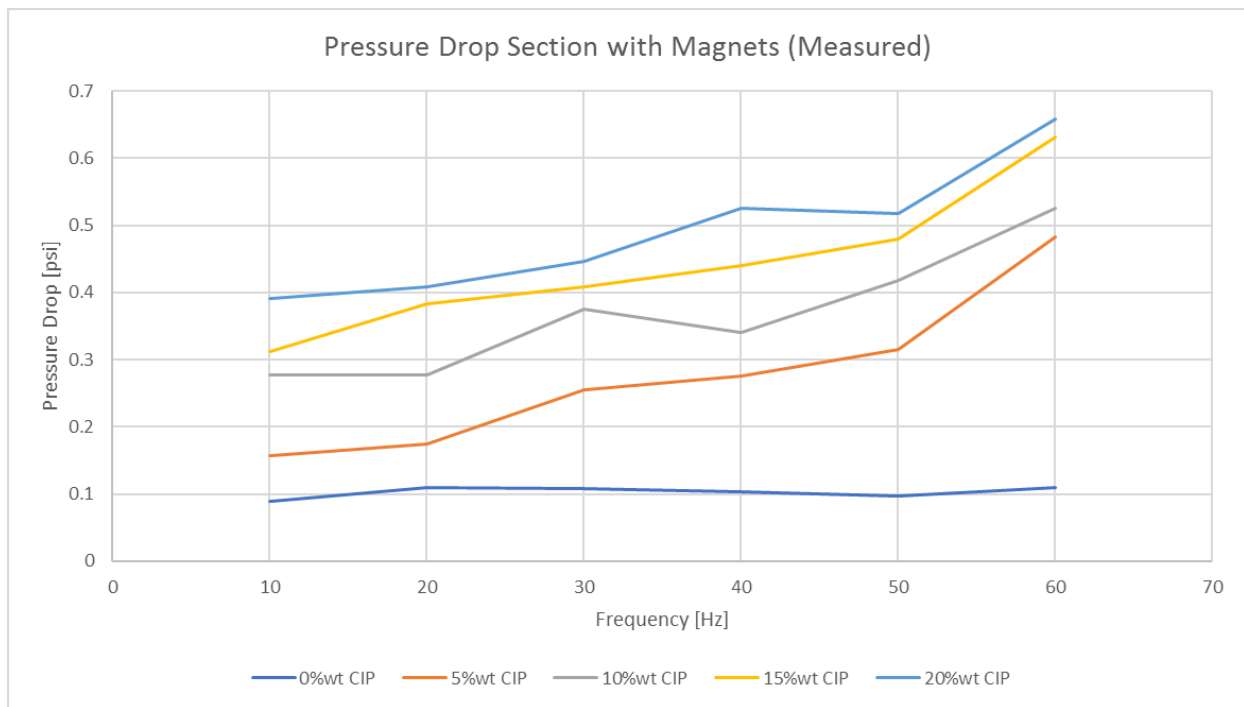


Fig. 35. Pressure Drop Measured at different flow rates, %wt of CIP for the section containing the magnet arrangement.

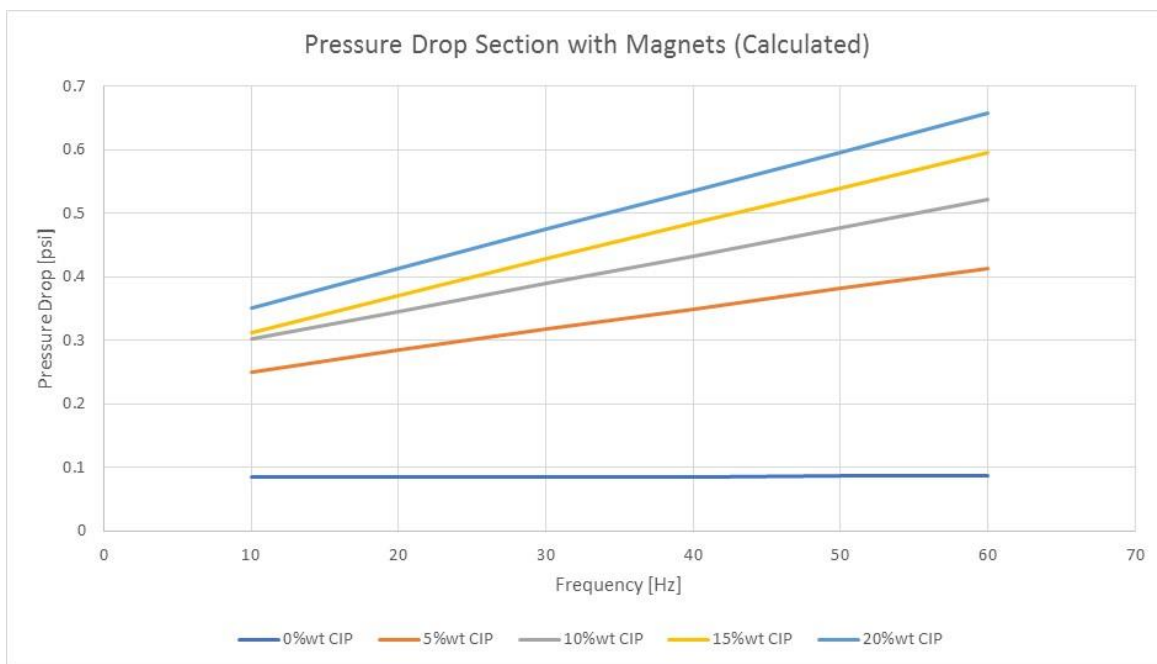
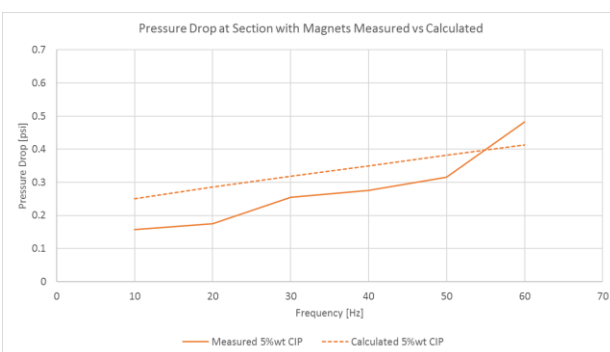
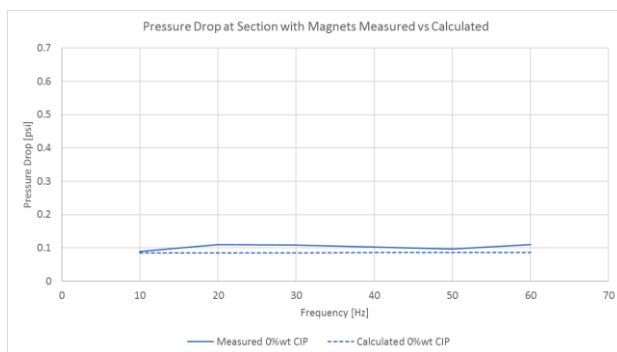


Fig. 36. Pressure Drop Calculated at different flow rates, %wt of CIP for the section containing the magnet arrangement.

An example of calculation for determining the values from Table 8 are detailed in Appendix G. In both scenarios, with and without magnetic field, the calculated and the real pressure drop display a good matching with an average error of 5.6% at high flow rates and 18% at low flow rates, see Fig. 35, 37 and 37. From the rheogram of the sample S5 can be observed that at low flow rates the fluid exhibits a bump-like behavior of the shear stress. It has been documented that the Laponite RD produces strong gels when static and at low shear rates and developing a steadier shear stress behavior at higher shear rates. In that sense, the Hershel and Bulkley model used for the pressure drop estimation does not provide a good fit at lower shear rates.



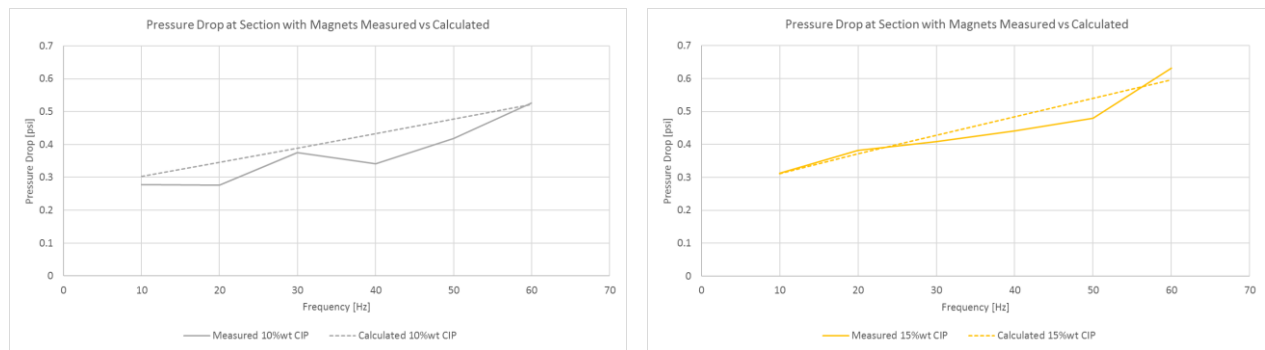


Fig. 37. Pressure Drop Measured vs Calculated.

Additionally, as observed in Fig. 35 and 36 the slope of the curves indicates that as the flow rate increases, the pressure drop increases. This is in agreement with the theory that the flow rate is directly related to the pressure drop when using the Hershel-Bulkley model (American Petroleum Institute, 2009). Similarly, as the CIP concentration is increased the pressure drop increases.. The Fig. 38 compares the pressure drop of the section with the magnets and the one without magnets.

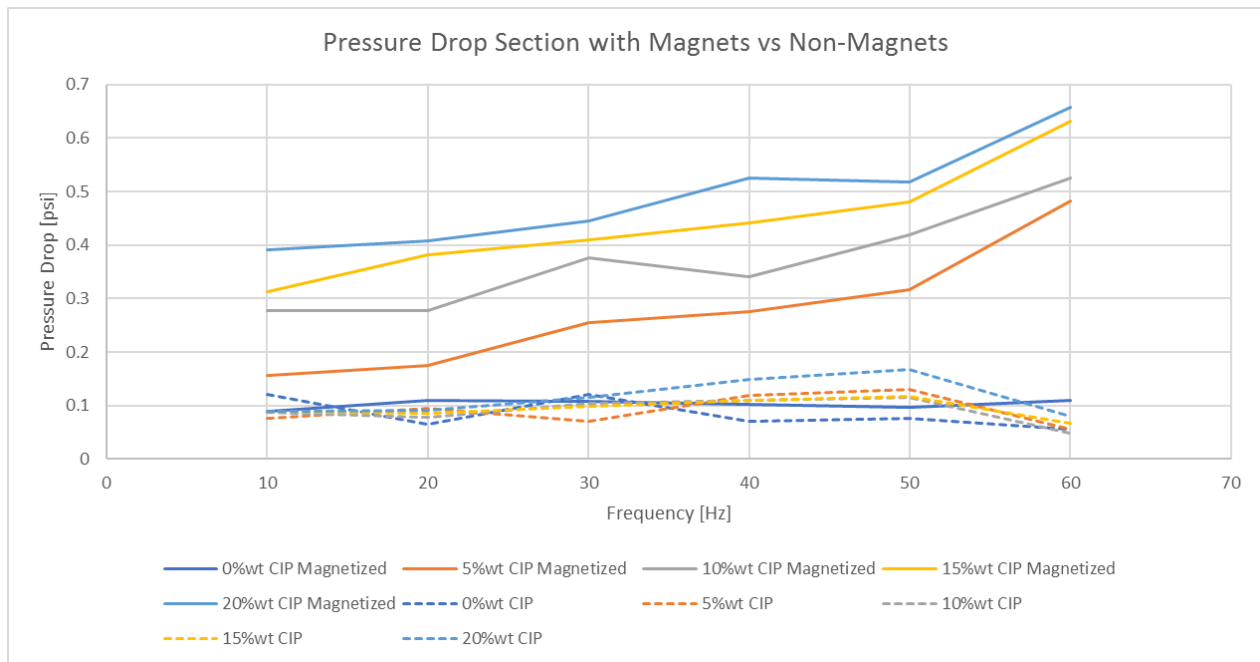


Fig. 38. Comparison of Pressure Drop between section with Magnets and the section without Magnets

The dashed lines represent the pressure drop of the section without magnets. As the CIP concentration increases, there is not a significant increase in the pressure drop. On the other hand, the continuous lines

represent the pressure drop measured in the section where the magnets are located. In this case, a significant increase in the pressure drop as the concentration of the CIP increases. This coincides with the theory (Rich et al., 2012) that the field-induced chaining of iron particles grows as the CIP concentration increases. In this study the author associates the magnitude of the MRF yield stress to the characteristic inner-particle magnetic attractive forces at different CIP concentrations. Similarly, other authors (Martin & Anderson, 1996) established that the yield stress exhibits a linear dependence on the fraction of the magnetic particles.

## UPSCALING TO MODEL FROM PROTOTYPE

### 5.1. Dimensionless Analysis

One of the main objectives to build the prototype is having the opportunity to predict the pressure behavior in real operations while drilling a well. If a dimensional analysis indicates that a phenomenon is described by a functional relationship between non-dimensional parameters, then a prototype to model similarity can be used to predict the MRF behavior in a well.

A dimensional analysis is commonly performed by following the Buckingham's Pi Theorem:

1. If a phenomenon involves  $n$  relevant variables and  $m$  independent dimensions, then it can be reduced to relationship between  $n - m$  non-dimensional parameters  $\pi_1, \dots, \pi_{n-m}$ .
2. To construct those non-dimensional  $\pi$  groups:
  - a. Choose  $m$  dimensionally-distinct scaling variables (also known as repeating variables).
  - b. For each of the  $n - m$  remaining variables construct a non-dimensional  $\pi$  of the form

$$\pi = (\text{variable})(\text{scale1})^a(\text{scale2})^b(\text{scale3})^c \dots \dots \quad (\text{Eq. 22})$$

To estimate the pressure-drop, the relevant variables are as described in (Eq. 20). These relevant variables are:

$\Delta P, d, L, V, \rho, \beta$ , being the pressure drop, difference diameter outer pipe-inner pipe, length, annular velocity, density, CIP concentration is associated to the fluid density and Magnetic Field Strength is  $\beta$ .

$$[\Delta P] = \text{psi} = ML^{-1}T^{-2}$$

$$[L] = \text{ft} = L$$

$$[d] = \text{in} = L$$

$$[V] = \text{ft/min} = LT^{-1}$$

$$[\rho] = \text{Lg/gal} = ML^{-3}$$

$[\beta] = mTesla = L^{-1}I$ , is the dimension of Magnetic Potential

The independent dimensions are therefore  $m = 4$  (M, L, T and I)

Number of non-dimensional groups:  $6 - 4 = 2$

Choosing  $m (= 4)$  scaling variables: geometry (d), annular velocity (V), density ( $\rho$ ), and magnetic field strength ( $\beta$ ).

Forming dimensionless groups by non-dimensionalising the remaining variables:  $\Delta P$  and  $L$

$$\pi_1 = \Delta P * d^a * V^b * \rho^c * \beta^d$$

$$M^0 L^0 T^0 I^0 = (ML^{-1}T^{-2})(L)^a (LT^{-1})^b (ML^{-3})^c (L^{-1}I)^d$$

$$(M^{1+c})(L^{-1+a+b-3c-d})(T^{-2-b})(I^d)$$

$$M: 0 = 1 + c, c = -1$$

$$L: 0 = -1 + a + b - 3c - d, a = 0$$

$$T: 0 = -2 - b, b = -2$$

$$I: 0 = d, d = 0$$

$$\pi_1 = \Delta P * V^{-2} * \rho^{-1}$$

$$\pi_1 = \left( \frac{\Delta P}{\rho V^2} \right)_{Prototype} = \left( \frac{\Delta P}{\rho V^2} \right)_{Well}$$

From Length

$$\pi_2 = L * d^a * V^b * \rho^c * \beta^d$$

$$M^0 L^0 T^0 I^0 = (L)(L)^a (LT^{-1})^b (ML^{-3})^c (L^{-1}I)^d$$

$$(M^c)(L^{1+a+b-3c-d})(T^{-b})(I^d)$$

$$M: 0 = c, c = 0$$

$$L: 0 = 1 + a + b - 3c - d, a = -1$$

$$T: 0 = -b, b = 0$$

$$I: 0 = d, d = 0$$

$$\pi_2 = L/d$$

$$\pi_2 = \left(\frac{L}{d}\right)_{Prototype} = \left(\frac{L}{d}\right)_{Well}$$

Using the pressure drop recorded at the prototype at low flow rates, the following type curves can be generated from  $\pi_1$ :

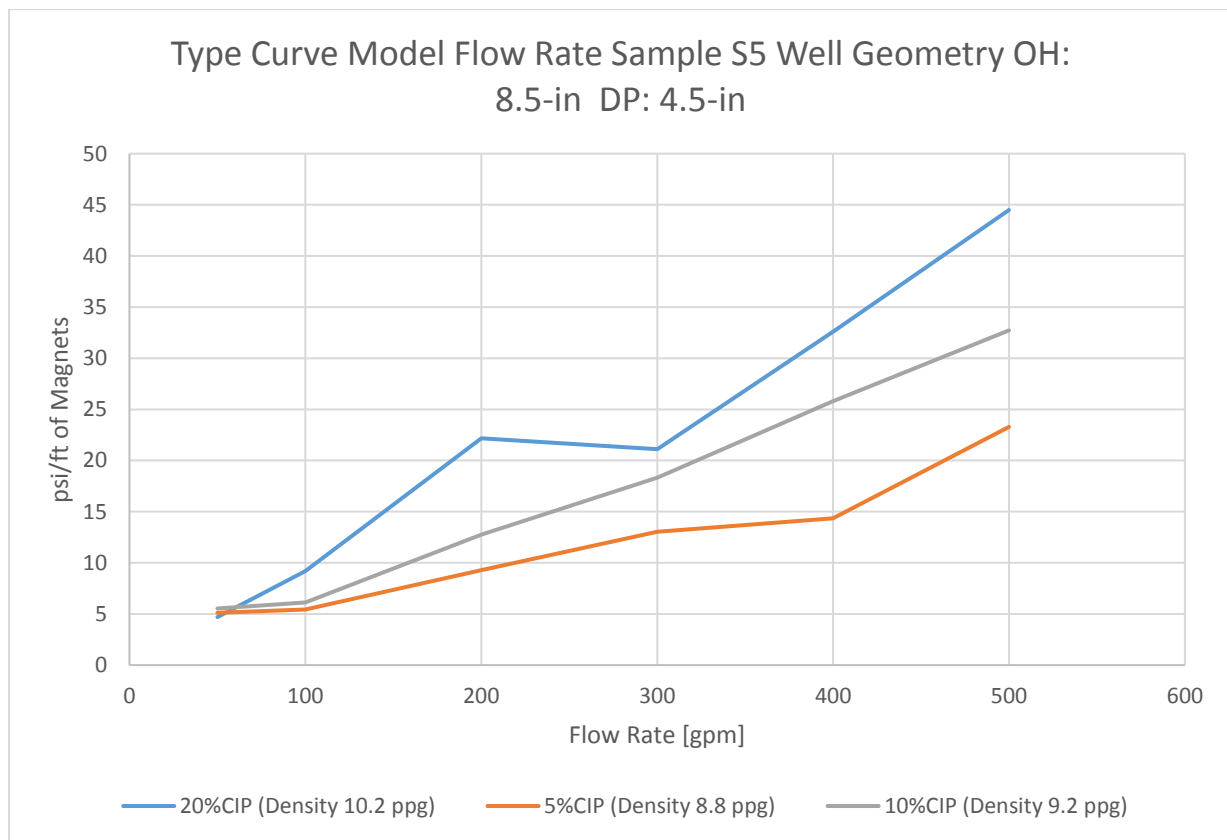


Fig. 39. Upscaled model from prototype. Flow rate vs psi/ft of magnets for sample S5 and well geometry OH: 8.5-in and DP OD: 4.5-in



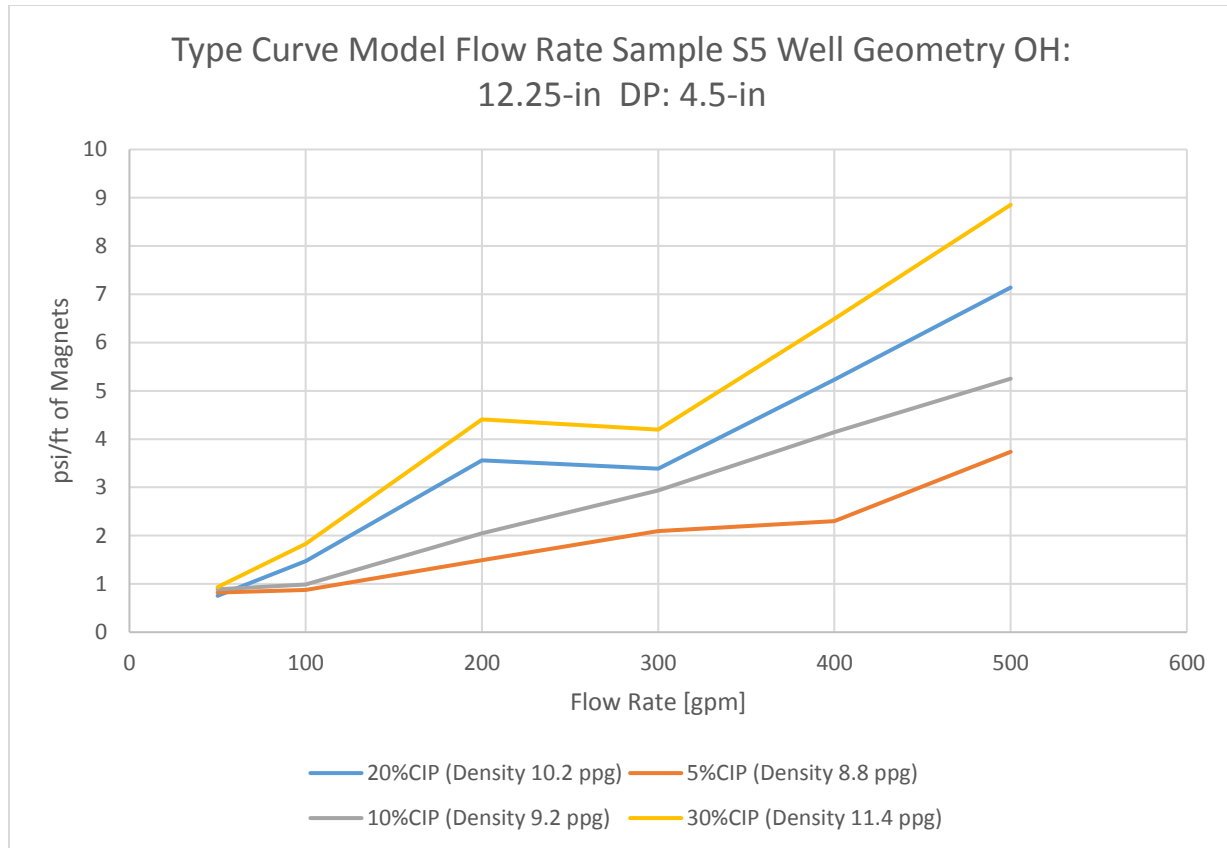


Fig. 40. Upscaled model from prototype. Flow rate vs psi/ft of magnets for sample S5 and well geometry OH: 12.25-in and DP OD: 4.5-in

Using the pressure drop generated above, a pressure profile can be modified at the bottom of the hole using permanent magnets to activate the MRF in front of magnetic source.

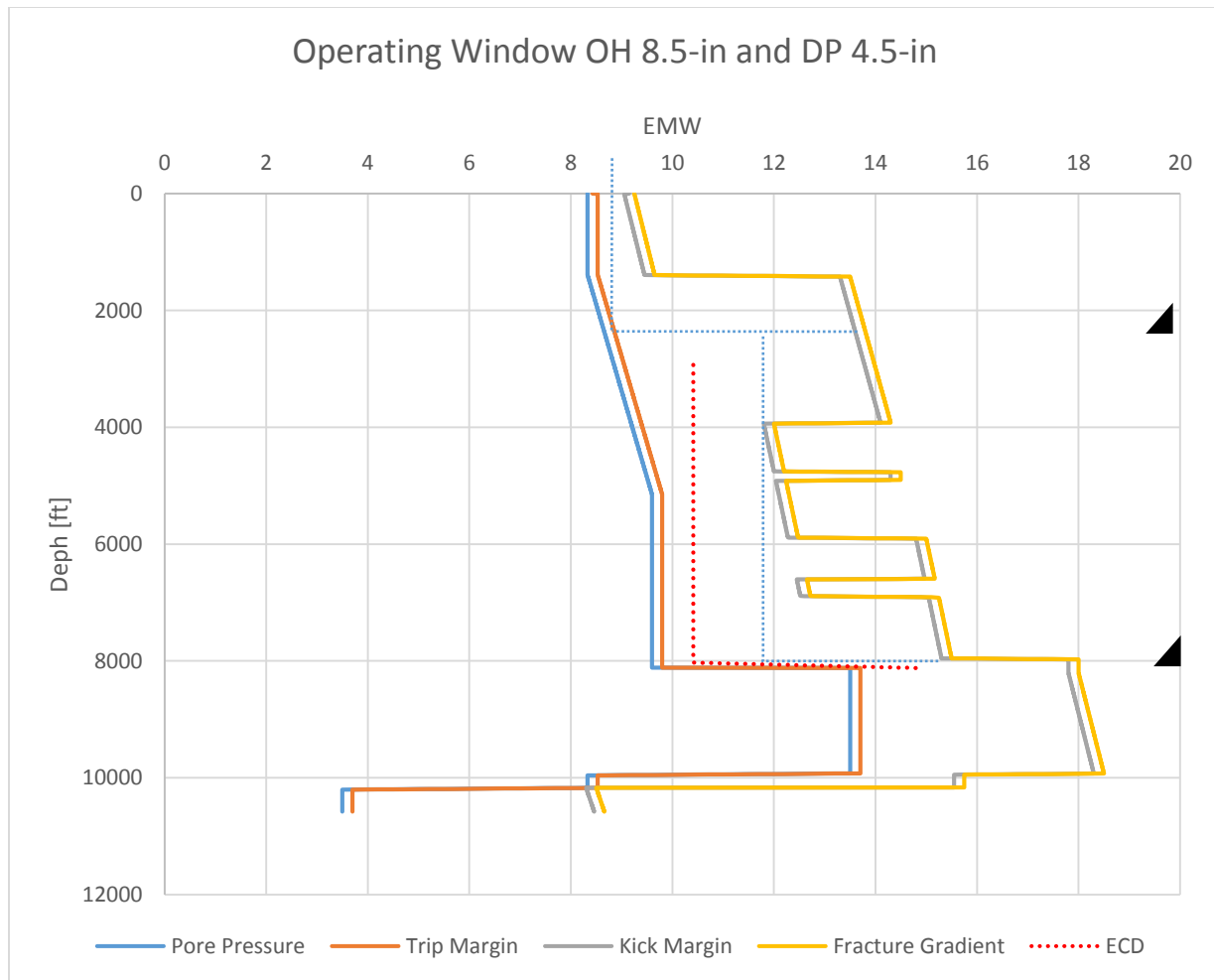


Fig. 41. Upscaled model from prototype. Depth vs EMW with magnet arrangement of 85-ft for sample S5 (CIP 20%wt) and well geometry OH: 8.5-in and DP OD: 4.5-in at 300 gpm.

The Fig. 41 describes the narrow operating window between the trip margin and the kick margin. One of the narrowest windows occurs close to 8000-ft. There is an abnormal pressure that makes a drastic increase of the equivalent pore pressure from near 9.8 ppge to 13.7 ppge, being the fracture gradient with its kick margin close to 15.3 ppge. This narrow window would require a casing to protect that section. To avoid setting a new casing, an 85-ft magnetic tool could be used at the proper flow rate to generate a pressure drop such that only the formations at and below the magnetic tool are affected by the pressure drop. Conventional MPD could not be used since that would increase the entire pressure profile and fracture at the depth of 4000-ft. From Fig. 39 at a flow rate of 300 gpm, the dimensionless analysis produced a drop pressure of about 20 psi/ft of magnets. Therefore, for the 85-ft of magnetic tool could produce enough

pressure to increase the EMW sequentially to be above the trip margin and below the kick margin. Thus, setting the casing at that depth would provide a zonal isolation of the weak zone and a higher room to use higher mud densities to overcome the abnormal pressure. A question mark remains in terms on the forthcoming operations after reaching the new depth using the MRF. Regularly, the BHA is pulled out of hole to run the casing and cement it. Stopping circulation will produce a reduction on the EMW and producing an underbalance condition consequently. Casing drilling could be advantageous to avoid stopping circulation.

Similarly, Fig. 42 describes the narrow operating window between the trip margin and the kick margin with another wellbore geometry. In this case the annulus is larger in comparison to the previous case study and therefore the pressure-drop achieved by the MRF is not at the same ratio. Using the prototype to model similarity from Fig. 33, at 300 gpm the pressure drop expected from the MRF in front of the magnets is of 3.5 psi/ft. To be able to create the pressure drop necessary to drill to 8123-ft, a length of 436-ft would be required. This is inconvenient in the sense that several stands need to be connected, cutting circulation momentarily. Because of this, a circulation at higher rates will produce a higher pressure drop or more conveniently a higher concentration of CIP will produce higher pressure drop.

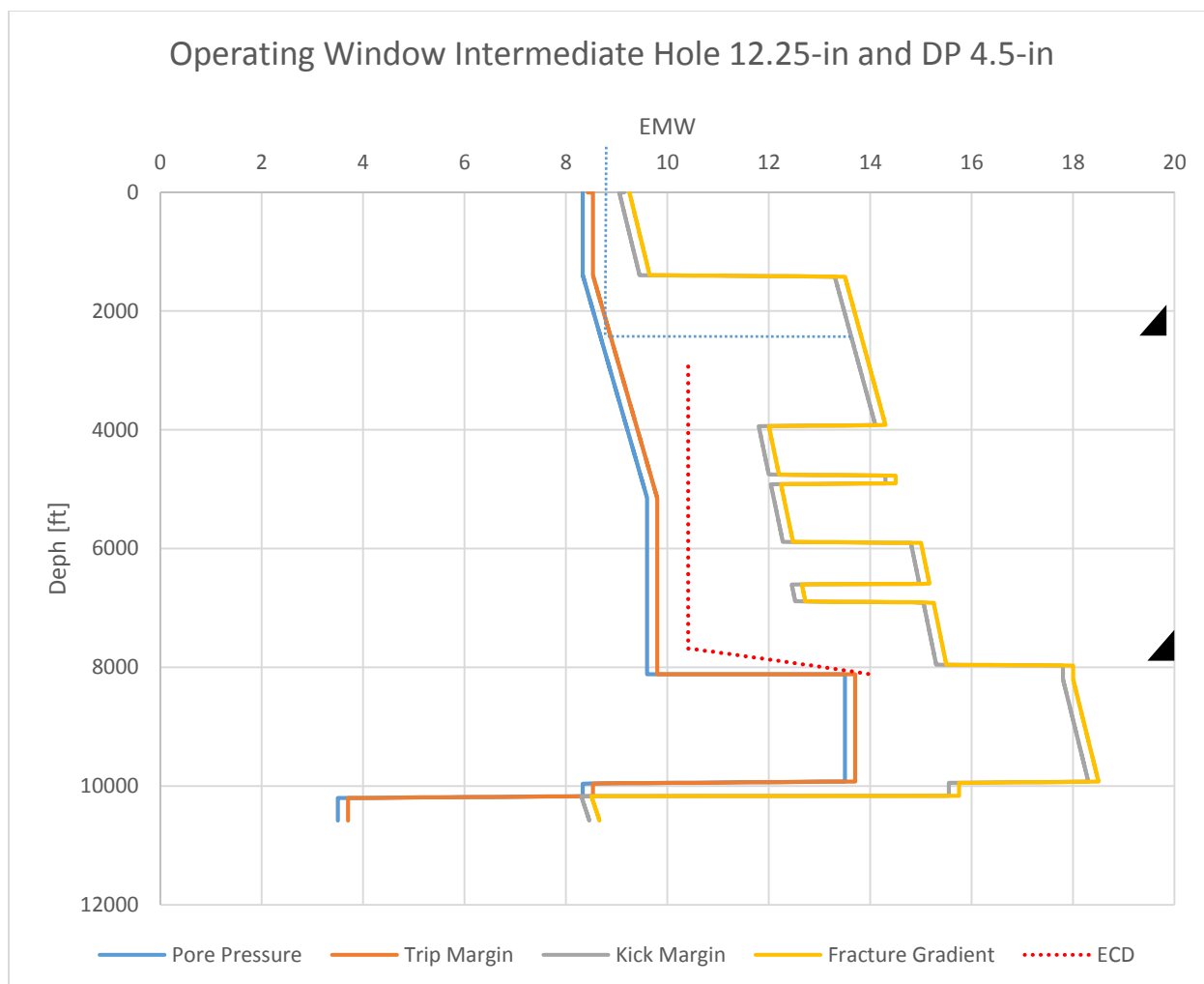


Fig. 42. Upscaled model from prototype. Depth vs EMW with magnet arrangement of 437-ft for sample S5 (CIP 20%wt) and well geometry OH: 12.25-in and DP OD: 4.5-in at 300 gpm.

Because of the challenge that the geometry supposes, a higher rate of 500 gpm and a concentration of CIP of 30% (Density 11.4-ppg) can generate a good pressure drop to shorten the length of the magnetic tool to 85-ft. Fig. 36 represents the ECD at the given conditions for a shorter tool.

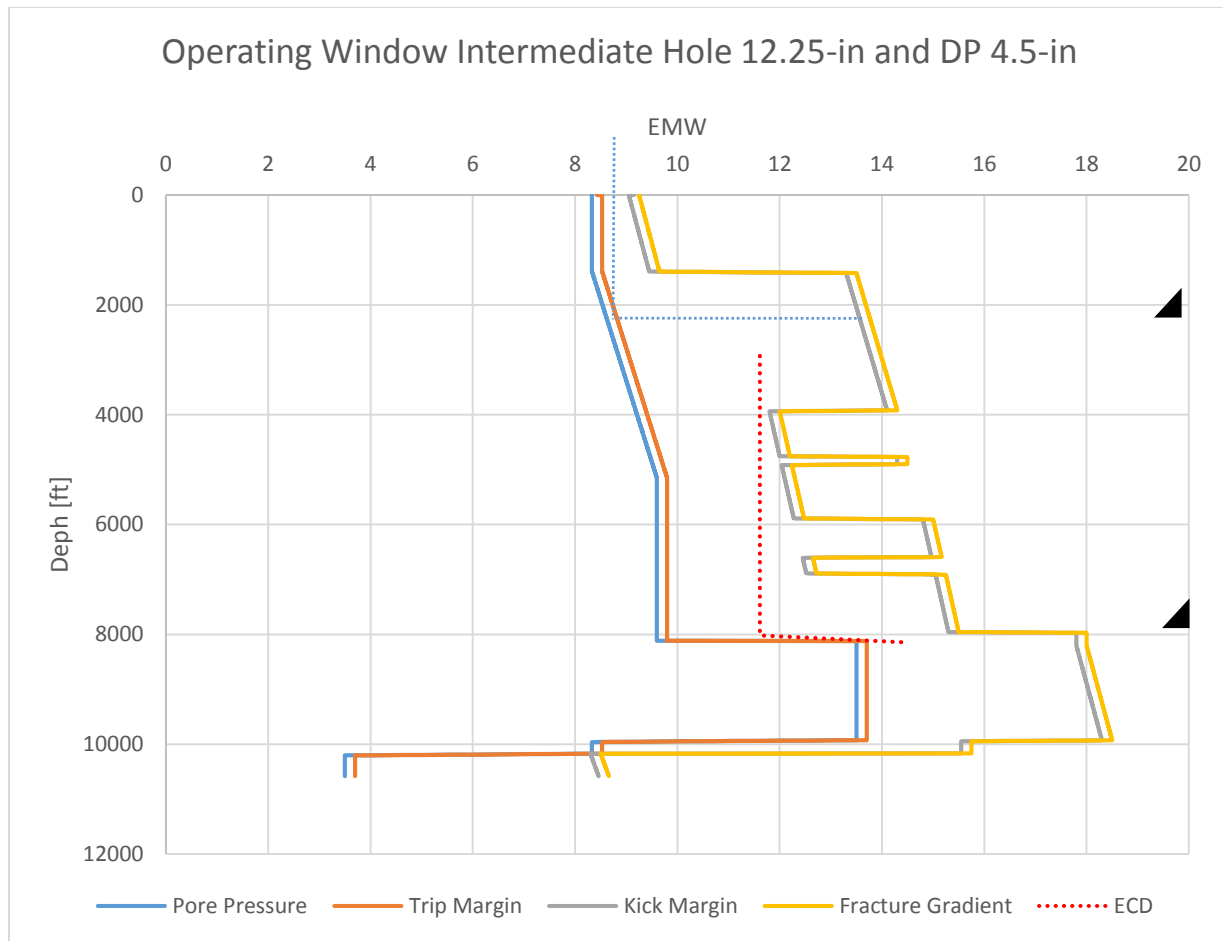


Fig. 43. Upscaled model from prototype. Depth vs EMW with magnet arrangement of 85-ft for sample S5 (CIP 30%wt) and well geometry OH: 12.25-in and DP OD: 4.5-in at 500 gpm.

Fig. 43. Exhibits an ECD above the trip margin and below the kick margin below the narrow operating window zone. In that sense, a modification on the flow rate and the concentration of CIP can represent an alternative to avoid settling a new casing.

## 5.2. Mason Number and Bingham Number:

The modeling of the MRF fluids has two perspectives: The microscopic modeling by examining the formation and destruction of the chain structures formed by the magnetizable particles in the presence of the magnetic field. The forces that form these chain structures are the viscous drag for the carrier fluid and the interparticle magnetic forces. The ratio of the interparticle magnetic forces to the viscous drag forces is known as the Mason number,  $Mn$  (Klingenberg, Ulicny, & Golden, 2007). To a larger scale, a controllable yield stress to an applied magnetic field can be represented by the Bingham number, which is the ratio of yield stress to

viscous stress. The Bingham number can be used to calculate flow rates, flow profiles and pressure losses in devices using the approximation to Bingham plastic fluids (Wereley & Pang, 1998). Also, an extrapolation of rheological measurements to higher shear rates can be achieved. Although the MRF evaluated in this research are better represented by the H-B model, an approximation can be used to upscaling purposes. Both Mason and Bingham numbers are dimensionless and represent fundamental descriptors of the MRF behavior at microscopic and macroscopic scales, respectively. Experimentally, (Sherman, Becnel, & Wereley, 2015) demonstrated that microscopic and macroscopic forces are linearly related and how the Mason/ Bingham relationship can inform the MRF fluid / Device design process. Mathematically these numbers are represented as follow and the derivations are encountered at (Sherman et al., 2015):

$$Bi = \frac{\tau_y}{\eta_{pl}\gamma_c} \quad (\text{Eq. 23})$$

$$Bi + 1 = \frac{\eta_{app}}{\eta_{pl}} \quad (\text{Eq. 24})$$

Where  $\tau_y$  is the magnetic field dependent Yield stress,  $\eta_{pl}$  is the plastic viscosity of the fluid, which is equivalent to the plastic viscosity without magnetic field and  $\gamma_c$  is the shear rate. The Bingham number is empirical, descriptive but does not provides information about what causes the MR effect. Interestingly, when the apparent viscosity  $\tau/\gamma$  is plotted against Mason the apparent viscosity curves collapse into a master curve of the apparent viscosity as function of the Mason number (Fig. 44). Thus, the Mason number acts as a non-dimensionalized input to relates to the Bingham number. This nondimensionalization of experimental data also allows to extrapolate to higher shear rates and different magnetic fields. Knowing these values, the Fanning friction number can be estimated to determine the pressure drop. Mathematically, the Mason number is expressed as function of the Magnetic Field intensity as follows:

$$Mn(H) = \frac{16\eta_c\gamma_c}{\mu_c\mu_0\beta^2H^2} \quad (\text{Eq. 25})$$

Where the  $\mu_0$  and  $\mu_c$  are the relative permeability of the particle and carrier fluid respectively. The measurement of these properties is required with a magnetometer.  $H$  is the magnetic field strength and

$$\beta = (\mu_p - \mu_c)/(\mu_p + 2\mu_c) \quad (\text{Eq. 26})$$

(Sherman, Becnel, & Wereley, 2015) experimentally demonstrated that the product of the Bingham number is a constant:

$$Bi Mn = 3\pi \frac{\tau_y/\tau}{\eta_{pl}/\eta_c} \quad (\text{Eq. 27})$$

$\tau_y/\tau$  is the normalized Yield Stress and  $\eta_{pl}/\eta_c$  the normalized viscosity.

The measurement of the of the apparent viscosity at different flow rates and different magnetic fields. Using Eq. 27 and Eq. 24 a plot of the normalized apparent viscosity to the Mason number is generated at different magnetic field. All the curves converge to a master curve in a very small variation. In that sense, if the relative permeability of the particle and the carrier fluids are known for a given magnetic field, the field dependent yield stress can be determined. Finally, Eq. 1 to Eq. 20 can be used for determining the pressure drop for a given geometry and flow rates.

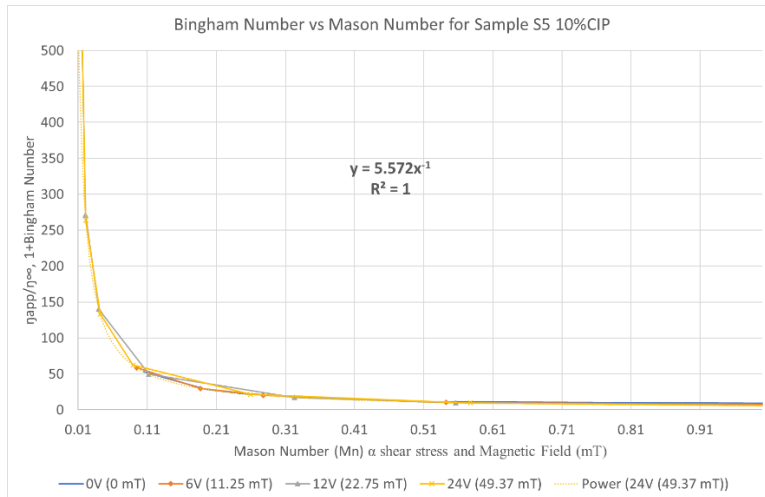


Fig. 44. Normalized apparent viscosity to Mason Number for Sample S5 10% CIP

## CONCLUSIONS AND FUTURE WORK

- A magnetic field responsive fluid was developed with the incorporation of Carbonyl Iron Powder (CIP), a magnetizable particle, on a water-bentonite dispersion. It has been shown that increasing the concentration of the CIP in the presence of a magnetic field is responsible for the modification of the rheological properties of the fluid. In that sense, a non-chemical rheology modification is presented experimentally. Particularly, the rheology effect can be predicted by determining the magnetic field dependent yield stress and the concentration of the magnetizable particles. The pressure drop on a laminar flow regime in a concentric annulus could be modeled considering the Herschel-Bulkley Model.
- The friction loss is as a function of the annular cross-sectional area, the fluid rheology and the flow rate. As the flow rate increases, the friction loss increases proportionally. As the annular cross-sectional area decreases, the friction loss increases. Additionally, the pressure drop increases as the fluid yield stress non-newtonian fluids increases. Therefore, the pressure drop is also a function of the CIP concentration of the MRF and the intensity of the magnetic field.
- For downhole or surface equipment applications with the use of MRF, two simplified variables are required to be known to create the desired effect. On the one hand, the field dependent yield stress as a function of the CIP concentration. On the other hand, the field dependent magnetic field as a function of the magnetic field intensity. An optimized balance between these two variables can provide the feasibility of its applications.
- A packing effect development was observed after the MRF sample S0 remained static for a period of 60 hours. The preliminary interpretation is that this effect could be created through the built-up of the magnetizable particles in front of a magnetic field. This suggests that, depending on the magnetic geometry and strength, and the design of the MR fluid, the magneto-rheological effect versus the physical blockage because of magnetic particles built-up around the magnet behaves differently.



- In the case of the experiments performed with sample S0, the pressure drop effect can be increased as a function of the time exposure to the magnetic field and to a lower extent, to the instantaneous rheology modification when the MRF crosses in front of the magnetic field.
- Pressure drop per unit length measurements in the two sections that did not contain magnets were the same. This suggests that effectively, and as expected, the rheology modification due to the magnetic field occurs only in front of the magnets. This represents an advantage to the MRF to modify its rheology locally when required and being capable to reverse to its original conditions in the absence of a magnetic field.
- Most of the literature studied the rheology of the MRF on two-plates rheometers with gap between the two plates of 0.5 mm (Rich et al., 2012). This geometry and narrow slot hinders the effect that sedimentation may have on the rheology measurements. On the contrary, the rotational viscometer used in this study propends the settling of the particles due to gravitational forces due to the larger distance from the Bob to the bottom of the cup. Because of this, some shear stresses and therefore yield stresses could have been underestimated as the concentration of the CIP decrease in front of the Bob as the particles settled. The reading at higher concentration of CIP after several cycles of magnetization and demagnetization showed erratic or lower expected values. The remaining magnetization of the particles, if any, can lead to the agglomeration of the particles and its subsequent sedimentation. The remaining magnetization of the particles was not studied but could be of interest to determine if the cycles of magnetization and demagnetization provoke any hysteresis in terms of rheology changes and exacerbation of the particle sedimentation.
- The dynamic field dependent yield stress was obtained by decreasing the shear rate and extrapolating the measured stress values to the shear rate equivalent to  $0 \text{ s}^{-1}$ . This model is represented by the Modified Power Law model known as Herschel-Bulkley. Curve fitting was used to determine the yield shear stress ( $\tau_0$ ), the flow index ( $n$ ), and the fluid consistency ( $k$ ).

- For this research, to protect the integrity of the electromagnets, the effect of temperature in the behavior of the MRF was not evaluated. However, it is expected that the temperature may have a direct impact in the behavior of the MRF. Principally, the temperature affects the magnetization behavior of the magnetizable particles, the base fluid shear viscosity, and the carrier fluid thermal expansion.
- It was observed that at shear rates larger than  $400 \text{ s}^{-1}$ , the shear stress decreased as the shear rate increased. The theory associates this type of behavior to thixotropic fluids or fluids that form strong gels at low shear rates. In this sense, it is logical to accept an MRF with gelling properties that withhold the high density magnetizable particles static or at low shear rates and that behaves more as a conventional pseudoplastic fluid at higher shear rates. Further study is needed to overcome the effect of sedimentation at higher shear rates or after cycles of magnetization and demagnetization.
- The sample S8a and S0, which used Bentonite as the stabilizer, exhibits a good development of shear stress but as shown in Appendix F, this mixture produces an aggravated corrosion issue of the CIP particles, later in time. This phenomenon was broadly observed during the experimental phase. Future studies are required to determine the main causes. A hypothesis is that the montmorillonite, the main component of the Bentonite, a mineral from the group of phyllosilicates is structurally formed by aluminum and magnesium arranged octahedrally in form of oxides and hydroxides, is provoking the accelerated oxidation of the ferrous components of the CIP. Therefore, the ferric oxide  $\text{Fe}_2\text{O}_3$  responsible for the brown color in the sample is forming from either the dissolved  $\text{O}_2$  in the water or from the oxygen free radicals from the Silicon Dioxide  $\text{SiO}_2$  that constitutes about 61.4% of the Montmorillonite. The samples that did not contain bentonite as the stabilizer did not exhibit any corrosion even after two months of preparation, whereas the samples containing bentonite were all corroded. This suggests that the oxidation is primarily due to the Silicon Dioxide rather than the  $\text{O}_2$  dissolved in water.

- The samples that contained silicone oil as the carrier fluid and stearic acid as the stabilizer (Sample S1 and S6) are the ones that exhibited the highest and fastest sedimentation among the samples. For future works, mixing an emulsion and defining the proper emulsifier to increase the interfacial tension could provide better results in terms of lowering the settling ratio. On the other hand, the samples with carrier fluid water and Laponite RD exhibited a higher sedimentation control as the concentration of Laponite RD increased. However, extremely high concentration of Laponite RD (larger than 2%) produce aggravated gelation that makes the MRF behave more as a cross-linked fluid. As presented before, the MRF require to remain fluid in OFF states and only to develop higher rheology under the influence of the magnetic field. The optimum concentration of Laponite RD is 1.5% because it has low rheology and good control against particle settling.
- From the samples studied, the particle settling is developed at an early stage between the first week after mixing (168 hours). Later than that, the settling ratio remains almost steady.
- While evaluating the circulating MRF Sample S5 subject to a magnetic field in the outlet of the flow-loop, it was observed that the pressure in all the transducers increased simultaneously at a same proportion of 0.5 to 0.8 psi per activation of the electromagnets. This is the main principle of Managed Pressure Drilling (MPD) where a surface choke aperture regulates the amount of back pressure to apply to the system to control the bottom hole pressure. The industry have manual operated chokes with dedicated personnel controlling the choke apperture. There are also automatic chokes that can be regulated based on a hydraulic software. In both cases, manual or automatic chokes are formed by a physical restriction that modifies its flowing area. Since the drilling mud circulates at higher flow rates, the solids contained in the mud can erode the physical restriction of the choke. In that sense, an electromagnetic choke that activates the flowing MRF could create a flow restriction and therefore a back pressure. Additionally, the electromagnetic choke could provide a finer aperture of the choke when the magnetic field is modified accordingly.

- Based on the correlations and the pressure behavior of the MRF in presence of a magnetic field, the hypothesis is that a higher pressure-drop can be generated when the length of the permanent magnets is increased. Similarly, as the magnetic field is increased the pressure drop increases. For future works, a modification of the length of the magnet arrangement will provide the evidence to these claims.

## REFERENCES

- Abbasy, I., & Ritchie, B. (2010). Challenges in Completing Long Horizontal Wells Selectively. *SPE Drilling & Completion*. Retrieved from <https://www.onepetro.org/download/journal-paper/SPE-116541-PA?id=journal-paper%2FSPE-116541-PA>
- Alexeyenko, A. V., & Aramco, S. (2014). SPE-172173-MS Statistical Approach to Forecasting Fluid Loss Solutions, (April), 21–24.
- Almond, K., Coull, C., Spe, P. K., Smith, J., Smith, M. V, Baker, S. P. E., ... Spe, S. W. (2002). SPE 77519 Improving Production Results in Monobore , Deepwater and Extended Reach Wells Tier I : Open Hole Completion.
- American Petroleum Institute. (2009). API Recommended Practice 13D – Rheology and hydraulics of oil-well drilling fluids.
- Ashtiani, M., & Hashemabadi, S. H. (2015). An experimental study on the effect of fatty acid chain length on the magnetorheological fluid stabilization and rheological properties. *Colloids and Surfaces A: Physicochemical and Engineering Aspects*, 469, 29–35. <https://doi.org/10.1016/j.colsurfa.2014.12.046>
- Ashtiani, M., Hashemabadi, S. H., & Ghaffari, A. (2015). A review on the magnetorheological fluid preparation and stabilization. *Journal of Magnetism and Magnetic Materials*, 374, 716–730. <https://doi.org/10.1016/j.jmmm.2014.09.020>
- Ashtiani, M., Hashemabadi, S. H., & Ghaffari, A. (2015). A review on the magnetorheological fluid preparation and stabilization. *Journal of Magnetism and Magnetic Materials*, 374, 711–715. <https://doi.org/10.1016/j.jmmm.2014.09.020>
- Back to Basics*. (2013). Retrieved from [www.aiche.org/cep](http://www.aiche.org/cep)
- Bårdsen, J., Hazel, P., Vasques, R. R., Hjorteland, Ø., Welltec, A. S., & Eikeskog, Ø. (2014). Improved Zonal Isolation in Open Hole Applications.
- Beirute, R. M. (1978). Flow Behavior of an Unset Cement Plug in Place. *Spe*, (SPE 7589). <https://doi.org/10.2118/7589-MS>
- Bossis, G., Lemaire, E., Volkova, O., Clercx, H., & Lemaire, ) E. (1997). Magnetorheology of magnetic holes compared to magnetic particles. *Structure-Enhanced Yield Stress of Magnetorheological Fluids Journal of Applied Physics*, 41, 91. <https://doi.org/10.1122/1.550838>
- Brian Mitchell Southern, B., Ahmadian, M., & Corina Sandu Fernando Goncalves, C. D. (2008). Design and Characterization of Tunable Magneto-Rheological Fluid-Elastic Mounts. Retrieved from [https://vtchworks.lib.vt.edu/bitstream/handle/10919/32654/Southern\\_MSME\\_05\\_30\\_08.pdf?sequence=1](https://vtchworks.lib.vt.edu/bitstream/handle/10919/32654/Southern_MSME_05_30_08.pdf?sequence=1)
- Brown, E., Thomas, R., & Milne, A. (1990). The Challenge of Completing and Stimulating Horizontal Wells. *Oilfield Review*.
- Cho, M., Lim, S., Jang, I., ... H. C.-I. T. on, & 2004, undefined. (n.d.). Encapsulation of spherical iron-particle with PMMA and its magnetorheological particles. *Ieeexplore.ieee.org*. Retrieved from <https://ieeexplore.ieee.org/abstract/document/1325724/>
- Daneshy, A. (2011). Hydraulic Fracturing of Horizontal Wells: Issues and Insights. *SPE Hydraulic Fracturing Technology Conference*, (January), 24–26. <https://doi.org/10.2118/140134-MS>

- Elizabeth Premalatha, S., Chokkalingam, R., & Mahendran, M. (2012). Magneto Mechanical Properties of Iron Based MR Fluids. *American Journal of Polymer Science*, 2(4), 50–55. <https://doi.org/10.5923/j.ajps.20120204.01>
- Ermila, M., Eustes, A. W., & Mokhtari, M. (2012). Using magneto-rheological fluids to improve mud displacement efficiency in eccentric annuli. *SPE Eastern Regional Meeting*, 17–29. Retrieved from <http://www.scopus.com/inward/record.url?eid=2-s2.0-84873803403&partnerID=tZOtx3y1>
- Estrada, J., Akbari, B., & Nielsen, G. (2018). Use of Magnetorheological Fluids for Pressure Drop Generation. In *Offshore Technology Conference*. Offshore Technology Conference. <https://doi.org/10.4043/28749-MS>
- Ghalambor, A., Salehi, S., Shahri, M. P., & Karimi, M. (2014). Integrated Workflow for Lost Circulation Prediction. *SPE International Symposium and Exhibition on Formation Damage Control*. <https://doi.org/10.2118/168123-MS>
- Goncalves, F., Güth, D., & Maas, J. (2015). Characterization and modeling of the behavior of magnetorheological fluids at high shear rates in rotational systems. *Journal of Intelligent Material Systems and Structures*, (January), 114. <https://doi.org/10.1177/1045389X15577646>
- Hajalilou, A., Amri Mazlan, S., Lavvafi, H., & Shameli, K. (2016). *Field Responsive Fluids as Smart Materials*. <https://doi.org/10.1007/978-981-10-2495-5>
- Hajalilou, A., Amri Mazlan, S., Lavvafi, H., & Shameli, K. (2016). Magnetorheological (MR) Fluids (pp. 13–50). [https://doi.org/10.1007/978-981-10-2495-5\\_3](https://doi.org/10.1007/978-981-10-2495-5_3)
- Hajalilou, A., Amri Mazlan, S., Lavvafi, H., & Shameli, K. (2016). Models and Modes in MR Fluids (pp. 51–65). [https://doi.org/10.1007/978-981-10-2495-5\\_4](https://doi.org/10.1007/978-981-10-2495-5_4)
- Hecker, M. T., Barry, M. D., Ryan, J. T., Ruiz, V. F., Stevens, P., & Development, E. (2011). SPE 146361 First Installation of Alternate Path Openhole Packer Providing True Zonal Isolation in Openhole Gravel Packs, (Block 15), 1–11.
- Hills, R., & Yurgelevic, S. M. (2003). ( 12 ) United States Patent -A- WITHOUT ADDITIVES, 2(12).
- Hyeok Park, J., Hyun Kwon, M., & Park, O. (n.d.). *Rheological Properties and Stability of Magnetorheological Fluids using Viscoelastic Medium and Nanoadditives* (Vol. 18). Retrieved from [https://link-springer-com.libezp.lib.lsu.edu/content/pdf/10.1007%2F978-1-4939-9063-1\\_1.pdf](https://link-springer-com.libezp.lib.lsu.edu/content/pdf/10.1007%2F978-1-4939-9063-1_1.pdf)
- Javier, U., Krishna, R., Jaime, P., Oscar, J., & John, P. (2016). Low Solids Shear Dependent Fluid System to Plug Zones for Preventing Fluid Influx and Loss.
- Joseph, M., Jin, H., Hoon, H., Oh, B., & Sinha, S. (2011). Colloids and Surfaces A : Physicochemical and Engineering Aspects Magnetic carbonyl iron suspension with organoclay additive and its magnetorheological properties. *Colloids and Surfaces A: Physicochemical and Engineering Aspects*, 377(1–3), 103–109. <https://doi.org/10.1016/j.colsurfa.2010.12.029>
- Kang Hyun Song, Bong Jun Park, & Hyoung Jin Choi. (2009). Effect of Magnetic Nanoparticle Additive on Characteristics of Magnetorheological Fluid. *IEEE Transactions on Magnetics*, 45(10), 4045–4048. <https://doi.org/10.1109/TMAG.2009.2025390>
- Karimi, M., Ghalambor, A., Montgomery, M., Moellendick, E., & Corporation, T. (2011). SPE 143656 Formation Damage and Fluid Loss Reduction due to Plastering Effect of Casing Drilling, (Lcm). <https://doi.org/10.2118/143656-MS>
- Kelessidis, V. C., Dalamarinis, P., & Maglione, R. (2011). Experimental study and predictions of pressure

- losses of fluids modeled as Herschel-Bulkley in concentric and eccentric annuli in laminar, transitional and turbulent flows. *Journal of Petroleum Science and Engineering*, 77(3–4), 305–312. <https://doi.org/10.1016/j.petrol.2011.04.004>
- Klingenberg, D. J., Ulicny, J. C., & Golden, M. A. (2007). Mason numbers for magnetorheology. *Journal of Rheology*, 51(5), 883–893. <https://doi.org/10.1122/1.2764089>
- Kolekar, S. (2014). Preparation of Magnetorheological Fluid and Study on Its Rheological Properties. *International Journal of Nanoscience*, 13(2), 1450009 (1-6). <https://doi.org/10.1142/S0219581X14500094>
- Laun, H. M., Kormann, C., & Willenbacher, N. (1996). Rheometry on magnetorheological (MR) fluids. *Rheologica Acta*, 35(5), 417–432. <https://doi.org/10.1007/BF00368993>
- Liu, X., Lu, H., Chen, Q., Wang, D., & Zhen, X. (2013). Study on the preparation and properties of silicone oil-based magnetorheological fluids. *Materials and Manufacturing Processes*, 28(6), 631–636. <https://doi.org/10.1080/10426914.2013.773017>
- Liu, Y. D., Choi, H. J., & Choi, S.-B. (2012). Controllable fabrication of silica encapsulated soft magnetic microspheres with enhanced oxidation-resistance and their rheology under magnetic field. *Colloids and Surfaces A: Physicochemical and Engineering Aspects*, 403, 133–138. <https://doi.org/10.1016/J.COLSURFA.2012.04.002>
- Loginov, A., & International, T. A. M. (2015). Innovative Borehole Treatment Utilising Inflatable Packer Straddle System Technology.
- Malik, A. R., Leal, J. A., Asiri, M. A., Ogundare, T. M., Soriano, E., Vega, R., & Lopez, A. (2016). Overcoming Open Hole Multistage Acid Fracturing Challenges in Saudi Arabian Carbonate Reservoirs with Swellable Packers, Best Practices and Dynamic Evaluation. *SPE/IADC Middle East Drilling Technology Conference and Exhibition*. <https://doi.org/10.2118/178159-MS>
- Martin, J. E., & Anderson, R. A. (1996). Polarization forces and conductivity effects in electrorheological fluids. *Induced Fibration of Suspensions Journal of Applied Physics*, 104, 91. <https://doi.org/10.1063/1.471176>
- Modular, T., & Series, R. (n.d.). Physica MCR Physica MCR Modular Compact Rheometer Physica MCR.
- Nair, S. D., & Ferron, R. D. (2014). Set-on-demand concrete. *Cement and Concrete Research*. <https://doi.org/10.1016/j.cemconres.2013.12.001>
- Nair, S. D., Wu, Q., Cowan, M., & Oort, E. Van. (2015). Cement Displacement and Pressure Control Using Magneto-Rheological.
- Rich, J. P., Doyle, P. S., & McKinley, G. H. (2012). Magnetorheology in an aging, yield stress matrix fluid. *Rheologica Acta*, 51(7), 579–593. <https://doi.org/10.1007/s00397-012-0632-z>
- Rivenbark, M., & Appleton, J. (2013). Cemented Versus Open Hole Completions: What is Best for Your Well? *Proceedings of 2013 SPE Middle East Unconventional Gas Conference & Exhibition*, (January), 28–30. <https://doi.org/10.2118/163946-MS>
- Sairam, P. K. S., Pangu, G., & Gajji, B. (2015). Innovative and Modular Equipment Design for Rheology and Compatibility Measurement of Complex Wellbore Fluids.
- Sherman, S. G., Becnel, A. C., & Wereley, N. M. (2015). Relating Mason number to Bingham number in magnetorheological fluids. *Journal of Magnetism and Magnetic Materials*, 380, 98–104.

<https://doi.org/10.1016/j.jmmm.2014.11.010>

Stair, T., & Makowiecki, G. (2016). SPE/IADC-178212-MS Improved Validation Method for Annular Casing Packers, (January), 26–28.

Tang, H. S., & Kalyon, D. M. (2004). Estimation of the parameters of Herschel-Bulkley fluid under wall slip using a combination of capillary and squeeze flow viscometers. *Rheologica Acta*.  
<https://doi.org/10.1007/s00397-003-0322-y>

Vryzas, Z., Kelessidis, V. C., Bowman, M. B. J., Texas, A., & Nalbantian, L. (2017). SPE-183906-MS Smart Magnetic Drilling Fluid With In-Situ Rheological Controllability Using.  
<https://doi.org/10.2118/183906-MS>

Wang, D., Zi, B., Zeng, Y., Hou, Y., & Meng, Q. (2014). Temperature-dependent material properties of the components of magnetorheological fluids. *Journal of Materials Science*, 49(24), 8459–8470.  
<https://doi.org/10.1007/s10853-014-8556-x>

Wereley, N. M., & Pang, L. (1998). Nondimensional analysis of semi-active electrorheological and magnetorheological dampers using approximate parallel plate models. *Smart Materials and Structures*, 7(5), 732–743. <https://doi.org/10.1088/0964-1726/7/5/015>

Whitfill, D., Wang, H., & Systems, H. F. (2005). SPE 95561 Making Economic Decisions To Mitigate Lost Circulation.

Zitha, P. L. J., & Wessel, F. (2002). Fluid Flow Control Using Magnetorheological Fluids. *Proceedings of SPE/DOE Improved Oil Recovery Symposium*, 1–10. <https://doi.org/10.2523/75144-MS>



## APPENDIX A: MAGNETIC FIELD MEASUREMENTS AT VISCOMETER BOB.

Table A1. Magnetic Field [mTesla] measured at the Viscometer Bob

Standard						
	Voltage	6V	12V	18V	24V	48V
Location						
1		7	12	49	27	57
2		11	22	40	55	102
3		16	32	50	71	138
4		11	26	45	51	120
5		9	19	30	40	80
6		11	22	35	43	105
7		15	29	45	58	130
8		10	20	20	50	99

Rotor		
	Voltage	48V
Location		
3		117
7		95

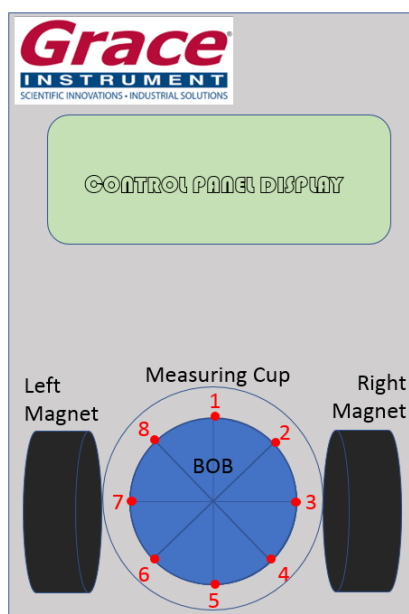


Fig. A1. Red dots indicate the location of measurement of the magnetic field [mT]

Voltage is at the top in [volts]. Magnetic field strength measured values are in [mT].

Locations are all on the outside of the bob (therefore the exact measurement area) and are parallel to the magnetic field lines. All magnetic field lines go from one magnet to the other. The magnets appear to be setup so that one has its south magnet facing the fluid and the other has its north magnet facing the fluid.

Locations as in Fig. A1:

All measurements have the bob in place, and the rotor not in place. The cup was also in place for those measurements.

Additional measurements were without the cup or the bob, but with the rotor in place. They could be slightly lower because the location is slightly farther from the magnets because of how the bob and rotor are located.

Highlighted values are low values likely due to the magnets not being in the correct place. Also the electromagnet, and the cup for that matter, tilt slightly to the left side.

**APPENDIX B: CERTIFICATE OF ANALYSIS CARBONYL IRON POWDER (AMERICAN ELEMENTS)**

Table B1. Certificate of analysis of 99.5% Carbonyl Iron Powder used for the experimental phase



THE MATERIALS SCIENCE COMPANY®

10884 WEYBURN AVE. LOS ANGELES, CA 90024  
TEL: 310-208-0551 • FAX 310-208-0351 • E-MAIL: shipping@americanelements.com

**CERTIFICATE OF ANALYSIS**  
**99.5% (metals basis) Carbonyl - Iron Powder**

**Fe**

**Product Code: CBL-FE-025M-P.10UM**

**Lot #: 6971282447-460**

**CAS #: 7439-89-6**

**Description: Powder**

<u>Analysis</u>	<u>%</u>
Fe	98.6
C	0.68
O	0.18
N	0.10

## APPENDIX C: MAGNETIC FIELD READINGS AT THE PERMANENT MAGNETS

Table C1. Magnetic Field [mTesla] measured at the permanent magnets in different locations

Magnetic Field [mTesla]					
Small	Small	Large	Large	Degrees	Distance
S over N	N over S	N over S	S over N	from the	from the
322	108 N	313 N	325	0	0
298	162 N	288 N	290	45	0
273	99 N	278 N	270	90	0
234	112 N	325 N	260	135	0
241	108 N	280 N	365	180	0
255	124 N	300 N	270	225	0
216	190 N	318 N	310	270	0
264	180 N	308 N	300	315	0
14	*	60 N	63	0	0.25
6	*	45 N	40	0	0.5
5	*	31 N	25	0	0.75
4	*	15 N	13	0	1
6	*	17 N	16	0	1.25
4	*	11 N	12	0	1.5
2	*	9 N	7	0	1.75
1	*	6 N	3	0	2

\*Due to the thickness of the epoxy/paint coating, as well as the opacity of the paint the probe is not certain to be located at above the magnets

Individual	Readings		
		1	4
	Location	Large	Small
		N over S	S over N
On magnet	downstream	186 N	206 S
	middle	306 N	247 S
	upstream	336 N	267 S
In-Between Magnet	downstream	61 N	
	middle	70 N	78 S
	upstream	57 N	

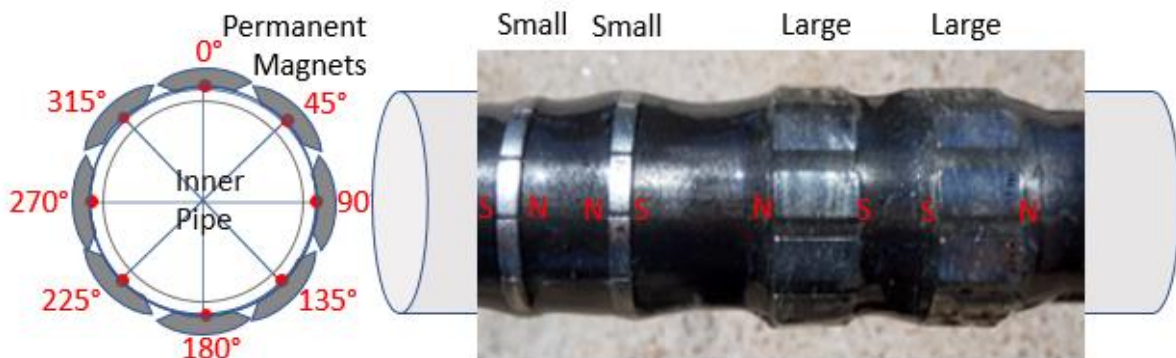


Fig. C1. Magnetic Field Measurement at permanent magnets

APPENDIX D: PUMP MOTOR SPECIFICATIONS

**BALDOR • RELIANCE** Product Information Packet: VEM3611T - 3HP,1760RPM,3PH,60HZ,182TC,3632M,TEFC,F1

Nameplate NP3441LUA															
CAT.NO.		VEM3611T													
SPEC		36A003S266G2													
HP		3													
VOLTS		230/460													
AMPS		8.4/4.2													
RPM		1760													
FRAME		182TC				HZ		60		PH		3			
SF		1.15		CODE		K		DES		B		CLASS		F	
NEMA NOM. EFF		89.5		PF		75									
RATING		40C AMB-CONT													
CC		010A		USABLE AT 208V						9					
ENCL		TEFC		SER											
DE		6206		ODE		6205									
VPWM INVERTER READY															
CT8-60H(10:1)/VT3-60H(20:1															
50Hz 3HP 190/380V 9.6/4.8A														SF1.0	

Fig. D1. Pump motor VEM3611T – 3HP specifications

APPENDIX E: PRESSURE RELIEF VALVE DISCHARGE ORIFICE AREA DETERMINATION

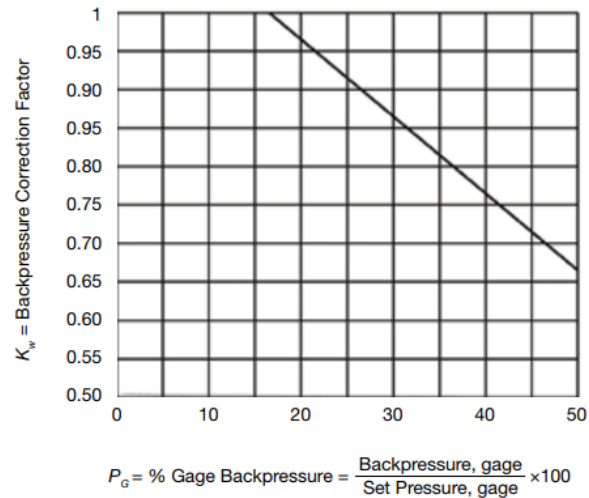


Fig. E1. Backpressure correction factor at different vs the ratio of backpressure and set pressure (*Back to Basics*, 2013)

$K_w$  is the adjusted factor for backpressure (unitless). This value is 1.0 for conventional relief valves in liquid service. For balanced-bellows relief valves the value is generally obtained from the manufacturer. The Fig. E1 provides preliminary values. The set pressure is the value at which the relief is expected. For this experimental setup is 100 psi. The back pressure is the atmospheric pressure.

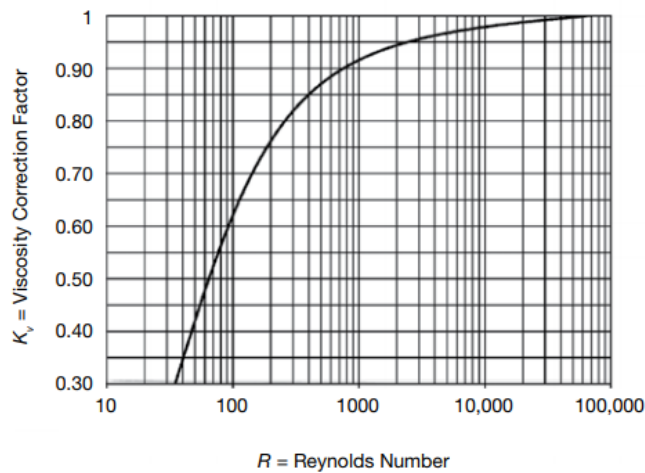


Fig. E2. Viscosity Correction Factor vs Reynolds Number (*Back to Basics*, 2013)

Determining the proper viscosity correction requires an iterating process since the area must be known to determine the Reynolds number. Assume  $K_v$  equal to 1.0 to determine the Reynolds number. This factor includes the discharge velocity based on the viscosity of the fluid.

## APPENDIX F: STUDY OF RHEOLOGY AND SETTLING RATIO OF SAMPLES S1, S2, S3, S4, S6, S7A, S7B, S8A, S8B, S9 AND S9A

### Sample S1:

The silicone oil high viscosity provides a high viscosity of the mixture. The stearic acid didn't dissolve in the silicone oil at room temperatures. While mixing, the friction of the impellers increased the temperature of the mixture, at 120°F the stearic acid pallets dissolved completely.

The sample was tested at different concentrations of CIP measuring the rheology at different magnetic fields. It was observed a rapid reaction of the mixture when a magnetic was on or off as shown on Fig. F1.



Fig. F1. Sample S1 CIP 15wt% reaction to 48V ON/OFF

However, it is observed after 10 seconds of applied magnetic field how the CIP particles tend to separate from the mixture, leaving the silicone oil and the stearic acid as a separate phase. Additional mixing at higher shear rates homogenizes the mixture to its original form.

Additionally, at high shear rates and high magnetic field, the readings exceeded the maximum torque of the equipment. The results of the rheology measurements are presented in Fig. F2:



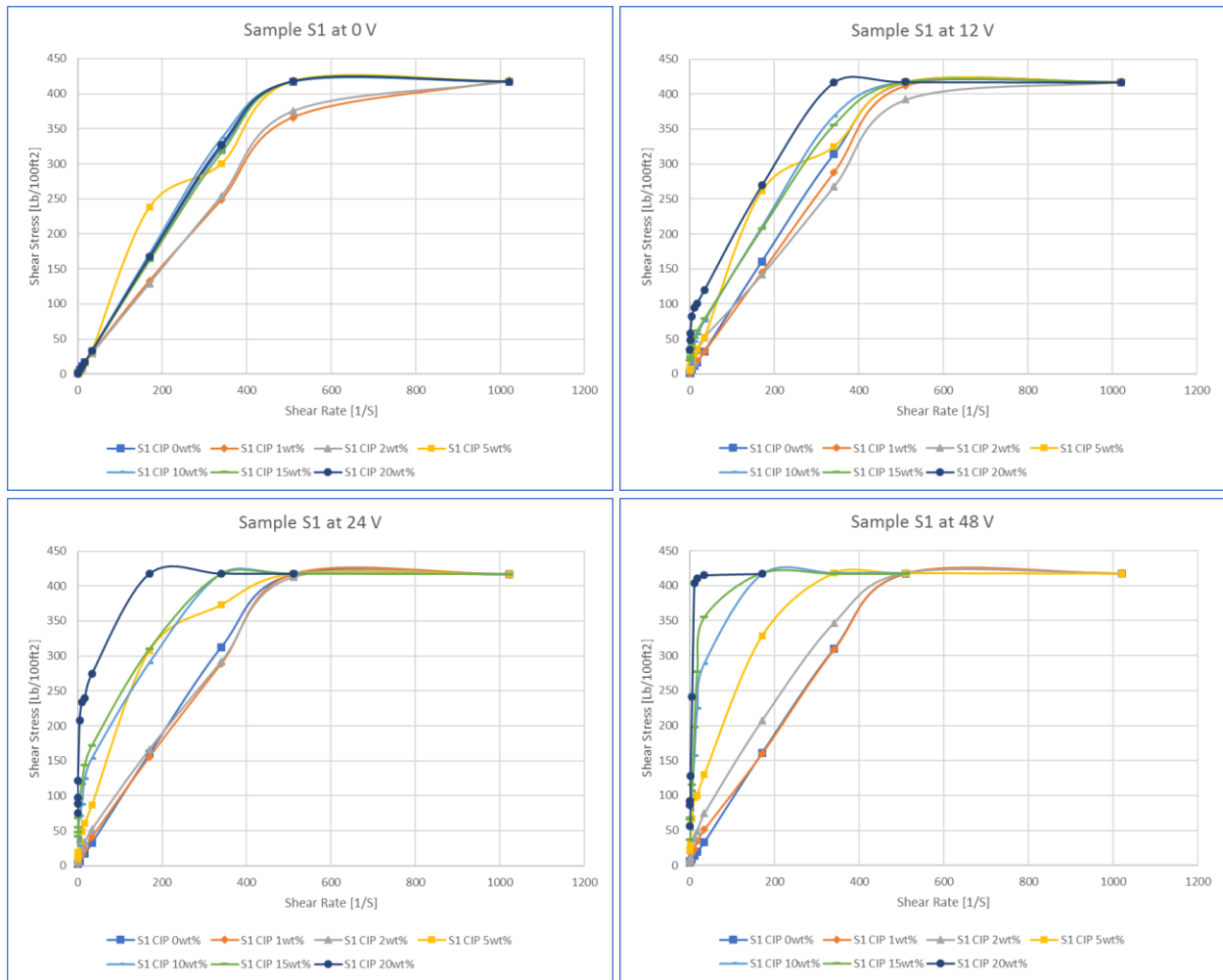


Fig. F2. Rheology behavior of Sample S1 at different magnetic fields.

It is observed how at lower shear rates the shear stress increases as the concentration of CIP increases and the magnetic field increases. The sample with CIP 5%wt (Yellow) at magnetic fields 24V and below showed higher shear stresses in comparison to the other concentration's trends. At shear rates of 500 [1/S] and higher, there is not evident increase of the shear stress as a function of both, the CIP concentration and magnetic field. However, it is important to consider that at 48V and CIP 20%wt, the readings exceeded the rheometer capabilities.

The mixture separated as two different phases in less than 24 hours 20/80 CIP 5%wt and 50/50 as shown in F CIP 20%wt, as shown below in Fig. F3.

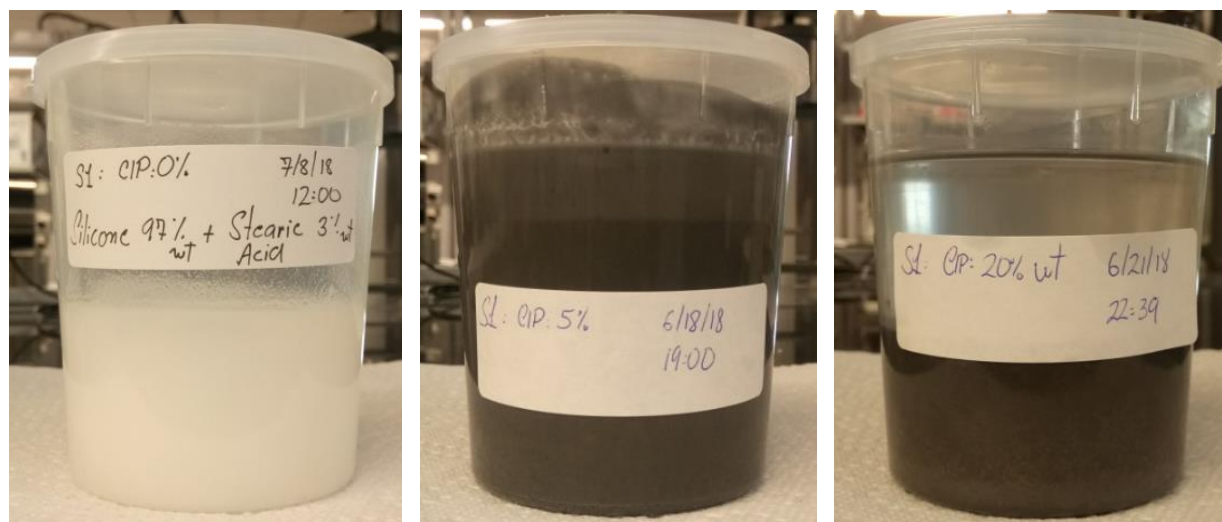


Fig. F3. Study of sedimentation of Sample S1

The rheology results shown a very interesting behavior, where at lower shear rates the shear stress is increased by the magnetic field and CIP concentration. These results strengthen the background theory from the literature review. Also, the capability of this sample to activate and deactivate simultaneously with the application of the magnetic field was the more evident among all the sample tested so far. The main setback of this sample is the considerable high particle settling. Additionally, the fact that a high temperature (120°F) required to dissolve the pallets of stearic acid in the silicone oil provides a logistic complication in terms of mixing it at room temperatures (PERTT Lab). Finally, the use of silicone oil increases even more the costs of the fluid and challenges even more the cleaning of the flow loop. Other than that, the results obtained, and the phenomena observed was very interesting.

### Sample S2:

To avoid the degradation of the Laponite RD pallets, the pH was increased to 10 by adding 1.8 mM NaOH and 4.1 mM NaHCO<sub>3</sub>. While agitating, the 3%wt of Laponite RD was added. After a few minutes the polymer reacted, and a highly viscous fluid was produced, having the consistency of a cross-linked gel. Also, in static conditions the fluid formed gelled rapidly. The gels were broken easily by adding motion to

the system. The gels didn't form homogenously, showing higher gelation at the bottom of the metal cup. While in agitation and before the activation of the polymer, the CIP was added to create a more homogenous mixture. The consistency of the mixture showed probably a low pumpability.

In comparison to the sample 1, the sample 2 did not return to the fluid form after removing the magnetic field. In fact, only after rotating at high shear rates the CIP particles build-up could dissolve.

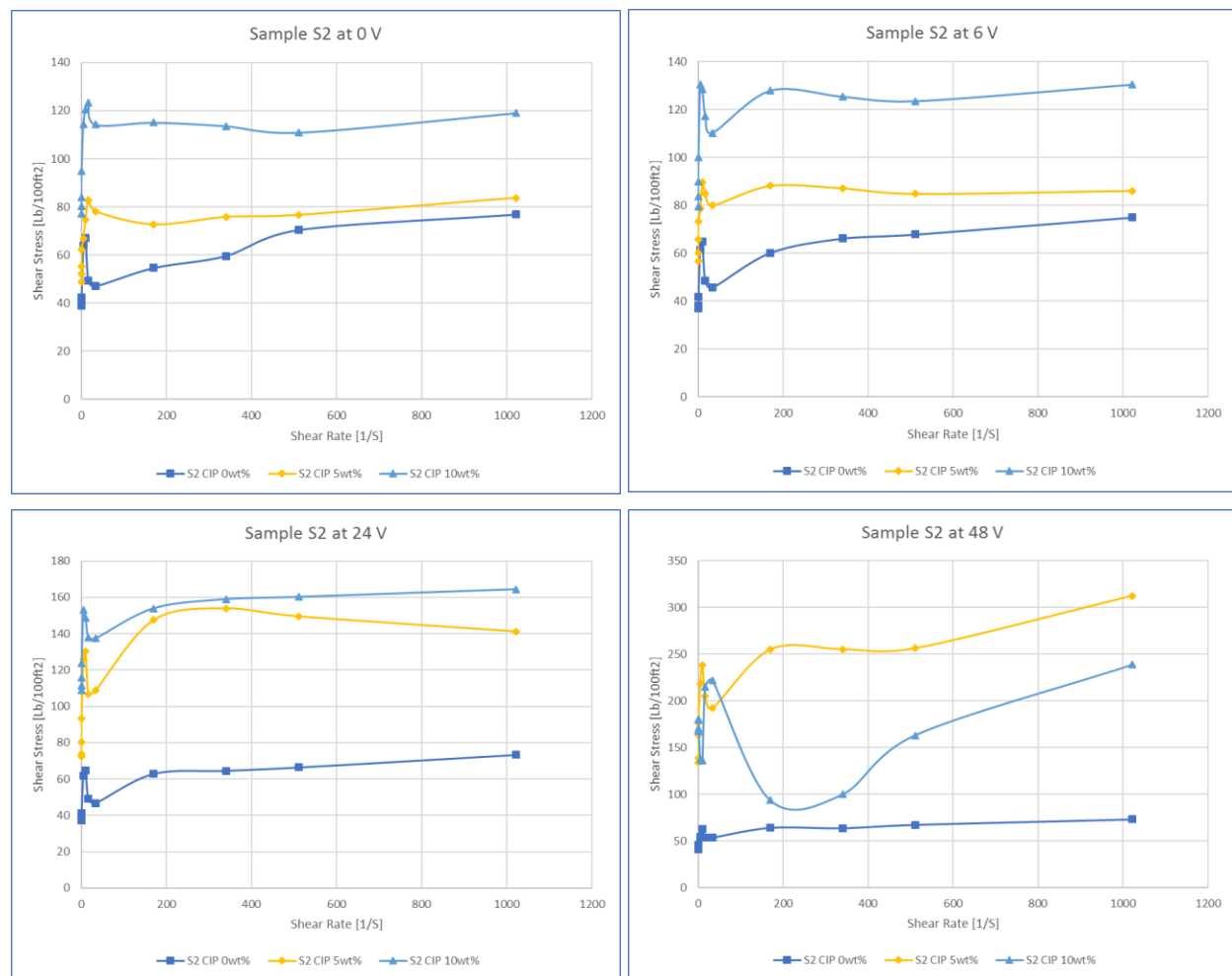


Fig. F4. Rheology behavior of Sample S2 at different magnetic fields.

It can be observed a gelling (aging) effect at low shear rates showing a peak in the shear stress. It was observed physically how the fluid gelled rapidly when static. To get a better understanding of this type of fluid, further recipes with lower concentration of Laponite RD were produced. At 48V the shear stress for the highest concentration 10%wt had a lower shear stress in comparison to the 5%wt. When the metal cup was removed, CIP particles were settled down at the bottom, this potentially explain why at 48V the rheologies were lower.

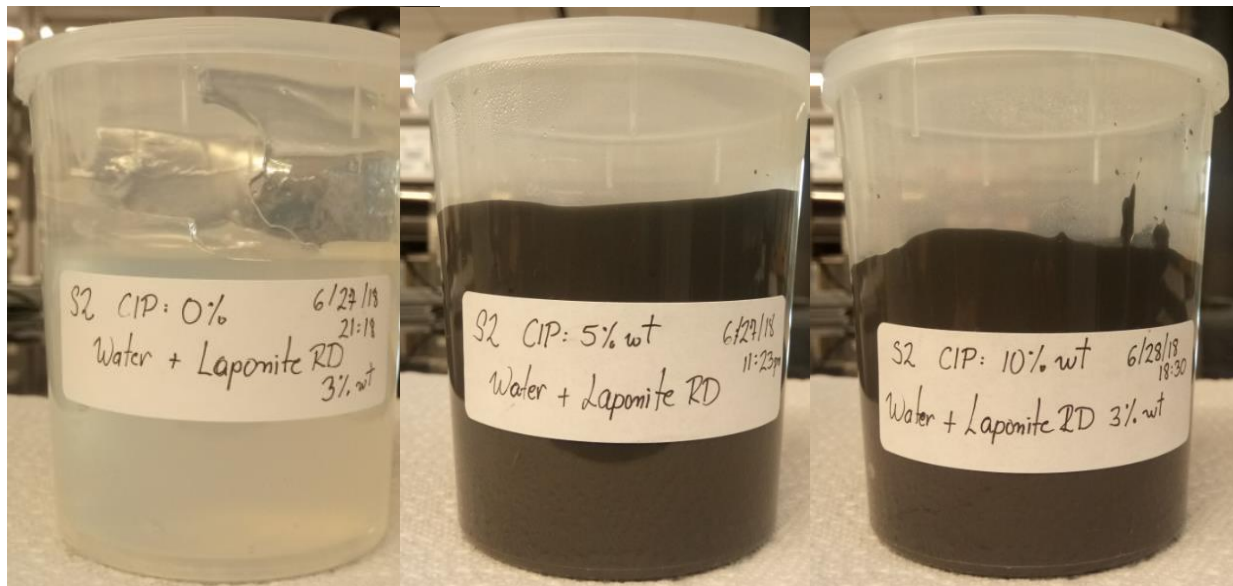


Fig. F5. Particle Settling Sample S2

The particle setting was negligible, even after two weeks to particle settling was observed Fig. F5. The positive aspects of this combination are the low/negligible particle settling. Additionally, the use of water as the carrier fluid provides an easier logistics and lower prices of the fluid. A potential setback is the high viscosity, it rises doubt of its pumpability due to its consistency. And perhaps, more importantly, the shear stress was not considerable high if it is compared to the sample 1, the later achieved 400 Lb/100 ft<sup>2</sup> whereas the sample 2 hardly achieved the 300 Lb/100 ft<sup>2</sup>. Probably, the high viscosity is not allowing a proper alignment of the particles. Because of this, further combinations with lower concentration of Laponite RD were tested and evaluated, as follows.

### Sample S3:

This sample produced a more aqueous mixture with low viscosity in comparison to Sample S3. The Laponite RD and the CIP dissolved easily. No gelation or clogs of fluid were identified.

The rheology values were in general low. Additionally, a low gelling effect was observed at low shear rate as compared to sample 2.

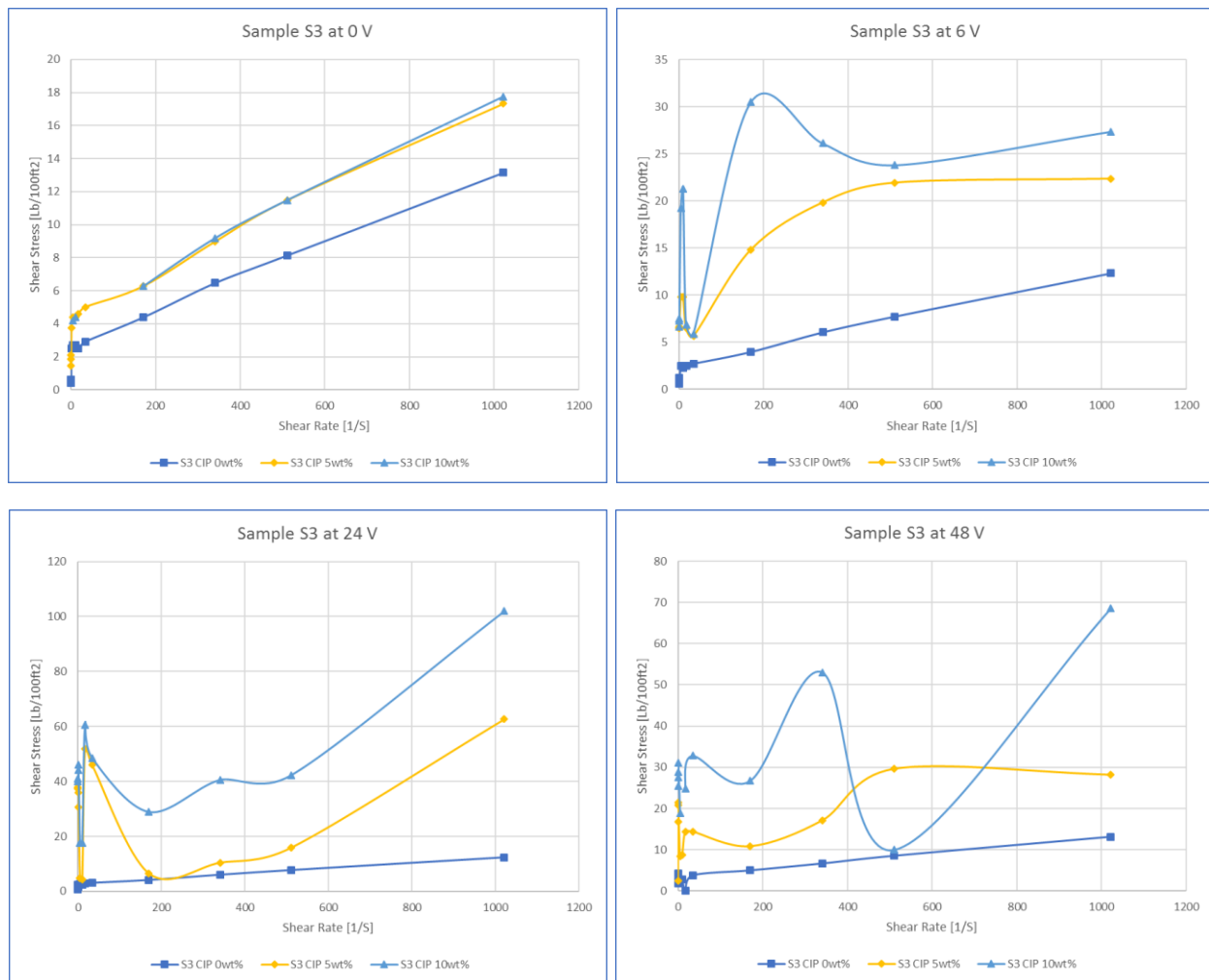


Fig. F6. Rheology Measurements Sample S3

At higher concentration of CIP the higher the shear stress produced. However, in general the shear stress values were low in comparison to the samples 1 and 2. In that sense, it is possible to argue that the rheology properties of the MRF are a direct function of the carrier fluid with the corresponding additives, in this case the Laponite RD. Finally, as the CIP concentration increases, the shear stress tends to decrease. Possibly, the low capability of this fluid to hold the solid particles produced this low rheologies. However, this mixture produced a fluid with low capabilities of controlling the particle settling as observed in Fig. F6. In fact, even with no CIP content, the mixture segregated. The higher the concentration of CIP, the higher the particle settling for this sample.

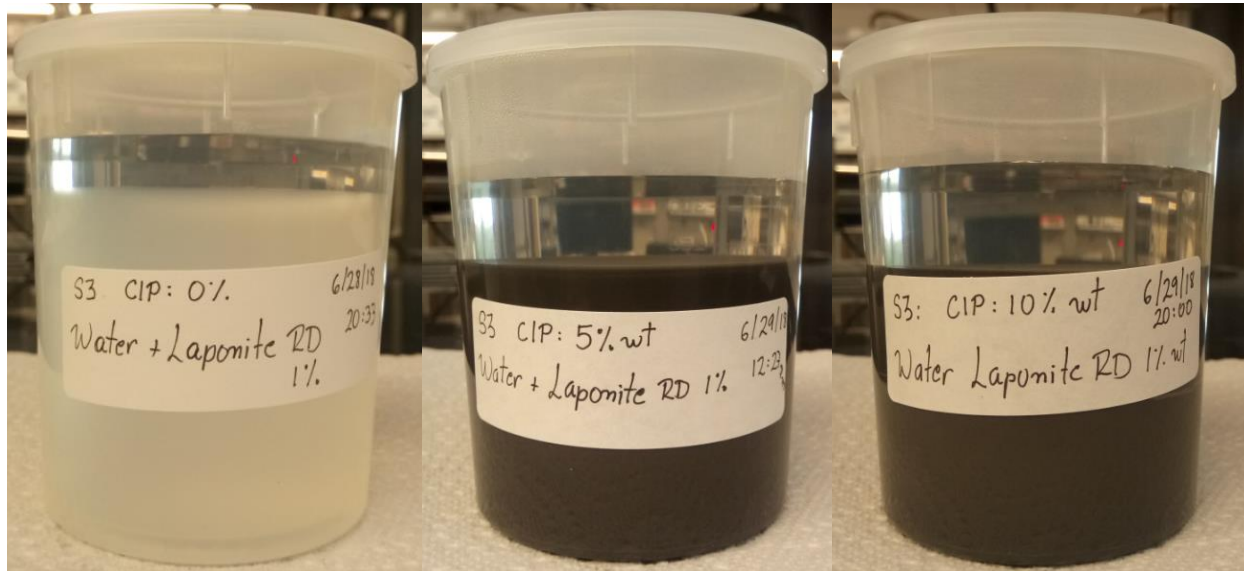


Fig. F7. Settling Ratio Sample S3

This mixture produced a fluid with low capabilities of controlling the particle settling. In fact, even with no CIP content, the mixture segregated. The higher the concentration of CIP, the higher the particle settling for this sample. In that sense, Sample 3 is not a good candidate for MRF due to its low rheological properties, high particle settling and low shear stresses, specially at higher magnetic fields.

#### Sample 4:

The mixing was regular, as the other samples using the agent Laponite RD. After five minutes of mixing, the polymer activated and again some gels were formed at the bottom. In comparison to sample 2, sample 4 was more fluid and homogeneous.

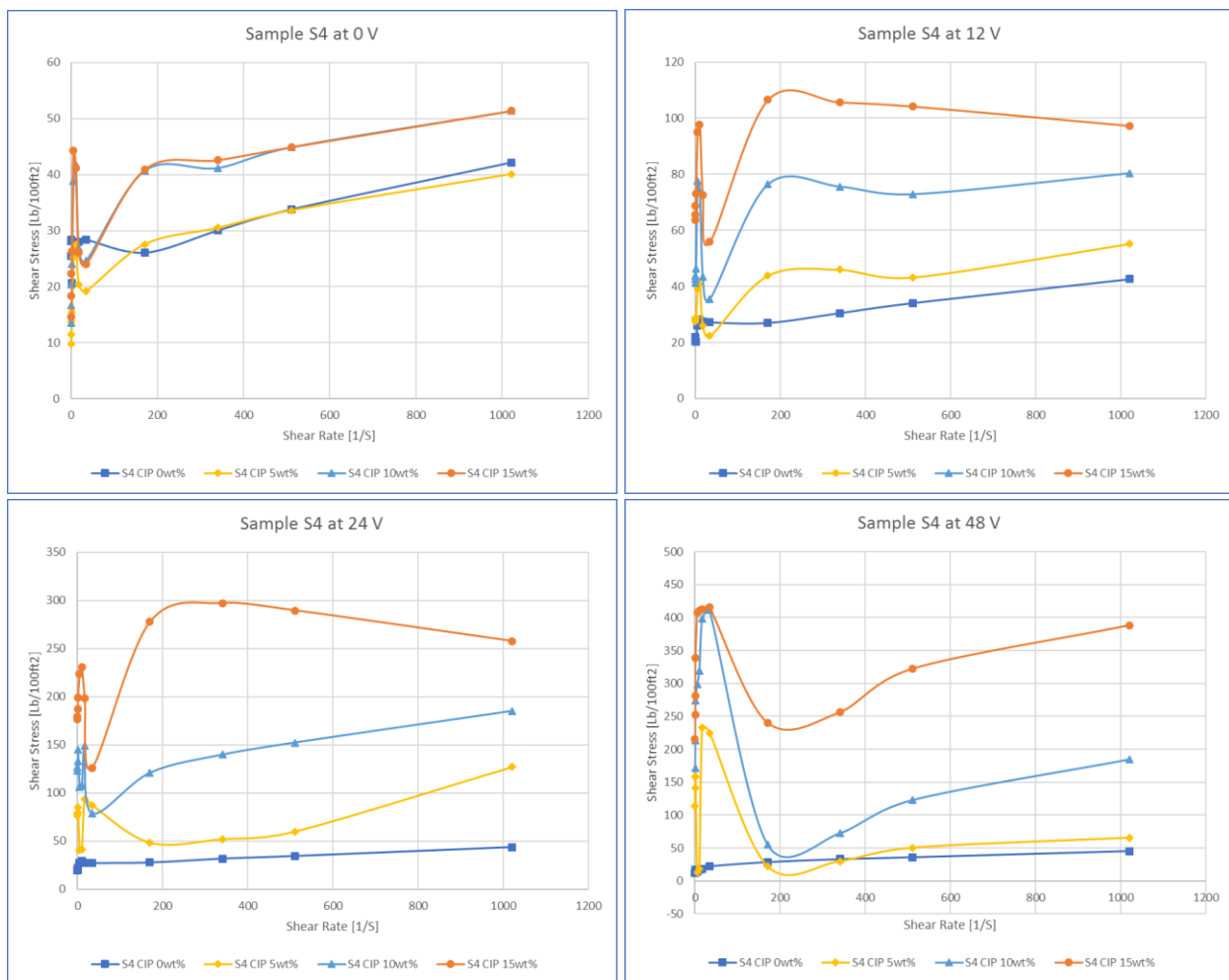


Fig. F8. Rheology of Sample S4

As with the other samples with Laponite RD, there is a clear gelling (aging) effect at low shear rates that normalizes after 200 [1/S] as observed in Fig. F8. In terms of shear stress, at very low and very high shear rates the shear stress was close to 400 Lb/100 ft<sup>2</sup> which is one of the highest observed during the experimentation phase.

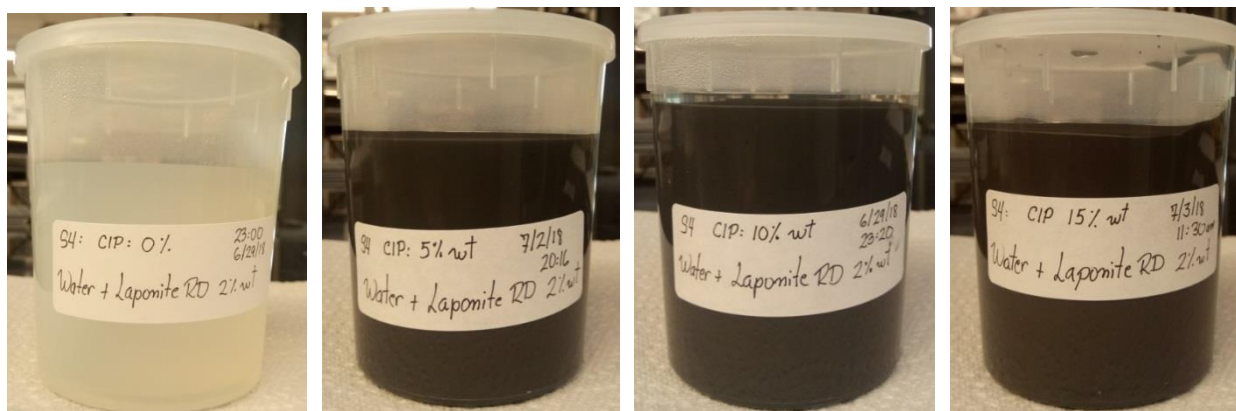
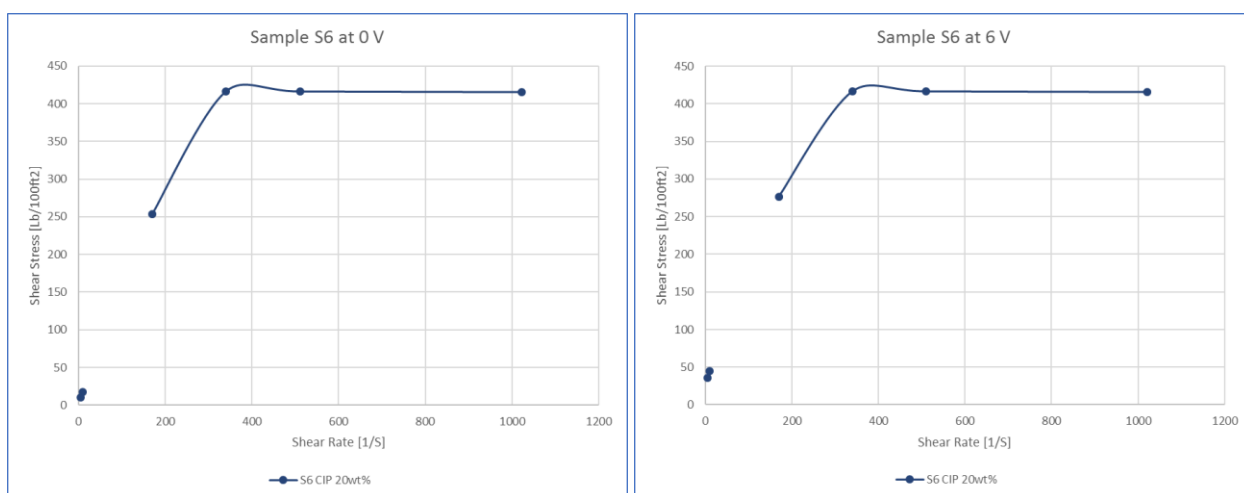


Fig. F9. Particle Settling Sample S4

This sample in general showed a good consistency and a low tendency for the particles to settle down as shown in Fig. F9. However, it is still evident to see the two phases (water + additives) in a ratio of 5% approximately.

This sample remains as a good candidate for MRF. It showed relatively high shear stresses as the magnetic field increased. There is not evident overlapping of the rheology curves at different CIP concentration and constant magnetic field, as observed at low shear rates in the samples studied to this point. The particle settling is still low to be considered as a setback.

### Sample 6:





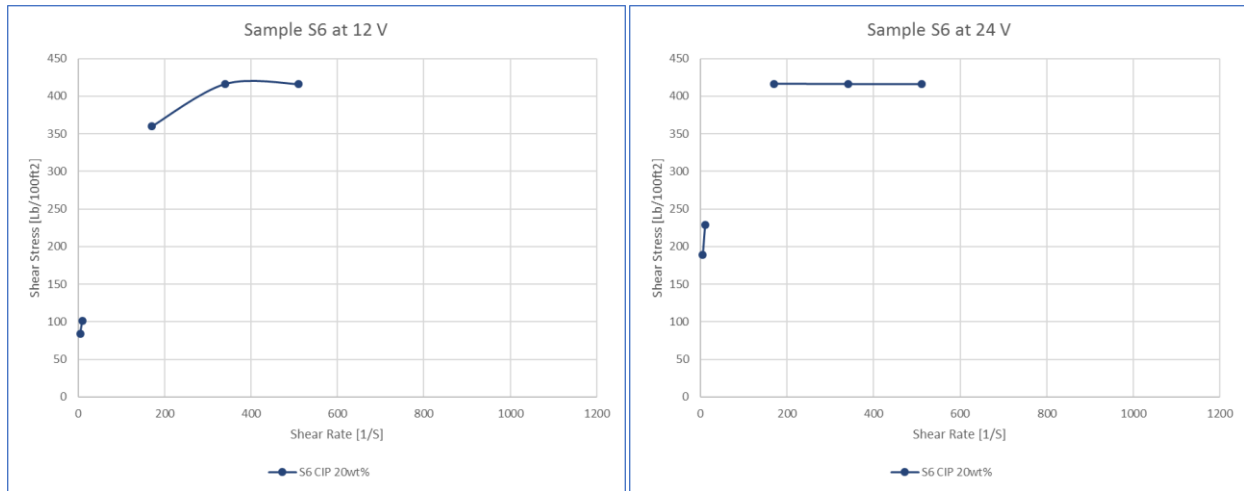


Fig. F10. Rheology of Sample S6

As the temperature decreased, the viscosity and shear stress increased as expected for the high viscosity silicone. The low shear rate readings were not obtained since the bob unlatched due to the high viscosity of the sample. The particle settled at a very fast ratio. Not good candidate for MRF.

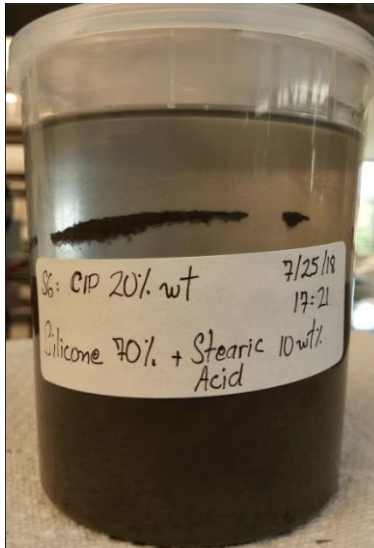


Fig. F11. Particle Settling Sample S6

## Sample 7

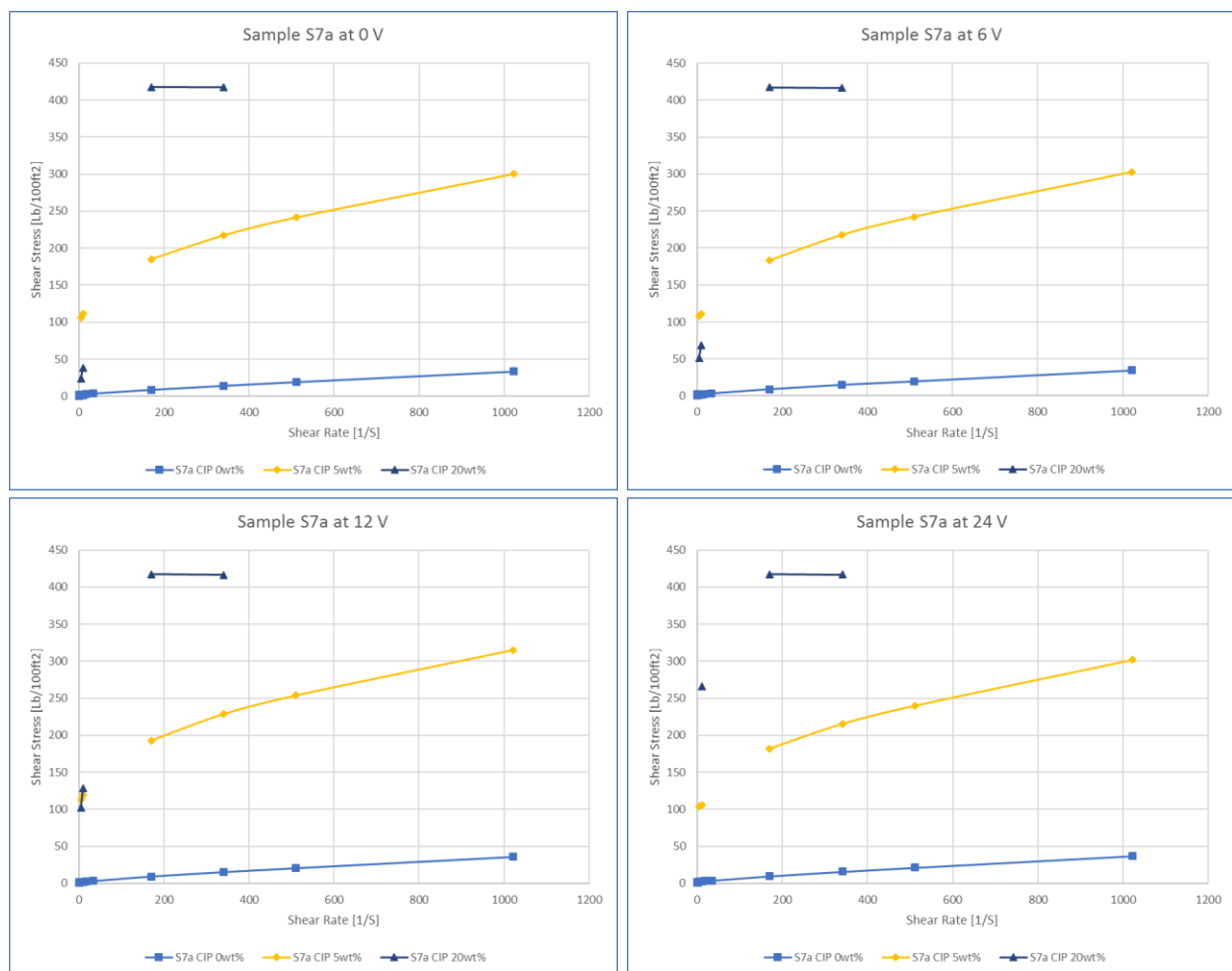


Fig. F12. Rheology of Sample 7a

The consistency of the sample was too thick that fluid almost looked completely gelled, perhaps non-pumpable. My impression is that after the pre-hydration of 24 hours the fluid looked pumpable but after mixing it again at the mixer strong gels creating almost no vortex. The bob detached from the shaft from the viscometer. Because of this the measurement at low shear rates were not taken. The fluid was highly viscous at almost none magnetic field. This aspect makes this sample not a good candidate.

## Sample S8

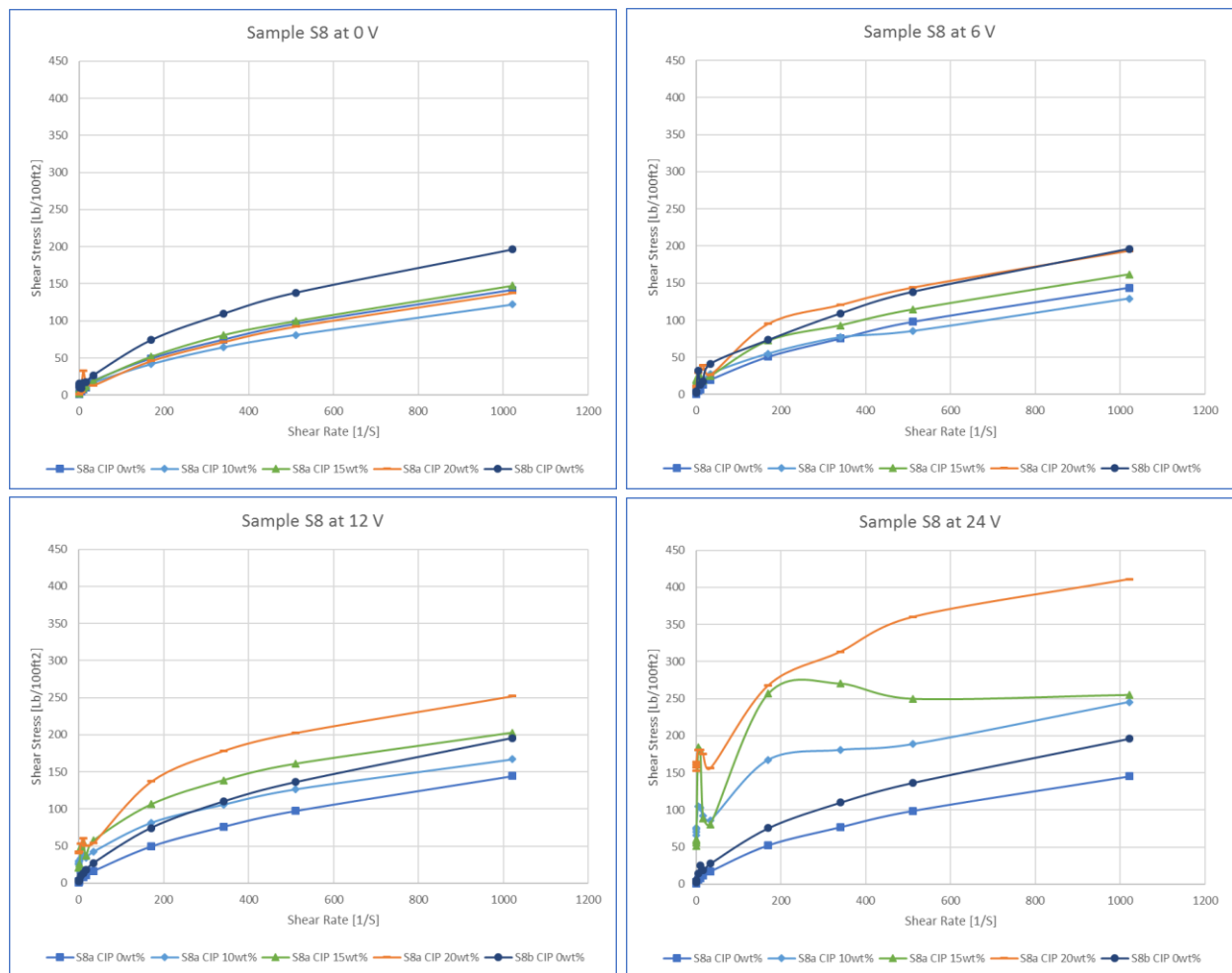


Fig. F13. Rheology of Sample S8

First the CMC was added and mixed for 10 min. Then, the Bentonite was added. The rheologies show an extremely good behavior in terms of what is expected from a pseudoplastic fluid. Also, the shear stress increases accordingly with the magnetic field intensity and the CIP concentration. However, after 20 day of mixed the fluid started to become greener. The CIP particles started to corrode, and the sedimentation of the particles increased exponentially.



Fig. F14. Particle Settling Sample S8a

## Sample 9

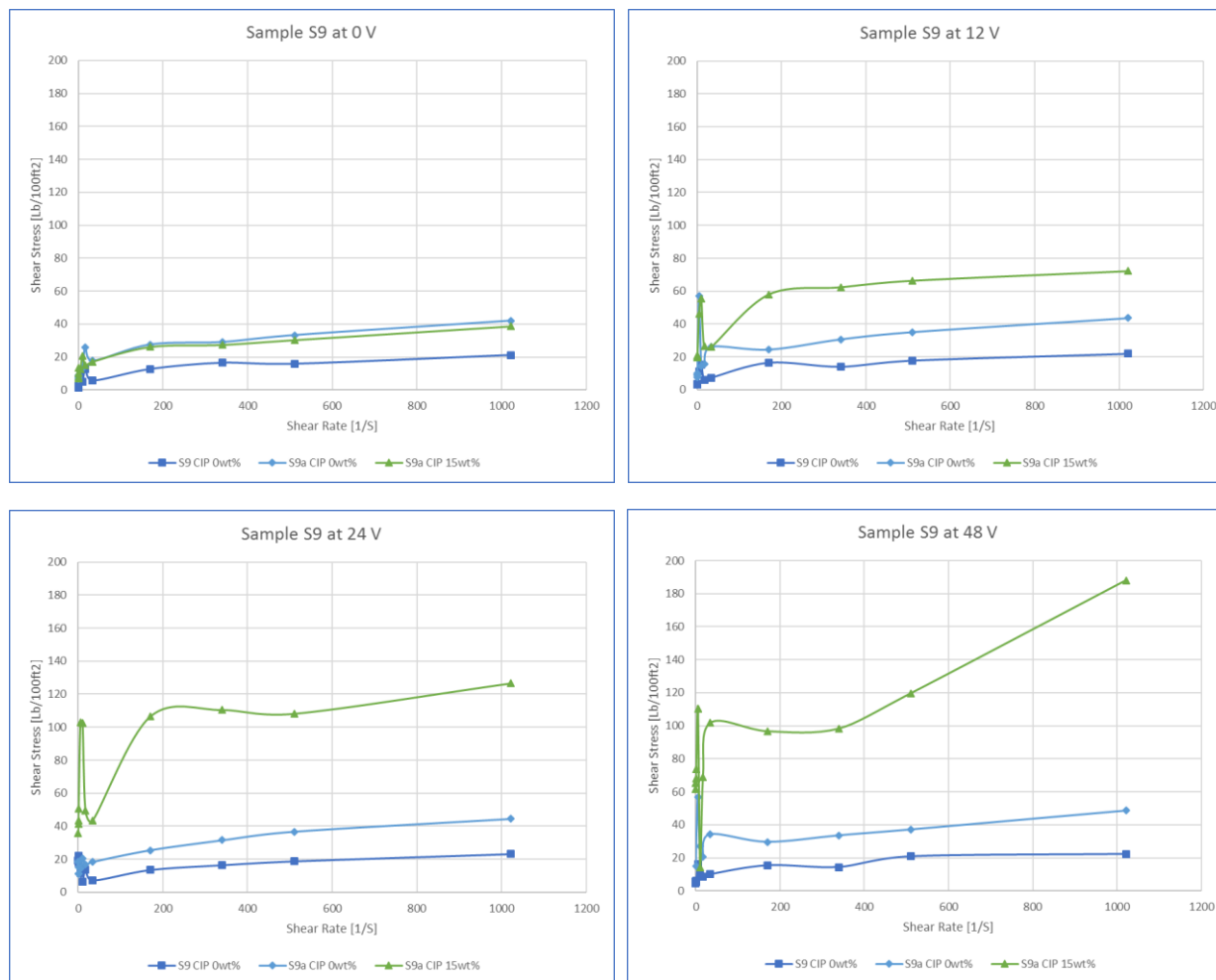


Fig. F15. Rheology of Sample S9

First the CMC was added and mixed for 10 min. Then, the Bentonite was added. The mixture produces a high amount of foam. This sample does not produce a good development of shear stress at higher concentration of CIP. The foam also affected the rheology measurements.

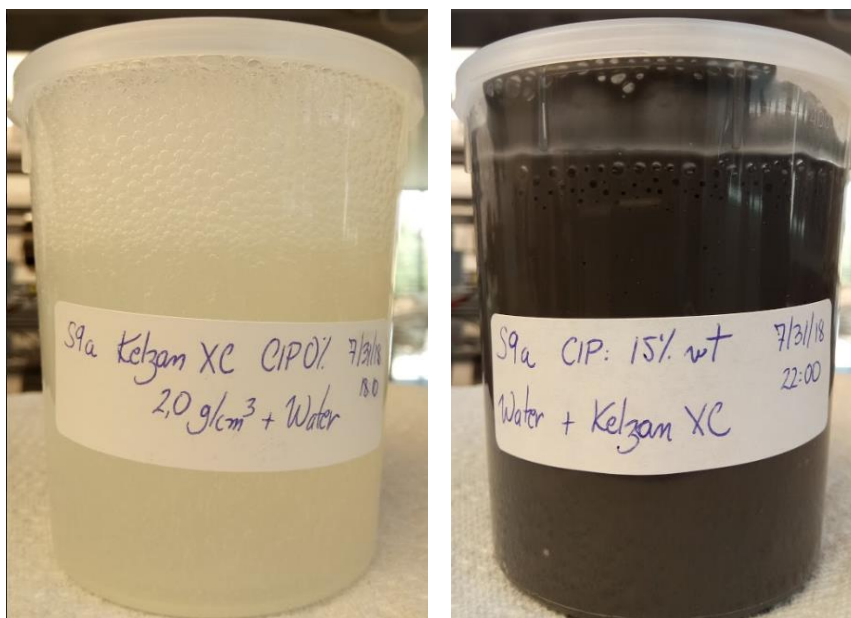


Fig. F16. Particle Settling Sample S9a

## APPENDIX G EXAMPLE OF CALCULATION FOR PRESSURE DROP

At 24 volts the rheological parameters are represented in the following table G1:

Table G1. Rheology measurements from Couette Viscometer

Speed [rpm]								
600	300	200	100	20	10	6	3	
Shear Rate [1/S]								
1021.38	510.69	340.46	170.23	34.046	17.023	10.21	5.1069	
382.62	392.64	375.10	353.38	183.37	257.3099	298.0368	286.1319	Deflect [°]

At 0 volts the rheological parameters are represented in the following table G2:

Table G2. Rheology measurements from Couette Viscometer

Speed [rpm]								
600	300	200	100	20	10	6	3	
Shear Rate [1/S]								
1021.38	510.69	340.46	170.23	34.046	17.023	10.21	5.1069	
37.593	27.77	23.182	19.214	15.2464	15.4553	17.335	15.6641	Deflect [°]

The fluid shear stress can be represented as a function of the Yield stress, consistency index, shear rate and flow behavior index. Using curve fitting, these parameters can be determined.

$$\tau = \tau_0 + k\dot{\gamma}^n \quad (\text{Eq. 1})$$

For the curve fitting at 24 volts

$$n = 0.689,$$

$$k = 1.52975 \text{ Lbf s}^n/100 \text{ ft}^2 \text{ or } 728.16 \text{ eq cP, and}$$

$$\tau_0 = 241.98587 \text{ Lbf}/100 \text{ ft}^2$$

The flow index measures the degree to which the fluid is shear thinning  $n < 1$ .

The average velocity of the fluid in pipe or annulus is inversely proportional to the cross-sectional area of the conduit:

$$V_a = \frac{24.51 Q}{d_h^2 - d_p^2} \quad (\text{Eq. 3})$$

Where  $V_p$  and  $V_a$  correspond to the average velocity [ft/min] in pipe and annulus, respectively.  $Q$  is the flow rate [gpm].  $d_h$  and  $d_p$  are the diameter [in] of the outside geometry and pipe, respectively.

$$V_a = \frac{24.51(21.1)}{4.0^2 - 1.66^2} = 39.047 \text{ ft/min}$$

The nominal shear rate  $\gamma$  first must be converted to shear rate at the wall  $\gamma_w$  to calculate the pressure drop. The well geometry correction factor  $B_a$  is a function of the rheological parameter flow index  $n$  and the type of conduit.

$$B_a = \left[ \frac{(3-\alpha)n+1}{(4-\alpha)} \right] \left[ 1 + \frac{\alpha}{2} \right] \quad (\text{Eq. 4})$$

Where  $\alpha$  is 0 for geometry factor for pipe and 1 for annulus.

$$B_a = \left[ \frac{(3-1)0.689+1}{(4-1)} \right] \left[ 1 + \frac{1}{2} \right] = 1.7256$$

The field viscometer correction factor  $B_x$  is also a function of the flow index  $n$  and the type of bob/sleeve combination.

$$B_x = \left[ \frac{X^{\frac{2}{n}}}{nX^2} \right] \left[ \frac{X^2-1}{\frac{2}{X^{\frac{2}{n}}-1}} \right] \quad (\text{Eq. 5})$$

Where X is the 1.0678 in the standard bob/sleeve combinations R1B1.

$$B_x = \left[ \frac{1.0678^{\frac{2}{0.689}}}{(0.689)1.0678^2} \right] \left[ \frac{1.0678^2-1}{\frac{2}{1.0678^{\frac{2}{0.689}}-1}} \right] = 1.0292$$

The combined geometry shear-rate factor is defined as  $G$

$$G = \frac{B_a}{B_x} \quad (\text{Eq. 6})$$

$$G = \frac{1.7256}{1.0292} = 1.6766$$

The shear rate at the wall  $\gamma_w$  required to determine the shear stress at the wall is calculated as follows:

$$\gamma_w = \frac{1.6GV_p}{d_p} \text{ or } \gamma_w = \frac{1.6GV_a}{d_h - d_p} \quad (\text{Eq. 7})$$

$$\gamma_w = \frac{1.6(1.6766)(39.047)}{4.0 - 1.66} = 44.7632 \text{ s}^{-1}$$

The frictional pressure losses are directly proportional to the shear stress at the wall  $\tau_w$ , where  $\tau_f$  is the shear stress at the wall in viscometer units.

$$\tau_f = \left[ \frac{4-\alpha}{3-\alpha} \right]^n \tau_y + k\gamma_w^n \quad (\text{Eq. 8})$$

$$\tau_f = \left[ \frac{4-1}{3-1} \right]^{0.689} 227.00 + (44.7632)^{0.689} = 313.88^\circ$$

$\tau_w$  in engineering units.

$$\tau_w = 1.066\tau_f \quad (\text{Eq. 9})$$

$$\tau_w = 334.6 \frac{Lb}{100ft^2}$$

The frictional losses are also a function of the flow patterns characterized by laminar, transitional and turbulent flow regimes.

The Reynolds number (generalized) determines the flow regime and applies for both pipe and annulus.

$$N_{ReG} = \frac{\rho V^2}{19.36\tau_w} \quad (\text{Eq. 10})$$

Where  $\rho$  is the density in [Lb/gal] of the fluid and  $V$  is the average velocity for pipe or annulus in [ft/min].

$$N_{ReG} = \frac{9.62 (39.047)^2}{19.36(334.6)} = 2.26$$

The critical Reynolds number  $N_{CRe}$  is the value of  $N_{ReG}$  where the flow regime changes from laminar flow to transitional flow.

$$N_{CRe} = 3470 - 1370n \quad (\text{Eq. 11})$$

$$N_{CRe} = 3470 - 1370(0.689) = 2526.07$$

The pressure losses in pipes and annuli are a function of the Fanning friction factor  $f$  which is a function of the rheological properties, the flow regime and generalized Reynolds number. A generalized expression of Fanning friction factor  $f$  for any Reynolds number and flow regime includes intermediate terms for laminar  $f_{lam}$ , transitional  $f_{trans}$  and turbulent  $f_{turb}$  flow regimes.

$$f_{lam} = \frac{16}{N_{ReG}} \quad (\text{Eq. 12})$$

$$f_{lam} = \frac{16}{2.26} = 7.07964$$

$$f_{trans} = \frac{16N_{ReG}}{N_{CRe}^2} \quad (\text{Eq. 13})$$

$$f_{trans} = \frac{16(2.26)}{2526.07^2} = 5.6667 \text{EXP}(-06)$$

$$f_{turb} = \frac{a}{N_{ReG}^b} \quad (\text{Eq. 14})$$

Where

$$a = \frac{\log_{10}(n) + 3.93}{50} \quad (\text{Eq. 15})$$

$$a = \frac{\log_{10}(0.689) + 3.93}{50} = 0.07536$$

$$b = \frac{1.75 - \log_{10}(n)}{7} \quad (\text{Eq. 16})$$

$$b = \frac{1.75 - \log_{10}(0.689)}{7} = 0.273$$

$$f_{turb} = \frac{0.07536}{2.26^{0.273}} = 0.06032$$

The pipe roughness effect on friction increases in fully developed turbulent flow. Since this is not case of the current experiment, the pipe roughness effect is considered negligible.



$$f_{intermediate} = (f_{transitional}^{-8} + f_{turbulent}^{-8})^{-1/8} \quad (\text{Eq. 17})$$

$$f_{intermediate} = (5.666EXP(-6)^{-8} + 0.06032^{-8})^{-1/8} = 5.666EXP(-6)$$

$$f = (f_{intermediate}^{12} + f_{laminar}^{12})^{1/12} \quad (\text{Eq. 18})$$

$$f = (5.666EXP(-6)^{12} + 7.079^{12})^{1/12} = 7.6363$$

Where  $f$  is the Fanning friction factor, dimensionless.

Finally, the pressure drop expression for a fixed length  $L$  is expressed as follows:

$$\Delta P_{pipe} = \frac{1.076\rho V_p^2 f L}{10^5 d_p} \quad (\text{Eq. 19})$$

$$\Delta P_{annulus} = \frac{1.076\rho V_a^2 f L}{10^5 (d_h - d_p)} \quad (\text{Eq. 20})$$

$$\Delta P_{annulus} = \frac{1.076(9.62)39.047^2(7.6363)(1ft)}{10^5(4-1.66)} = 0.51503 \text{ psi/ft in the presence of the magnets}$$

The length of the entire magnet arrangement is 6.5-in (0.5416 ft). The distance from pressure transducer P3 to P4 is 4.0 ft. Following the same calculation, the pressure drop without magnetic field (0 Volts) the values are the following:

$$n = 0.15,$$

$$k = 10.29801 \text{ Lbf s}^n/100 \text{ ft}^2 \text{ or } 4932.746 \text{ eq cP, and}$$

$$\tau_0 = 0 \text{ Lbf}/100 \text{ ft}^2$$

The friction loss is:

$$\Delta P_{annulus} = \frac{1.076(9.62)39.047^2(1.3623)(1ft)}{10^5(4-1.66)} = 0.09188 \text{ psi/ft without magnets}$$

$$\Delta P_{annulus} \text{ transducer } P4 - P2 = (3.4584 \text{ ft}) \left( 0.09188 \frac{\text{psi}}{\text{ft}} \right) + (0.5416 \text{ ft}) \left( 0.51503 \frac{\text{psi}}{\text{ft}} \right) = 0.5967 \text{ psi}$$

The measured value was 0.631239 psi

$$\text{Error} = \frac{\#Experimental - \#Theoretical}{\#Theoretical} * 100 = \frac{0.631239 - 0.5967}{0.5967} * 100 = 5.78\%$$

## VITA

John Estrada was born in Bogotá D.C., Colombia, on March 25<sup>th</sup>, 1985. He received a bachelor's degree in petroleum engineering in 2008 from Universidad Nacional de Colombia. During his bachelor studies he evaluated the technical and economical impact of Cluster Drilling in the Llanos Basin in Colombia. Also, in 2008, he did an internship with the artificial lift division with Schlumberger specialized in electro-submersible pumps. After obtaining his engineering degree he was an instructor at a technical school oriented to Oil & Gas personnel and was involved in a seismic project in Puerto Lopez, Meta Province, Colombia. In 2010, he started working with Halliburton Colombia in the division of Zonal Isolation. The most relevant projects he developed during his time in Halliburton included cementing operations for In-Situ combustion wells for the Chichimene and Quifa Fields. In 2015, he was transferred to Halliburton Argentina where he was involved in projects for the exploitation of Vaca Muerta, a shale oil and shale gas reservoir located at the Neuquén Province.

In 2016, he joined the Craft and Hawkins Department of Petroleum Engineering at Louisiana State University as a M.S. candidate, and the Magnetorheological Fluids research group led by Dr. Babak Akbari. During his time at Louisiana State University he held different assignments as Teaching Assistant including courses of Well Control, Mud Lab, Well Design Production and Fundamentals of Drilling Engineering.